Translation termination mechanism studied by solution state NMR

Li, Yan

2012

Li, Y. (2012). Translation termination mechanism studied by solution state NMR. Doctoral thesis, Nanyang Technological University, Singapore.

https://hdl.handle.net/10356/50711

https://doi.org/10.32657/10356/50711

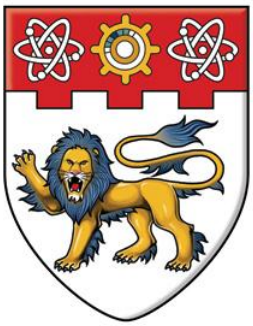

NANYANG TECHNOLOGICAL UNIVERSITY

TRANSLATION TERMINATION MECHANISM STUDIED BY SOLUTION STATE NMR

LI YAN

School of Biological Sciences

2012

Translation termination mechanism studied by solution state NMR

Li Yan

School of Biological Sciences

A thesis submitted to the Nanyang Technological University

in fulfillment of the requirement for the degree of

Doctor of Philosophy

2012

Acknowledgements

Foremost, I would like to express my sincere gratitude and thanks to my supervisor A/Prof. Dr. Konstantin Pervushin for his constant encouragement and support during my Ph.D. study and research, for his patience, motivation, enthusiasm, and immense knowledge. His guidance has helped me throughout my research and writing of this thesis. I could not have imagined having a better advisor and mentor for my Ph.D. study.

I would like to express my gratitude to Mr. Wong Leo E and Mr. Bertrand Russell for their help during this research. I would like to thank Ms. Sun Huihua for her support and encouragement. I am very thankful to Dr. Heike Summer and Mr. Lai Tenghow for their help in wet lab experiments. I would like to thank Mr. Edward Tan and Dr. Xiao Zhou for their suggestions and support with NMR Experiments.

I would like to thank all my other laboratory colleagues for their support: Ms. Bai Yang, Ms. Shubhadra Pillay, Mr. Zhang Yizhong, Mrs. Liu Rubing, Ms. Zhao Jing, Dr. Alistair Irvine, Ms. Margaret Phillips, Dr. David Steven Libich, Mr. Wei Lei, Ms. Rachel Lim Sing Mei and Dr. Ranjith Kumavath.

I am grateful to the School of Biological Sciences, Nanyang Technological University, Singapore for providing a Ph.D scholarship without which this work would not have been possible. This research was also supported by Singapore Ministry of Education AcRF grant T207B3205.

I dedicate this thesis to my father and mother whom I owe all that I have become today. I also thank my brother and all my family members who are always proud of my academic achievements and have supported me all the time.

Contents

List of figures

Introduction

Results

Discussion

List of tables

Abbreviations

CARA	Computer Aided Resonance Assignment
DNA	Deoxy ribo-Nucleic Acid
D_2O	deuterium oxide
DSS	2, 2-dimethyl-2-silapentane-5-sulfonate
E.coli	*Escherichia coli*
eRF1	eukaryotic polypeptide release factor 1
eRF3	eukaryotic polypeptide release factor 3
Hs-eRF1	human eRF1
HSQC	Heteronuclear Single Quantum Correlation
IPTG	Isopropyl β-D-thiogalactopyranoside
NMR	Nuclear Magnetic Resonance
NOE	Nuclear Overhauser Effect
NOESY	Nuclear Overhauser Effect SpectroscopY
MES	2-(N-morpholino) ethanesulfonic acid
PMSF	phenylmethanesulfonyl fluoride
PTC	Peptidyl Transferase Center
$Q^{122}FM(Y)F^{126}$	4-site mutant T122Q+S123F+L124M+L126F
RDC	Residual Dipolar Coupling
RF1	Polypeptide release factor 1
RF2	Polypeptide release factor 2
RF3	Polypeptide release factor 3
RNA	RiboNucleic Acid
RMSD	root mean squre deviation
RRF	Ribosome Recycling Factor
SDS-PAGE	SDS-polyacrylamide gel electrophoresis
St-eRF1	*Stylonychia* eRF1
TROSY	Transverse Relaxation Optimized Spectroscopy

Abstract

Translation termination occurs when one of three stop-codons (UAA, UGA, or UAG) in mRNA reaches the ribosomal A site. In eukaryotes, class-I release factor (eRF1) directly recognizes all three stop-codons in the A site on the small ribosomal subunit and stimulates peptide release. N-domain of eRF1 plays an important role in the stop-codon recognition; however, the precise mechanism of stop-codon discrimination by eRF1 remains obscure, hindering drug development targeting aberrations at translation termination. Through comparison of the solution structure of $Q^{122}FM(Y)F^{126}$ mutant, the Y125F mutant of eRF1 N-domain and the wild type eRF1 N-domain which are determined, we built the correlation between the structure and the stop-codon recognition and found that the conserved GTS loop adopts alternate conformations. We propose that structural variability in the GTS loop may underline the switching between omnipotency and unipotency of eRF1, implying the direct access of the GTS loop to the stop-codon. Also, we proposed a model of eRF1 bound to the A site of eukaryotic ribosome.

Chapter I Introduction

Structural biology of translation termination in prokaryotes and eukaryotes

1.1 Termination of translation of messenger RNA by the Ribosome

1.1.1 Protein synthesis

Protein biosynthesis is a multi-step process which starts with amino acid synthesis and transcription of DNA into messenger RNA, which in turn is decoded by the ribosome to produce a polypeptide capable spontaneously or in assisted manner to fold into an active protein. The cell's cytoplasm of bacteria is the place where small and large ribosomal subunits are located and mRNA is translated while in eukaryotes translation occurs across the membrane of the endoplasmic reticulum. The ribosome decodes mRNA triplet codons by facilitating binding of charged transfer RNA with complementary anticodon sequences to that of the mRNA via canonical Watson-Crick base pairing resulting into a codon-anticodon mini helix as it was evinced in the X-Ray structure of *T.Thermophilus* pre-translocation complex containing three molecules of tRNA, one mRNA and a paromomycin molecule in the A-site of ribosome. Crystal structures of the 30S ribosomal subunit in complex with messenger RNA and cognate transfer RNA in the A site, both in the presence and absence of the antibiotic paromomycin, have been solved at 3.3 Angstrom resolution by V. Ramakrishnan group in 2000 (*1*). However, the structure of the translation termination complex is still not available at present, so it is quite useful to solve the NMR structure of the N-domain of eRF1.

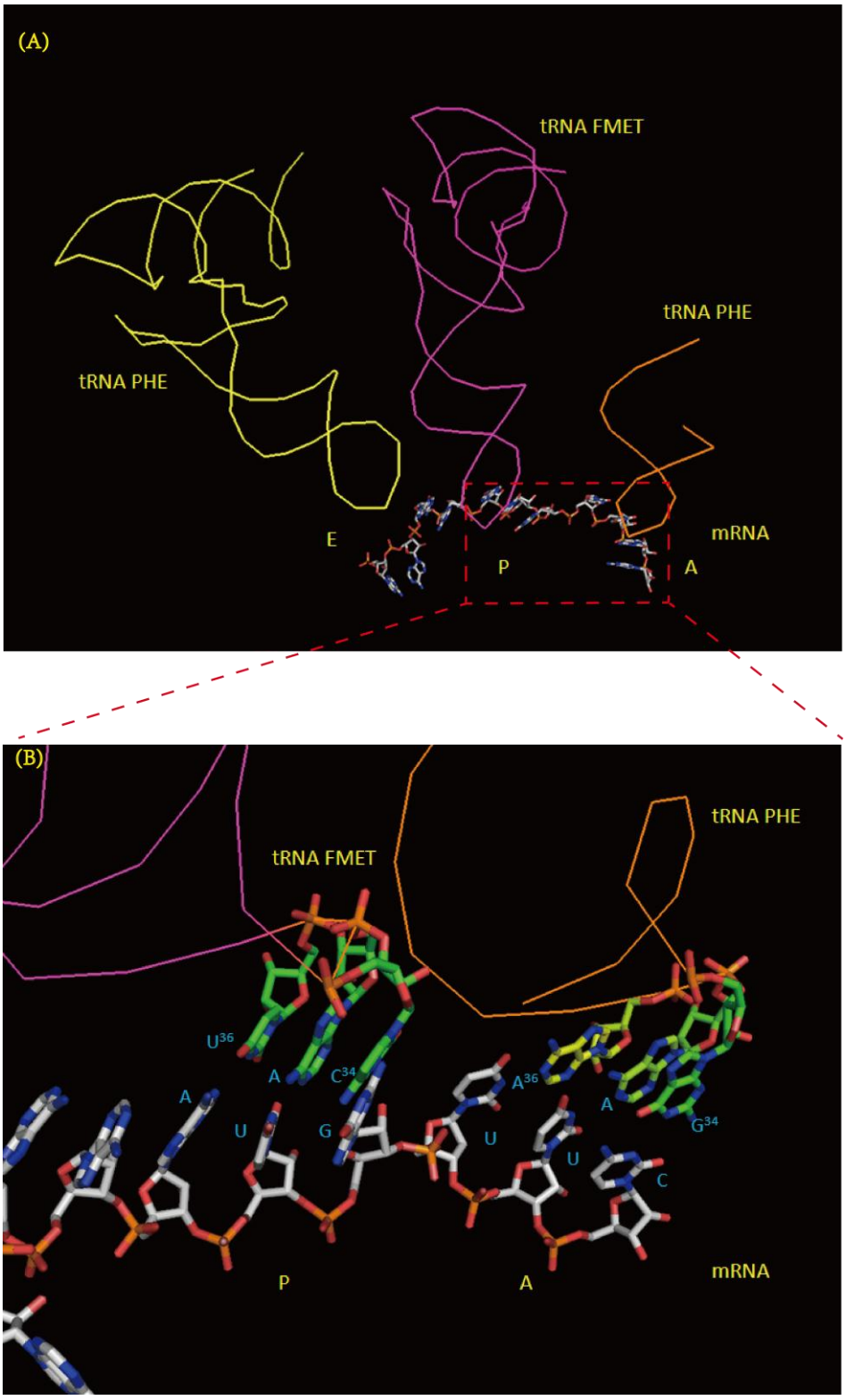

Figure 1.1: Canonical Watson-Crick base pairing between codons and anticodons at the A and P sites of the pre-translocation ribosomal complex (PDB code1IBL) (*1*). mRNA fragment is shown by the sticks representation; cognate tRNAs are yellow, magenta and brown, respectively; anticodon stem-loop bound at the A site.

1.1.2 Translation termination

The final step in protein synthesis is the hydrolysis of the ester bond of the peptidyl tRNA and release of the nascent polypeptide. This occurs when one of three translation termination codons (UAA, UGA, or UAG) in mRNA is found in the ribosomal A site (*2, 3*). The stop-codons are nucleotide triplets within messenger RNA that signals termination of translation. In the standard genetic code in RNA these stop-codons are designated as UAG ("amber"), UAA ("ochre") and UGA ("opal"). They occur at different frequencies in genomes of different organisms. Hydrolysis of the peptidyl-tRNA ester bond in the peptidyltransferase center in the large ribosomal subunit depends on these stop-codons and protein release factors which recognize stop-codons by structurally different mechanisms than tRNA base pairing. Release factors are markedly different and not closely homologous between prokaryotes and eukaryotes (*4-7*). In prokaryotes the two kinds of class-I release factors possess different decoding capability: RF1 recognizes exclusively UAA ("ochre") and UAG ("amber") as stop-codons, while RF2 terminates translation at UAA ("ochre") and UGA ("opal") (*4-6*). In contrast, eukaryotic eRF1 is unrelated in primary structure to the prokaryotic proteins (*7*) and recognizes all three stop-codons (*8-10*). Class-II release factors (RF3 in prokaryotes; eRF3 in eukaryotes) bind GTP or GDP and stimulate class-I RF activity (*11, 12*).

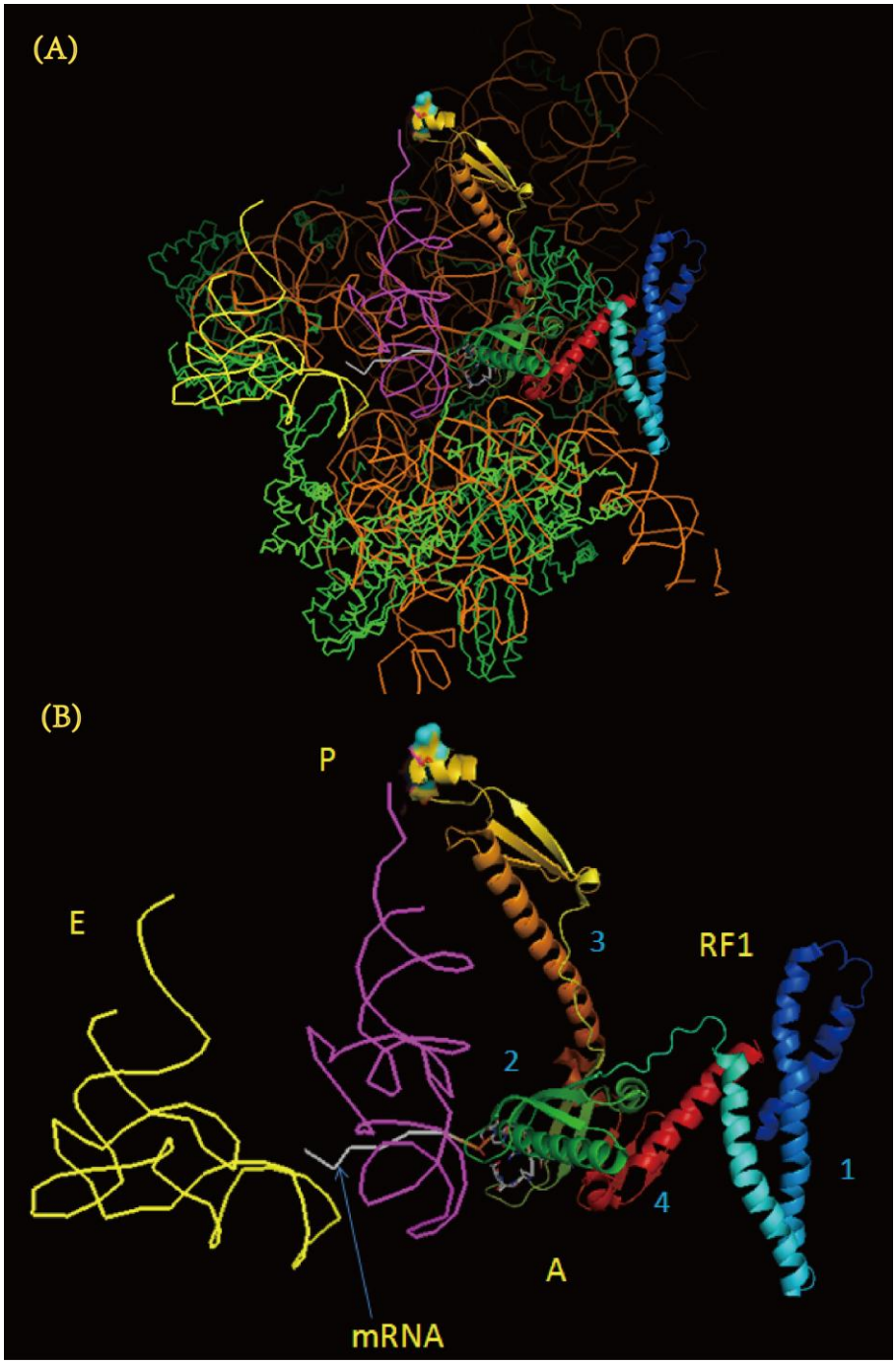

Figure 1.2: Structure of *T.Thermophilus* translation termination complex with RF1. (A) Structure of *T.Thermophilus* translation termination complex (PDB code 3D5C) (*13*) with RF1 protein in the A-site of ribosome. The location of the peptidyltransferase center in the large subunit 70S is highlighted by blue spheres indicating GGQ motif at the top of RF1 protein (shown by the ribbon representation and colored using rainbow color scheme). mRNA is grey, tRNAs are yellow and magenta. (B) The same figure as above but all ribosomal proteins and rRNA are removed from the view. Domains of RF1 are numbered.

1.1.3 Laying down structural foundations of ribosomal research

Ribosome's function is to assemble the 20 specific amino acid molecules to synthesize the particular protein molecule determined by mRNA sequence in cells. Ribosomes consist of RNAs and proteins called ribonucleoproteins and are divided into two subunits. The larger subunit binds to the tRNA and the amino acids while the smaller subunit binds to the mRNA. Ribosomes from bacteria and eukaryotes have different structures and RNA sequences. Prokaryotes have 70S ribosomes containing a small (30S) and a large (50S) subunit. Their small subunit has a 16S RNA subunit and 21 proteins. The large subunit contains a 5S RNA subunit, a 23S RNA subunit and 31 proteins. Differently, eukaryotes have 80S ribosomes containing a small (40S) and large (60S) subunit. Their 40S subunit has an 18S RNA (1900 nucleotides) and 33 proteins. The large subunit is composed of 5S RNA, 28S RNA, 5.8S RNA subunits and ~49 proteins.

The crystal structures of the 50S subunit from the archaeon *Haloarcula marismortui* (*14*) and the 30S subunit from *Thermus thermophilus* (*1, 15*) were published. Thus in 2009 the Nobel Prize in Chemistry was awarded to Venkatraman Ramakrishnan, Thomas A. Steitz and Ada E. Yonath for ribosomal structural studies. They independently solved high resolution 3D structures using X-Ray analysis revealing how different antibiotics attack bacterial ribosomes, thus laying down structural mechanisms of the

ribosome functions. Some antibiotics inhibit the monitoring mechanism of the molecular ruler; some hinder the formation of the connection between amino acids; others block the tunnel through which the nascent peptide chain leaves the ribosome. The discovery of the exact mechanism by which antibiotics bind to the ribosome stimulated scientists to develop new and more efficient drugs which are expected to save more human lives in the future.

1.2 Prokaryotic class-I release factor

In bacteriaRF1 and RF2 share high sequence similarity with RF1 recognizing UAA ("ochre") and UAG ("amber"), while RF2 recognizing UAA ("ochre") and UGA ("opal"), respectively. As two crystal structures were published: the crystal structure of EF-G:GDP (*16*) and the ternary complex EF-Tu:GTP:aa-tRNA (*17*), it was proposed that class-I RFs are an example of macromolecular mimicry (*18*). Later the crystal structure of Ribosome recycling factor (RRF) (*19*) showed RRF had high mimicry with tRNA as well. We can make a hypothesis that this mimicry might have evolved due to the specific structural constraints imposed by the extended ribosomal scaffold and not due to interactions with molecules outside the ribosome.

In class-I RFs, a tripeptide motif (PxT in RF1 and SPF in RF2) (*20*) confers stop-codon specificity. Recent crystal structures of the four

functional ribosome complexes (*13, 21-23*) which contain the class-I RFs and the three stop-codons have uncovered the molecular mechanisms by which RF1 and RF2 recognize UAA, UAG and UAA, UGA respectively. The fidelity of stop-codon recognition by RFs has been estimated to be 1 x 10^{-3} to 1 x 10^{-6} (*24, 25*). Although the correct discrimination of the cognate versus near-cognate tRNAs in A-site involves a subtle kinetic proofreading mechanism including Mg^{2+} ions and a number of ribosomal proteins (*15*), accurate recognition of stop-codons achieved by RFs is apparently without the help of a proofreading mechanism and is essential to prevent premature termination.

1.2.1 Conformation of class-I release factor upon recognizing stop-codon

The recent crystal structures suggest that class-I release factors bind to the A site on the 70S ribosome (*13, 21-23*). Compared the overall conformation of the ribosome in translation termination complexes with that of a 70S complex in which the A site is vacant (*26*), no large-scale conformational changes on the ribosome were induced by the binding of class-I release factors. As the 70S structures bound with RF1 in the presence and in the absence of E-site tRNA (*13, 23*) are similar, occupancy of the ribosomal E site does not affect the hydrolysis of peptidyl-tRNA mediated by release factors. The RF1- and RF2-bound termination

complexes (Figure 1.2) have similar structures, but quite different from those of the isolated class-I release factors. Class-I release factors have four domains (Figure 1.2B). Domain 1 (residues 1-116) is bound in the vicinity of the ribosomal GTPase-associated center. In the RF1-bound structures domain I does not interact with L11 stalk (*13, 23*); however, in the RF2-bound structures of the 70S termination complexes (*21, 27*), domain 1 interacts with the L11 stalk. Domains 2 and 4 are closely connected and form a compact superdomain (Figure 1.2) by multiple polar and nonpolar interactions. They have the functionally important PxT motif and SPF motif involved in stop-codon recognition. Domain 3 extends between the 30S and 50S ribosomal subunit; helix α7 of domain 3 (Figure 1.3) bridges the decoding head of the release factor with the universally conserved GGQ motif which is exposed in the loop on this face.

Upon binding to 70S ribosome, the switch loop's confirmation is changed. Thus, the rearrangement of the switch loop results in reorientation and extension of α7.

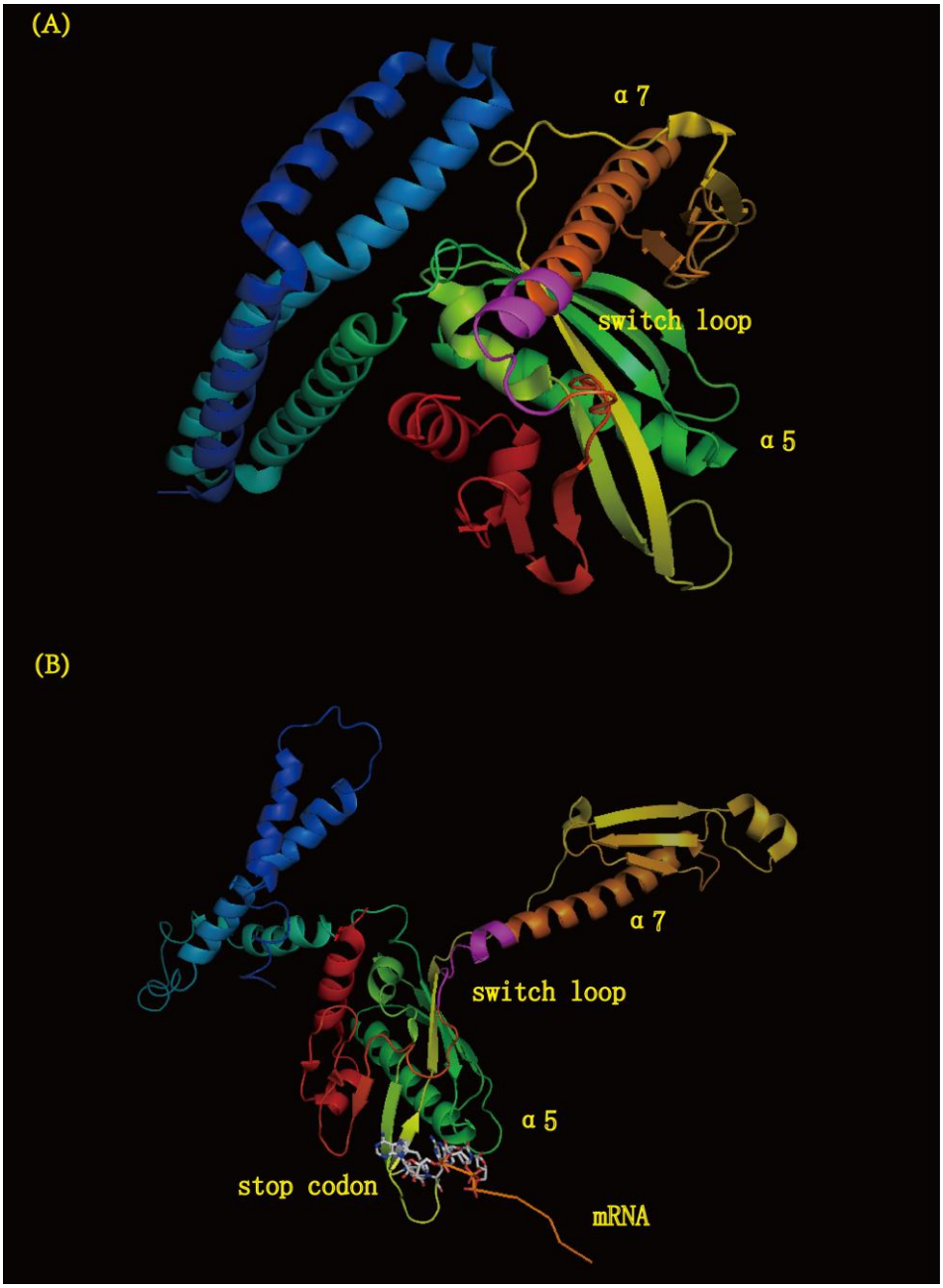

Figure 1.3: Comparison of structures of isolated RF2 and RF2 in translation termination complex. (A) Crystal structure of isolated RF2 (PDB code 1GQE) (*28*). RF2 is shown in ribbon representation. Switch loop is highlighted in magenta. (B) Crystal structure of RF2 in translation termination complex (PDB code 2WH1) (*21*). The ribosome and tRNA are not shown; RF2 is shown in ribbon representation; switch loop is magenta the mRNA is brown; the stop-codon is shown in the sticks representation.

1.2.2 Specificity at the first position of the stop-codon

Cytidine (C), uridine (U), adenosine (A) and guanosine (G) are the four possible nucleotides in mRNA, but only uridine, adenosine and guanosine are used in stop-codons (UAA, UAG, UGA). U is found only in the first position, whereas A and G can be either in the second or in the third position of the stop-codon. Thus the nucleotides of a stop-codon will be referred to as U1, A2 or G2, and A3, or G3. In the 70S-RF1 UAA complex, UAA is bound in a pocket formed by conserved elements of 16S rRNA and domain 2 of RF1, which contains the proposed PxT tripeptide anticodon motif. The specific recognition of the stop-codons relies on specific hydrogen bond patterns between N-terminal tips of helix α5 and U1 of stop-codons (Figure 1.4 & Figure 1.5). At the tip of helixα5 of RF1 two glycines (G116 of RF1 and G138 of RF2) pack against U1 of the stop-codon and thus discriminate sterically against the larger A and G. Three H-bonds formed between U1 and RF1: 4-keto moiety of U1 formed H-bonds with the backbone of E119 and the hydroxyl moiety of T186 (PxT motif in RF1); 3-amino moiety of U1 formed H-bond with backbone of G116 (Figure 1.4). Thus, a small nucleotide pocket and a precise H-bond pattern select for the canonical U in the first position of all three stop-codons (UAA, UAG and UGA). These H-bonds can explain why discrimination is strongest for the first base of the stop-codon (*24*). Similarly, RF2 utilizes H-bonds to specify

the selection of U in the first position: 4-keto moiety of U1 formed H-bond with the backbone of E119; 3-amino moiety of U1 formed H-bond with backbone of G116 (Figure 1.5). However, as the SPF serine residue is oriented towards the second base, there is no H-bond between 4-keto moiety of U1 and any of the SPF residues in RF2.

1.2.3 Selectivity at the second position of the stop-codon

The specificity of class-I release factors for the second nucleotide was defined by conserved amino acids of the PxT and SPF motifs of RF1 and RF2, respectively. In RF1, release factor specificity relies on the side chains of T186 of the PxT motif. In the 70S–RF1 UAA complex, A2 is sandwiched between U1 and H193 (Figure 1.4**)**, and packs against the side chains of P184 (PxT motif) and E119. Not only is an H-bond formed between hydroxyl group of T186 and the 4-keto moiety of U1, but also one H-bond is formed between hydroxyl group of T186 and 6-amino group of A2. Thus, the PxT motif of RF1 interacts with the first two stop-codon bases. These H-bonds define the specificity of RF1 for A2 at the second position.

Unlike RF1, RF2 specificity relies on the side chain of S206 of the SPF motif. The side chain of S206 of RF2 formed H-bond with the Watson-Crick face of either A or G at the second position of a stop-codon (Figure 1.5). S206 of RF2 adapts equally well with a 180° rotation of the side chain to

either the 6-amino moiety and the N1 atom of an A, or the 1-amino group of a G in this position (*21, 23, 27*). Therefore, this makes the versatility of RF2 to recognize either A or G in the second position (UAA and UGA).

However, it seems that T186 of the PxT motif and S206 of the SPF motif solely cannot determine the release factors specificity toward the second nucleotide. Substituting the PxT motif of RF1 with the SPF motif of RF2have structural clashes with the rest of the protein, thus it fails to modify RF1 specificity but instead renders RF1 inactive with any of the stop-codons (*29*). In contrast, substitution of the whole 13-residue recognition loop of RF1 with that from RF2 rendered RF1 active in response to either A or G the second position of a stop-codon. Therefore not only the PxT and SPF motifs but also other elements of the recognition loop define stop-codon specificity in this region.

Table 1.1: H-bond list of stop-codon and RF1/2

RF1	4-keto moiety of U1 formed H-bonds with the backbone of E119 and the hydroxyl moiety of T186 3-amino moiety of U1 formed H-bond with backbone of G116
	6-amino group of A2 formed H-bonds with hydroxyl group of T186
	N7 of the purine ring of A3 or G3 formed H-bond with side-chain hydroxyl group of T194 N6-amino group of A3 or the O6-keto group of G3 formed H-bond with side-chain amide group of the Q181
RF2	4-keto moiety of U1 formed H-bond with the backbone of E119 3-amino moiety of U1 formed H-bond with backbone of G11
	A2 or G2 formed H-bonds with the side chain of S206
	N6 amino group of A3 formed H-bond with side-chain hydroxyl group of T216

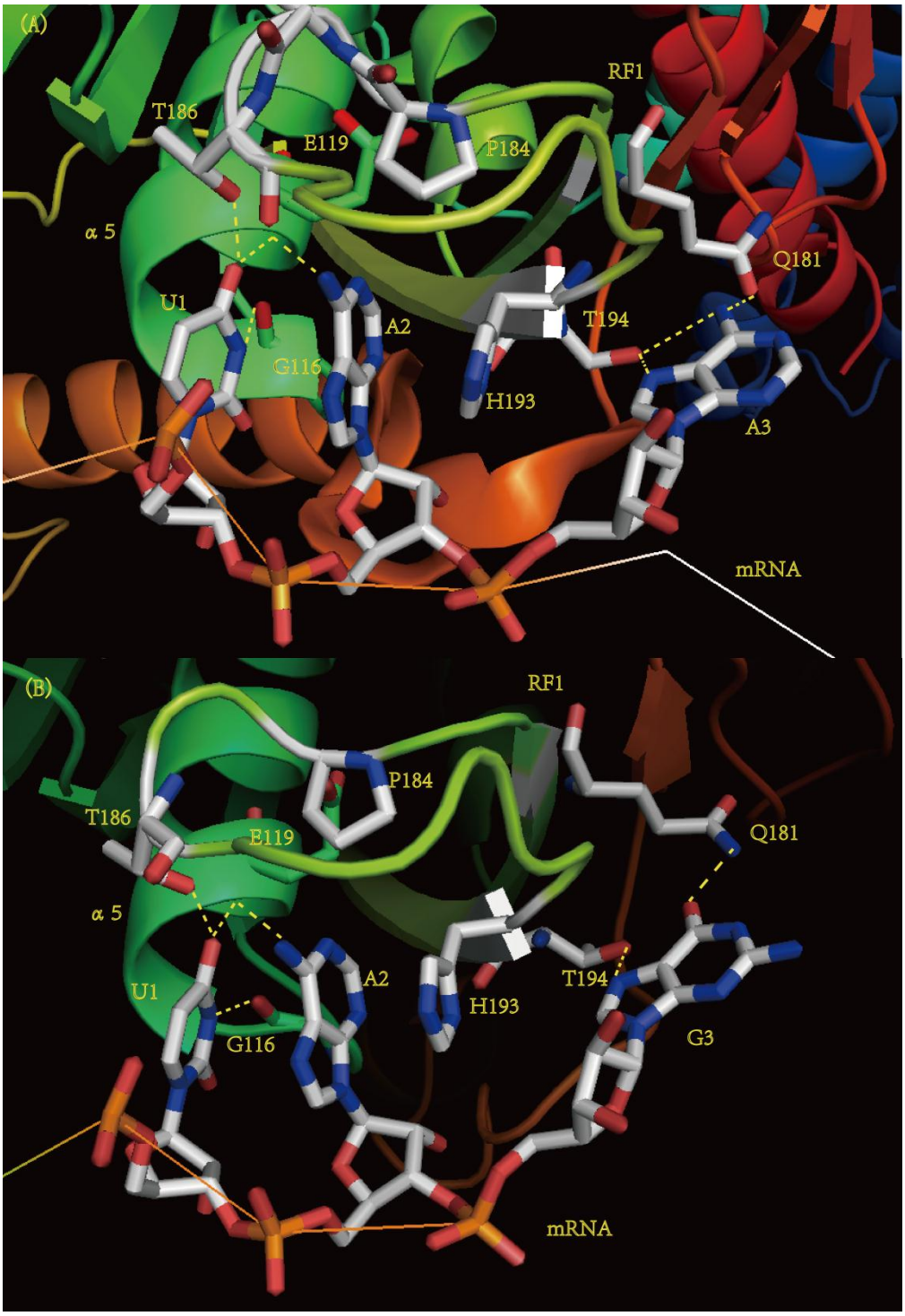

Figure 1.4: Specificity of RF1 with the first, second, third positions of the stop-codon. (A) Recognition of the stop-codon UAA by RF1 (PDB code 3D5C) (*13*). mRNA is orange; the stop-codon is shown by the sticks representation; RF1 is shown by the ribbon representation; H-bonds are shown by dashed lines. (B) Recognition of the stop-codon UAG by RF1 (PDB code 3MR8) (*23*). mRNA is orange; the stop-codon is shown in the sticks representation; RF1is shown by the ribbon representation; H-bonds were shown by dashed lines.

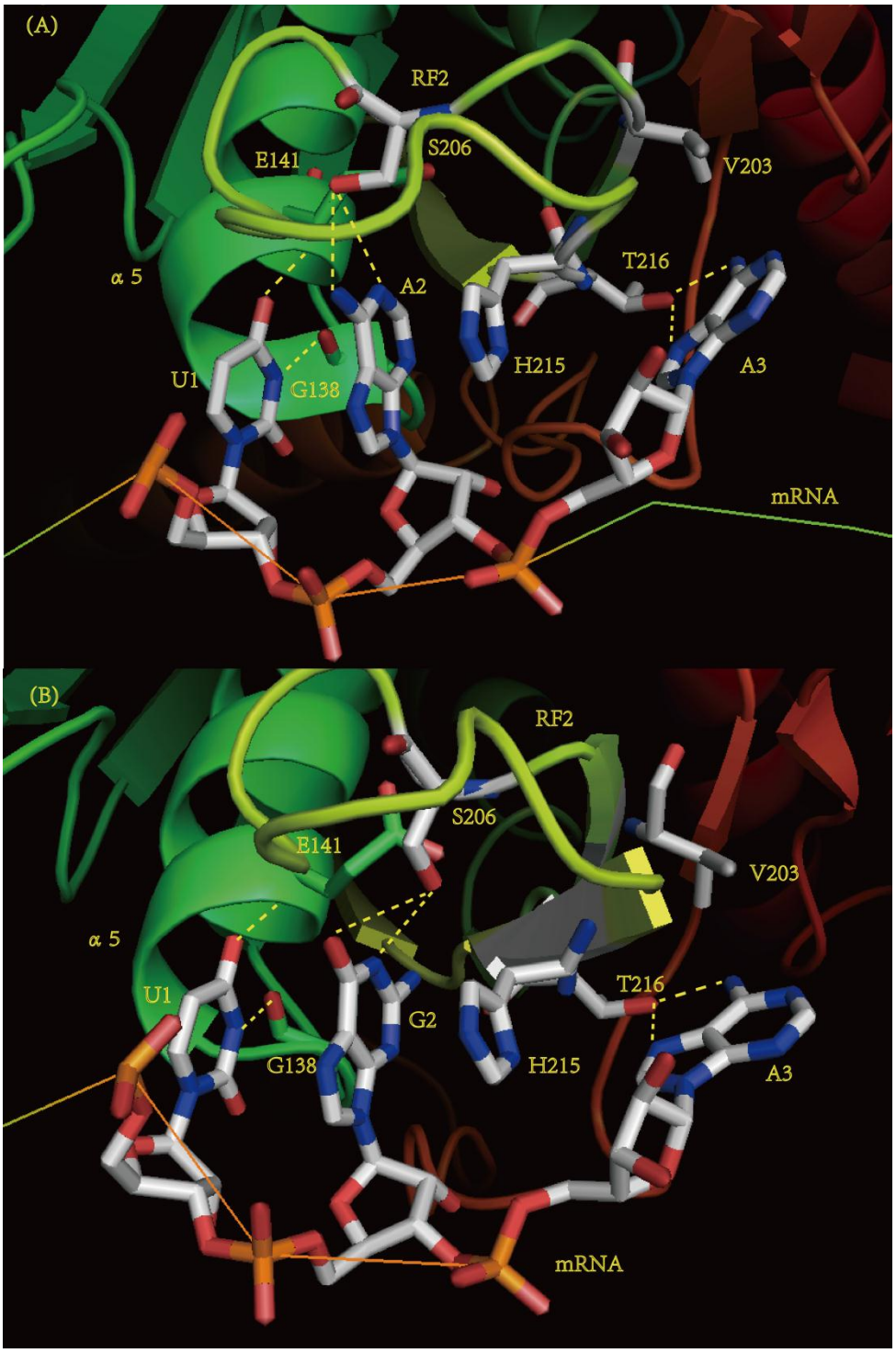

Figure 1.5: Specificity of RF2 with the first, second, third positions of the stop-codon. (A) Recognition of the stop-codon UAA by RF2 (PDB code 3F1G) (*27*). mRNA is orange; the stop-codon is shown by the sticks representation; RF2 is shown by the ribbon representation; H-bonds are shown by dashed lines. (B) Recognition of the stop-codon UGA by RF2 (PDB code 2WH1) (*21*). mRNA is orange; the stop-codon is shown by the sticks representation; RF2 is shown by the ribbon representation; H-bonds are shown by dashed lines.

1.2.4 Conformational changes and specific interaction at the 3rd position of the stop-codon

The N- and C-terminal ends of the recognition loop define the specificity for the third nucleotide located in the G530 pocket. A conserved histidine (H193 in RF1; H215 in RF2) stacks to the second base (Figure 1.4 & Figure 1.5) and makes a loop just after the PxT or SPF motif of RF1 or RF2. The side chain of the histidine inserts into between positions 2 and 3 and the third nucleotide of the stop-codon flips to another direction, thus the recognition of the third nucleotide by both RF1 and RF2 occur separately from the first two nucleotides. Mutation of this conserved histidine could affect the conformational change of complex and peptidyl-tRNA hydrolysis (*30*). A3 (or G3 in UAG) then stacks on G530 of 16S rRNA. The side-chain hydroxyl group of the universally conserved threonine (T194 in RF1 and T216 in RF2) forms H-bonds with N7 of the purine ring of A3 or G3 and N6 amino group of A3 (Figure 1.4 & Figure 1.5). At the N-terminal end of the recognition loop another conserved residue Q181 forms H-bonds with the 6-position of the third codon base. Comparing the two structures of RF1 bound to 70S ribosome (*13, 23*), it is revealed that RF1 can form an H-bond with the N6-amino group of adenine or the O6-keto group of guanine by rotating the side-chain amide group of the Q181, thus explaining how RF1 recognizes either A or G in the third position (Figure 1.4).

In RF2, which specifically recognizes A3, no residue equivalent to Q181 is found, instead a hydrophobic residue (V203 in *T. thermophilus* RF2) is in the place of Q181 (Figure 1.5). The position of the hydrophobic side chain would prevent H-bonding of the O6 of G2to water. As a result of a free-energy penalty due to desolvation of guanine whose dipole moment is significantly larger than that of adenine (*31*), discrimination against guanine in the third position could be achieved (*27*).

The crystal structures reveal that the tripeptides PxT and SPF are only partially responsible for specific codon recognition. Similarly in RF1 and RF2 the proline residue of the motifs primarily serves to create the proper conformation of the peptide loop despite significant differences in the amino acid sequence. Some other residues like the hydrophobic residues of the motifs (Ala, Val or Phe) which are involved in non-specific van der Waals contacts are also likely involved in conferring specificity. In another study, the two bases following the stop-codon which interact with RF1 and RF2 also influence the efficiency of translational termination(*32*).

1.2.5 Hydrolysis of the pepetidyl-tRNA bond in the PTC

The peptidyl-tRNA is protected from hydrolysis in a compact pocket of the peptidyltransferase center in protein synthesis (*33*). When RF1 or RF2 recognizes a stop-codon, the ester bond connecting the peptidyl moiety with

the terminal nucleotide A76 of peptidyl-tRNA is hydrolyzed. The universally conserved GGQ motif of class-I RFs is located in domain 3 following a short helical segment, and is involved in the catalysis of the hydrolysis reaction (*34-36*). The recent crystal structures (*13, 21-23, 27*) suggest the possible mechanism of peptidyl-tRNA ester bond hydrolysis.

The two glycines of the motif make a distinct backbone conformation which stacks the motif into the PTC next to A76 of tRNA. Mutation study shows that substitution of either glycine would move the peptide backbone away from the rRNA as a result of collisions of the Ala methyl group with G2583 and U2506 (*36*).

The side chain of Gln230points away from the scissile ester bond, in a pocket formed by PTC residues A2451, C2452, U2506 (23S rRNA) and their base moiety of A76. It is consistent with the mutational studies that substitution of the side chain glutamine has only a modest effect on catalysis (*35, 37-39*), whereas substitutions of the glycines have a more drastic effect (*35, 38, 40*). Possibly, the Gln230 side chain make contribution indirectly to catalysis through the coordination of a water molecule that can nucleophilically attack the peptidyl-tRNA carbonyl group (*35*), which is consistent with molecular dynamics simulations (*41*). As U2585 moves away from the peptidyl-tRNA bond in the presence of RF1, RF2 or a tRNA in the A site, the water molecule might gain access to the

active site thus deprotecting the carbonyl group for a nucleophilic substitution. Based on mutational data, A2602 is proposed to participate in catalysis (*42*). And A2602 is stacked in a cavity of the RFs, positioning the GGQ loop within a functional conformation into the PTC (*21*). The post-translational N-methylation of the Gln230 side chain increases termination efficiency (*39*), probably because the additional methyl group can fill the hydrophobic portion of the glutamine binding site (*41*).

Unlike the side chain of glutamine, the main chain amide group forms an H-bond with the 3'-hydroxyl group of A76 of the P-site tRNA, which is the leaving group of the hydrolysis reaction. This interaction is likely to stabilize the transition-state tetrahedral intermediate and the deacylated tRNA product. Mutation studies also reveal that replacing the conserved glutamine of with proline abolishes the affect catalytic activity. Possibly this mutation changed the backbone conformation and lost the H-bonding capability with the main chain amide group (*27*). The 2'-hydroxyl group of A76 of peptidyl-tRNA was suggested to be crucial for the peptidyl-tRNA hydrolysis reaction (*43, 44*). In another study, the complex structure which contains a substrate analogue Phe-NH-tRNA^{Phe} reveals that the water molecule possibly is coordinated by the critical 2'-hydroxyl group of A76 of the tRNA, A2451 of 23S rRNA, the main chain of the conserved glutamine (*22*). Taken together, both the main chain, and to some extent, the side

chain amide group of Gln230 are involved in the hydrolysis mechanism, but they are involved indifferent parts of the process.

1.2.6 Cooperativity between stop-codon recognition and peptidyl-tRNA hydrolysis

One crucial question is how the hydrolysis of peptidyl-tRNAin PTC is strictly coordinated with stop-codon recognition in the decoding site? Compared with the crystal structures of the isolated RFs (*28, 45*), the switch loop connecting domains 3 and 4 has a structural change which adopts a helical structure that extends helixα7 when bound to the ribosome (Figure 1.3). The SAXS structures show that class-I release factor has ‘‘compact’’ and ‘‘open’’ conformations in solution, which possibly correspond to those adopted upon crystallization in the free and ribosome-bound states, respectively (*46, 47*). The conformational change induces the docking of the GGQ motif into the PTC. The switch loop interacts with A1492, A1493 of helix 44 of 16S rRNA and A1913 of helix 69 of 23S rRNA and is positioned near ribosomal protein S12. Thus the switch loop possibly plays an important role in coordinating peptidyl-tRNA cleavage with stop-codon recognition.

Recent studies reveal that the switch loop and the connecting helix α7 play an important role in the cooperative coordination of stop-codon

recognition and peptidyl-tRNA hydrolysis. By using hydroxyl-radical probing, it is revealed that there are codon-dependent interactions between the switch loop and the ribosome (*48*). Mutational study shows that the interaction between the switch loop of RF1 and helix69 of 23S rRNA is involved in positioning the GGQ-bearing domain 3 in the active center, but are not directly involved in stop-codon recognition or peptidyl-tRNA hydrolysis (*23*). Kinetic assay shows that RF1 associates with ribosome in a similar association rate no matter a stop-codon or sense codon is present in the A site. However, dissociation of RF1 from stop-codons is as much as three orders of magnitude slower than from sense codons. These dramatic differences suggest that upon stop-codon recognition, class-I release factor undergoes conformation rearrangements resulting in an increased affinity of RF binding to the ribosome (*49*).

1.2.7 Prokaryotic class-II release factor (RF3)

RF3 is involved in the dissociation of the class-I RFs (*50-52*), whereas RRF and EF-G are involved in the dissociation and recycling of the ribosomal subunits. However, *in vitro* RF3 are not required in vitro for the peptide release reaction itself (*10, 11, 53*).

RF3 is a ribosomal GTPase, and binds to the 70S ribosome in complex with RF1 or RF2 in the GDP-state. GTP binds to RF3 and induces an RF3

conformation with high affinity for ribosome, thus leading to rapid dissociation of class-I release factor (*54*). Recently, there is no high-resolution structure of 70S–RF3 complex, but two cryo-EM structures of the E. coli ribosomal complex with RF3 (*55, 56*) could provide some initial insights. By cryo-electron microscopy it is revealed that the 70S–RF3 complex can adopt two different conformational states. In one state, RF3 is pre-bound to the ribosome, whereas in the other state RF3 contacts the ribosome GTPase center. Simultaneously, RF3 is changed from open conformation to a closed conformation, corresponding to rotational movement between the ribosomal subunits. And the tRNA molecule moves from the P site to the E site. Upon GDP-GTP exchange a hinge movement of RF3 of its GTPase domain could induce the release of the RF1/RF2.In the 30S subunit, RF3 binds to the region of helix 5 of 16S rRNA and ribosomal protein S12, which is a conserved binding site for several protein factors (*57, 58*). In the 50S subunit, as expected, the GTPase domain of RF3 interacts with the α-sarcin-ricin loop and protein L6 (*56*).

1.3 Eukaryotic class-I release factor (eRF1)

Eukaryotic and archaeal class-I release factors, eRF1 and aRF1, are both omnipotent and share high sequence similarity with each other but do not possess any obvious sequence homology with their bacterial counterparts

(*50*).

Structurally, Y-shaped eRF1 contains three distinct protein domains (Figure 1.6) (*7, 59, 60*) which perform different functions. N-domain recognizes the stop-codon at the decoding site of the 40S subunit. M-domain triggers hydrolysis of the peptidyl-tRNA ester bond in the peptidyltransferase center (PTC). M-domain contains a universally conserved GGQ motif which is located at the tip of the M-domain of eRF1 and is essential for peptidyl-tRNA hydrolysis. C-domain forms a complex interface with class-II release factor eRF3 (*61-64*).

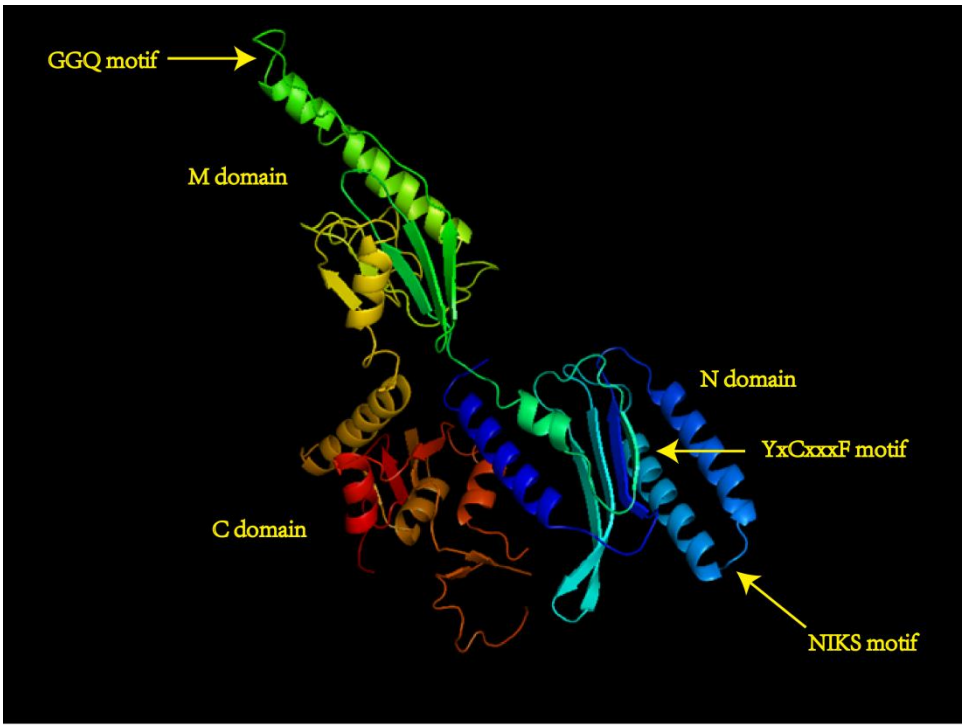

Figure 1.6: Crystal structure of eRF1 (PDB code 1DT9) (*7*). eRF1 is shown in the ribbon representation. NIKS, YxCxxxF and GGQ motifs are labeled.

1.3.1 Stop-codon recognition by eRF1

Despite availability of the crystal structure of isolated full-length eRF1 (*7*) and eukaryotic ribosome (*65, 66*), the mechanism of stop-codon recognition remains poorly understood. Over the last decade, various experimental approaches led to different models.

Among these models, the TASNIKS (*67, 68*) and YxCxxxF motifs (*69*) in N-domain of eRF1 were proposed to play a role in stop-codon recognition, forming the so-called non-linear model. In particular, experiments on photoactivatable cross-linking of a modified stop-codon to N-domain in a pre-termination complex pinpointed the NIKS motif as being positioned in proximity to the first U, and the YxCxxxF motif in proximity to the purines in the second and third stop-codon positions (*70, 71*).

Another model, known as the cavity model, was proposed based on a set of point mutations found to affect stop-codon readthrough in yeast. In this model, individual nucleotides of the stop-codon are accommodated into three defined cavities on the surface of N-domain (*72, 73*). Although both the non-linear and cavity models share some residues implicated in stop-codon recognition, they are not entirely compatible, thus requiring further experiments to resolve.

The recent structures of eRF1 in complex with eRF3 (*61*) showed that an ATP molecule as a crystallization additive is stacked in a pocket near the

anticipated site of stop-codon recognition. The adenine base of ATP interacts with some critical residues among whichE55, V71, Y125, and C127 were shown to be codon-specific by mutational studies (*69, 72, 74*). Thus it suggests that ATP binding to N-domain of eRF1 could mimic the interaction between the base and eRF1 decoding site. Thus it provides some insights to the mechanism of eRF1-stop-codon recognition.

1.3.2 Interaction between eRF1 andeRF3

The M-domain of eRF1 interacts with the peptidyltransferase center of the ribosome to trigger peptidyl-tRNA hydrolysis. Regardless of their origin and codon specificity, all class-I release factors share the universal conserved GGQ motif (*34*), which is required to trigger peptidyl-tRNA hydrolysis in eukaryotes. Mutations of either glycine residue in this motif were shown to abolish the RF activity of eRF1 both in vivo (*7, 38*) and in vitro (*34, 69*). It was proposed that Gln185 residue is in coordination with a water molecule and can mediate a nucleophilic attack on the ester bond of the peptidyl-tRNA in the P site. The C-domain of eRF1 has interaction with the C-terminus of class-II release factor eRF3 (*75*) and the binding of both factors is essential for fast kinetics of the translation termination (*76*). eRF3 contains a GTP-binding domain and eRF1's stimulation of eRF3's ribosome-dependent GTPase activity is codon independent(*77*). The

C-domain of eRF1 is not sufficient for stimulation of eRF3's GTP-binding and hydrolysis activities, and the M-domain of eRF1 is also required for both processes (*78*).

The exact mechanism by which eRF3 stimulates peptide release by eRF1 remains obscure. However, it is proposed that upon eRF3 binding, eRF1 undergoes a large conformational change to adopt a bent conformation (Figure 1.7). It reduced the distance between the GGQ motif and the decoding site to ~75 Å, and induced eRF1 to resemble a tRNA molecule. SAXS analysis showed that the eRF1-eRF3 complex adopts a conformation similar to that of the EF-Tu–GTP–tRNA complex (*17, 61*), which would likely result in increased affinity to the ribosome of eRF1in the eRF1/eRF3 complex compared with eRF1 alone.

Binding of the eRF1/eRF3/GTP complex to the ribosome would induce large conformational changes in a reconstituted in vitro system (*76*), which might be similar to that observed in the decoding center of the prokaryotic ribosome induced by RF1/RF2 binding (*13, 21, 27*), and consequently leading to optimal stop-codon recognition by eRF1. Upon GTP hydrolysis promoted by eRF1and the ribosome, the conformational changes in the switch regions of eRF3 would change the orientation of the M-domain of eRF1, thus GGQ motif is positioned optimally in the peptidyl-transferase center for peptide release.

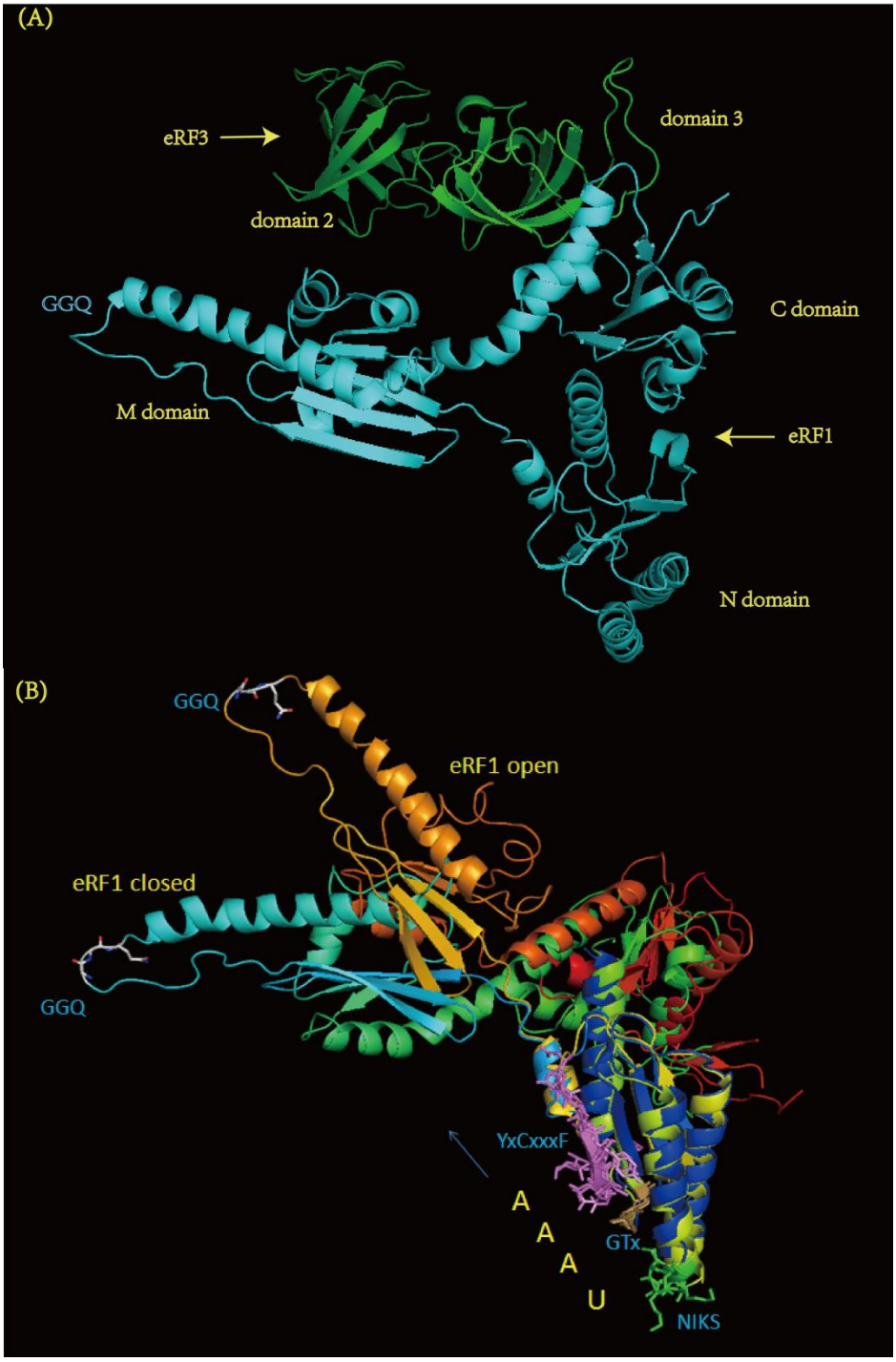

Figure 1.7: (A) Crystal structure of the eRF1 and eRF3 complex (PDB code 3E1Y) (*61*). eRF1 and eRF3 are shown in ribbon representation; eRF1 is colored with cyan; eRF3 is colored with green. (B) Comparison of the confirmations of isolated eRF1 (PDB code 1DT9) (*7*) and eRF1 in the complex with eRF3 (PDB code 3E1Y) (*61*). eRF1 is shown in ribbon representation; NIKS, YxCxxxF, GTx and GGQ motifs are shown in sticks representation; stop-codon (UAAA) are also labeled.

1.3.3 Translation termination is modulated by several ex-ribosomal proteins

Recently, several new players in translation termination have been identified (*79*). It reveals that reverse transcriptase of moloneymurine leukemia virus enhances suppression of termination and the binding of reverse transcriptase with eRF1 is required for an appropriate level of translational read-through (*80*). Using *Saccharomyces cerevisiae* as a model organism, the DEAD-box RNA helicase and mRNA export factor Dbp5, a member of the DEAD-box protein family, was discovered to play a role in translation termination (*81*). Dbp5 interacts with release factors and support eRF1 in stop-codon recognition, possibly because it can properly place the release factor on the stop-codon. Dbp5 shows genetic interactions with both termination factorseRF1 and eRF3. Upon its dissociation from eRF1, Dbp5 allows eRF3 to reach the complex. Moreover, Gle1 is Dbp5's interacting protein and inositol hexakisphosphate (IP_6) is Dbp5's co-factor. They are both involved in the translation termination process (*82*). Previously it was shown that Dbp5 and Gle1 play a role in mRNA export from the nucleus to the cytoplasm (*83*). Gle1 is uniquely positioned to coordinate the mRNA export and translation mechanisms. The iron-sulphur (Fe-S)-containing RNase L inhibitor (Rli1) has recently been shown to function in translation termination and recycling of the ribosomes (*84*). By

co-immunoprecipitation experiments, it is revealed that Rli1 interacts physically with eRF1 andeRF3 in *S.cerevisiae*. Also Rli1 was found genetic interaction with both eRF1 and eRF3. Taken together, all these novel termination factors in association with the release factors regulate more accurate stop-codon recognition.

1.4 Comparison of eukaryotic and prokaryotic release factor

1.4.1 Class-I release factors

eRF1 is the only eukaryotic factor involved in stop-codon recognition, and it recognizes all three stop-codons (*85*). RF1/2 and eRF1 have different structures (*7, 28, 45*), but the functionally relevant parts have a similar global configuration. eRF1 in the eRF1–eRF3 complex (*61*) have a more bent conformation than in the isolated state (*7*). Cryo-EM structure (*86*) and molecular dynamics simulations (*87*) show that RF1 or RF2 and eRF1 probably have overall similar conformations and positions on their respective prokaryotic and eukaryotic ribosome. N-domain of eRF1 functions in stop-codon recognition, corresponding to domains 2/4of RF1/RF2. However, the mechanism of stop-codon recognition is quite different, which is consistent with their different specificities. In eRF1, TASNIKS (*67, 68*) and YxCxxxF motifs (*69*) play a key role in stop-codon recognition, while PxT and SPF motif confer stop-codon specificity in RF1

and RF2, respectively (*20*). Both M-domain of eRF1 and domain 3 of RF1/RF2 which have conserved GGQ motif function in peptidyl-tRNA hydrolysis, and they have similar conformation (*86*), as both consist of a long helix.

1.4.2 Class-II release factors

The eukaryotic class-I eRF1 and class-II eRF3 form a complex in solution through their C-terminal domains (Figure 1.7) (*60, 62, 64*) and through M-domain of eRF1 (*78*).

The C-domain of eRF1possibly corresponds functionally to domain 1 of RF1/2. And RF1/2 interacts with the class-II RF3 factor (*38*) probably through domain 3 (*55, 56*) (Figure 1.7). The crystal structure of the eRF1–eRF3 complex suggests that M-domain of eRF1 interacts with the switch regions of eRF3 which are disordered in the isolated eRF3 (*75*). eRF1 binding to eRF3 increases the affinity of eRF3 for GTP and thereby promotes ribosome binding in the GTP form (*88, 89*). eRF3 shares little sequence similarity with prokaryotic class-II RFs except the conserved GTPase domain. eRF3 promotes eRF1-mediated peptide release in a GTP-hydrolysis-dependent manner rather than inducing class-I RF dissociation (*76, 90, 91*).

1.4.3 Hotspots involved in stop-codon recognition

Despite the exact mechanism by which eRF1 N-domain recognizes the stop-codons is not very clear, some hotspots of eRF1 N-domain are identified to play a role in stop-codon recognition. TASNIKS (*67, 68*) and YxCxxxF motifs (*69*) in N-domain of eRF1 were proposed to play a role in stop-codon recognition.

Besides these motifs, other residues are also involved in stop-codon recognition. GTS loop (G31, T32 and S33) of eRF1 had been previously suggested to be involved in stop-codon recognition on the basis of various indirect and direct data (*72, 92*). By performing a series of computational analyses to evaluate the conservation, accessibility, and structural environment of each amino acid located in N-domain, eight specific amino acid sites (G31, T32, G57,I62, K63, S70, L126 and C127) are found important for stop-codon recognition (*92*). The recent data on cross-linking of mRNA analogs to eRF1 reveals that region 121–131 (including the YxCxxxF motif), the GTS loop and V66 (in the region of the NIKS motif) are involved in stop-codon recognition (*71*).

Some ciliate species use alternative genetic codes, and one known change is the reassignment of stop-codons to sense codons. In *Euplotes,* UAA and UAG are still stop-codons but UGA is reassigned as a sense codon. By designing chimeric eRF1s, region 70-80 of eRF1 is supposed to

be responsible for UAR-only specificity and S70 in eRF1 plays a key role in changing stop-codon specificity (*93*). However, in *Stylonychia* and *Paramecium*, UGA is used as the only stop-codon, whereas UAA and UAG are translated to glutamine (*94*). The eRF1 factors from ciliates might provide some insights into the very basic principles of decoding of genetic information (*95, 96*). Substitutions of some amino acids located in the conserved region induced the UGA-only response. With introducing the St-eRF1 pentapeptide QFMYF (positions 122–126) UAA and UAG responses are eliminated in Hs-eRF1. This *Stylonychia* sequence in the context of human N-terminal domain converts the omnipotent eRF1 into a unipotent one. Thus the four-site mutant $Q^{122}FM(Y)F^{126}$ (T122Q +S123F +L124F +L126F) of N-domain of human eRF1 responds only to UGA. M124 and F126 strongly affect the QF discrimination ability depending on the sequence context (*97*).

In summary, various studies have identified many hot spots which play a role in stop-codon recognition (Figure 1.8). However, understanding of how the structure affects selectivity of stop-codon recognition is still unknown. Thus, we attempted to solve the structures of wild type N-domain and some mutants that only decode one or two of the stop-codons. These structures are aimed to expand our understanding of the mechanism of stop-codon recognition and potentially provide novel targets for anti-cancer drug

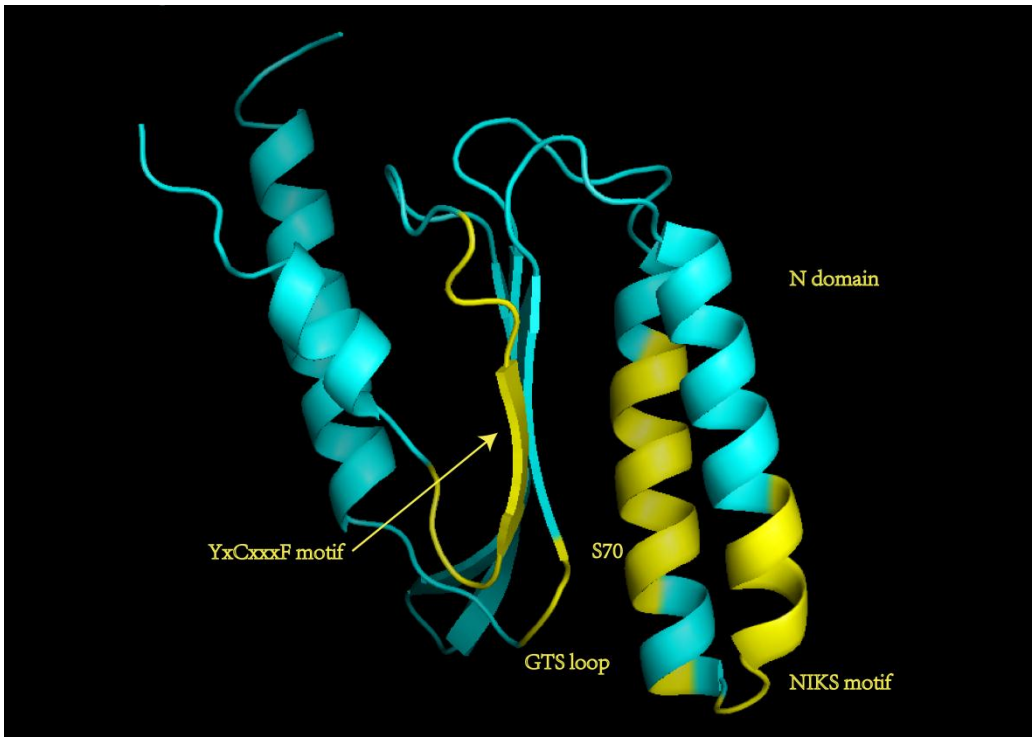

Figure 1.8: Hotspots of eRF1 N-domain which are involved in stop-codon recognition.

development. The latter is due to the fact that many genetic disorders are caused by mutations which introduce premature termination codons causing premature termination of translation of an mRNA template resulting in the production of truncated, non-functional proteins. The overall result of these cellular responses is a severe down regulation in the expression of specific proteins, some of which may be essential to the viability of the cell and/or the organism. Thus, intervention with the stalling of ribosome at the nonsense codons may provide promising therapeutic venue. This intervention might be based on the structures of eRF1 and its mutants along or in pre-termination complex with ribosome.

Chapter II Materials & Methods

2.1 Materials

DSS, $^{15}NH_4Cl$, $^{13}C_6$-glucose and L-phenylalanine (^{15}N, 98%) were from Cambridge Isotope laboratories; imidazole were from Sigma-Aldrich; MES, Glucose, $MgSO_4.7H_2O$, Thiamine, and PMSF were from AppliChem; $Na_2HPO_4.7H_2O$, KH_2PO_4 and NaCl were from Merck; all other chemicals were purchased from either Merck, Sigma-Aldrich or AppliChem. Protease inhibitor cocktail was from Roche; *Pf1* was purchased from Hyglos GmbH. pET23(+) vector was from Novagen. All of the synthesized RNA oligonucleotides were purchased from 1st BASE. HisTrap HP column, Superdex 75 prep grade column and Hitrap desalting column were from GE healthcare.

2.2 Buffers

Binding Buffer:

20 mM potassium phosphate buffer (pH 6.8)

100 mM KCl

25 mM imidazole

2 mM DTT

1 mM PMSF

Protease inhibitor cocktail

Elution Buffer:

20 mM potassium phosphate buffer (pH 6.8)

100 mM KCl

250 mM imidazole

2 mM DTT

1 mM PMSF

NMR Buffer:

20 mM MES buffer (pH 6.0)

100 mM KCl

0.1 mM DSS

2 mM DTT

96% H_2O/4% D_2O

2.3 Minimal medium

M9 salts are the minimal medium used for unlabeled and labeled growths of *E. coli* strains.

For 1L standard 5xM9 salts:

64 g $Na_2HPO_4.7H_2O$

15 g KH_2PO_4

2.5 g NaCl

5 g NH_4Cl

Dissolve the salts in double distilled water to a final volume of 1 L.

To prepare 1L M9 minimal medium:

200 mL of 5xM9 salts

2.0 g glucose

0.4940 g $MgSO_4.7H_2O$

0.0152 g $CaCl_2.2H_2O$

0.0100 g Thiamine

0.0100 g $FeSO_4.7H_2O$

After filtering each chemical into the medium, rinse the test tube with double distilled H_2O and filter the double distilled H_2O into the medium also. When finished, rinse the filter really well with ddH_2O and top up to 1 L.

2.4 eRF1 Mutagenesis

eRF1 N-domain mutants, namely $Q^{122}FM(Y)F^{126}$, Y125F, and E55Q were produced using QuikChange XL Site-Directed Mutagenesis Kit. The QuikChange XL system was used to make point mutations at T122Q+ S123F+L124M+L126F, Y125F, and E55Q.

2.5 Expression of protein samples

The DNA fragments encoding the wild-type, the $Q^{122}FM(Y)F^{126}$ mutant, Y125F mutant, and E55Q mutant of N-domain (residue 1-142) of human eRF1 with a C-terminal His tag (LEHHHHHH) were cloned into pET23(+)

vector under the phage T7 RNA polymerase promoter (*78, 98*) and were expressed in *Escherichia coli* Rosetta(DE3) host cells. Uniformly ^{13}C, ^{15}N-labeled wt N-domain, $Q^{122}FM(Y)F^{126}$ mutant, Y125F mutant and E55Q mutant were produced in minimal medium. The minimal medium contains 100 µg/ml ampicillin and 34 µg/ml chloramphenicol and is supplemented with extra 0.0456 g/L $CaCl_2$. The isotopically enriched protein were prepared using $^{15}NH_4Cl$ (1.0 g/L) and $^{13}C_6$-glucose (2.0 g/L) as the sole nitrogen and carbon sources. Competent Rosetta cells were used in the transformation process by electroporation. Expression was induced at an optical density (OD) of 0.6~0.8 with 0.2 mM IPTG at 37 ^{0}C, overnight. After 10 hours of additional growth, cells were then harvested by centrifugation at 8000 rpm, 4^{0}C for 20 minutes.

2.6 Purification of protein samples

The pellet from minimal medium was resuspended in Binding Buffer. The harvest culture was lysed by sonication (3s on, 3s off) at 4°C and the debris was spun down at 18000 rpm, 4°C for 30 minutes in a Beckman centrifuge.

The supernatant was applied to a HisTrap HP column using FPLC system (UNICORN), which was eluted with a 25–250 mM imidazole gradient using Elution Buffer. At last a buffer exchange was performed to remove the high amount of imidazole that is present in the protein sample by means of

gel-filtration chromatography on a Superdex 75 prep grade column or a series of Hitrap desalting column. The exchange buffer used were NMR Buffer at pH 6.0, the protein samples were then concentrated using Sartorius filter tubes with 10 kD cut-off (Sartorius Stedim) as the molecular weight of the protein is 17 kD. The concentration was measured with the NanoDrop ND-1000 spectrophotometer (NanoDrop Technologies), and the concentration of samples was about 0.5~1mM. Purity of the recombinant protein was confirmed by SDS-PAGE (15%, w/v). Based on the Mass spectrum, the molecular weight of uniformly ^{13}C, ^{15}N-labeled $Q^{122}FM(Y)F^{126}$ is 17.476 kD.

2.7 NMR spectroscopy

All NMR spectra were acquired using 600, or 700 MHz Bruker Avance II spectrometers. Chemical shifts were referenced to DSS directly for ^{1}H and indirectly for ^{13}C and ^{15}N spins. The raw data were processed using TopSpin 2.1 (www.bruker-biospin.com) and analyzed using the program CARA (www.nmr.ch). Linear prediction was used to improve spectral resolution in the indirect dimensions.

2.8 Backbone assignments

^{1}H, ^{15}N, and ^{13}C resonances of wt N-domain, $Q^{122}FM(Y)F^{126}$, Y125F, E55Q and NM-domain were assigned using 2D [^{1}H, ^{15}N]-TROSY (*99*), ^{1}H, ^{13}C-HSQC, 3D TROSY-HNCO,TROSY-HNCA and TROSY-HNCACB.

Reverse labeling of phenylalanine (*100*) and selective labeling of phenylalanine were used to resolve ambiguous phenylalanine assignments. Extra 100 mg/L unlabeled or ^{15}N-labeled phenylalanine was added to the medium just before induction to get specifically unlabeled or labeled sample. The dual amino acid-selective ^{13}C-^{15}N labeling technique (*101, 102*) were also employed to resolve ambiguous assignments in $Q^{122}FM(Y)F^{126}$. This technique utilizes protein samples in which the main chain carbonyl carbons of one amino acid type are labeled with ^{13}C and the amide nitrogens of another amino acid type are labeled with ^{15}N. The NMR signals of the amino acid residues that possess a $^{13}C\alpha$–^{15}N linkage can be extracted on the basis of the ^{13}C–^{15}N spin coupling.

2.9 Side-chain assignments

Side-chain ^{1}H and ^{13}C were assigned using iterative analysis of the 3D ^{15}N-NOESY-HSQC and ^{13}C-NOESY-HMQC spectra coupled with structure calculations. The ^{15}N-resolved NOESY spectra were collected in the phase-sensitive manner with mixing times of 200 ms.The^{13}C-resolved

NOESY spectra contain both aromatic and aliphatic carbons and hydrogens. The assignment process was facilitated by comparison with chemical shifts deposited in the Biological Magnetic Resonance Data Bank (www.bmrb.wisc.edu) for individual domains (*103-105*).

2.10 RDC measurements

Partial alignment of the proteins was induced by means of *Pseudomonas* Phage *Pf1,* Strained Polyacrylamide Gels or Otting Media. Approximately 10 mg/ml bacteriophage *Pf1* was sufficient to induce partial alignment of the protein. It takes approximately 2-3 days for complete sample preparation using strained Polyacrylamide Gels. 250 μl of gel solution would make sample volume height of approximately 20 mm. Sample concentration prior to diffusion into the gel was 0.6 mM. After diffusion, the concentration will drop to half its original amount, ~ 0.3 mM. The Otting media C8E5: Octanol is suitable for proteins, DNA and protein/DNA complex. A stock solution of C8E5 in NMR buffer was prepared to yield a final concentration of 30%. This was then diluted to 5% for the working protein sample. The correct weight of octanol was added, while vigorously shaking (vortex) it to achieve a final molar ratio of 0.85. The biphasic solution becomes transparent and opalescent upon formation of the Lα phases. The NMR sample consisted of 5 μl DSS, 10 μl D_2O, 105 μl protein (0.6 mM), 30 μl of C8E5:octanol

solution.

Residual dipolar couplings of wt N-domain and $Q^{122}FM(Y)F^{126}$ mutant were abstracted from the peak positions of 2D [^{1}H, ^{15}N]-TROSY and anti-TROSY cross-peaks in isotropic and anisotropic solvent conditions, respectively. The axiality and rhombicity of the alignment tensor were calculated using the program PALES (*106*).

2.11 ^{15}N relaxation experiments

The ^{15}N relaxation experiments for wt N-domain and $Q^{122}FM(Y)F^{126}$ were performed at 25°C on a 700 MHz Bruker Avance II spectrometer. Longitudinal relaxation time T_1 were measured with eight relaxation delays, 0.075, 0.15, 0.3, 0.375, 0.525, 0.675, 0.9375, 1.2 s. Transverse relaxation time T_2 were measured with eight relaxation delays, 12.5, 25, 50, 62.5, 87.5, 112.5, 156.25, and 200 ms. The spectra measuring ^{1}H–^{15}N NOE were acquired with a 2 s relaxation delay, followed by a 3 s period of proton saturation. In the absence of proton saturation, the spectra were recorded with a relaxation delay of 5 s. The exponential curve fitting and data analysis were carried out using the program Origin (Origin Lab).

2.12 Experimental restraints and NMR structure determination

NOE distance restraints for the calculated structures of wt N-domain and

$Q^{122}FM(Y)F^{126}$ mutant were obtained from ^{15}N-NOESY-HSQC and ^{13}C-NOESY-HMQC spectra, respectively. NOE distance restraints for the calculated structures of Y125F mutant and E55Q mutant were obtained from ^{15}N-NOESY-HSQC. Backbone dihedral angle restraints (φ and ψ) were derived from the backbone $^{13}C'$, $^{13}C_{\alpha}$, $^{13}C_{\beta}$, $^{1}H_{\alpha}$, $^{1}H_{\beta}$, $^{1}H^{N}$ chemical shift values using TALOS (*107*). Residual dipolar couplings which contain information regarding the orientation of the internuclear vector relative to the molecular susceptibility tensor were incorporated during the refinement process. Hydrogen bond restraints were obtained by identifying the slow exchange amide protons mainly in the regular secondary structures. Structure calculations were performed using the program CYANA 3.0 (*108, 109*) and visualized using the programs MOLMOL (*110*) and PyMOL (Delano Scientific). Quality of the final structures was assessed using the program PROCHECK-NMR (*111*).

Chapter III Results

3.1 Expression and Purification of mutants of eRF1 N-domain

3.1.1 Selection of N-domain mutants for NMR studies

In eukaryotes, the N-domain of polypeptide release factor eRF1 is involved in decoding all three stop-codons, UAA, UAG or UGA. In ciliates with variant codes, like *Stylonychia* and *Paramecium*, only one or two codons are conveying the stop of translation signal. Considering this kind of difference, mutants of eRF1 derived from systematic mutagenesis studies of N-domain motif swaps between ciliates and human eRF1 (*68, 69*) (Table 3.1) are selected and expressed, in an attempt to explore the mechanism by which the eRF1 recognizes the stop-codons.

Table 3.1: A list of selected eRF1 mutations localized in N-domain and the corresponding *in vitro* release factor activity of the full length eRF1 (*68, 69*). The release factor activity of the wild-type eRF1 was equal to 100%.

N-domain	UAA	UGA	UAG
$Q^{122}FM(Y)F^{126}$	0	90	0
C127A,N129A	5	62	0
E55Q	75	80	35
F131A	10	60	8
F131G	8	58	12
Y125F	100	100	34
N61S+S64D+N129P+K130Q	0	90	0
Stylonychiawt	0	90	0
Humanwt	100	100	100

The following mutant and wild-type constructs were expressed with sufficiently high yield enabling NMR structural studies:

A, $Q^{122}FM(Y)F^{126}$

B, wild-type N-domain

C, Y125F

D, E55Q

As the expression and purification processes for different mutants are quite similar, in the following sections the $Q^{122}FM(Y)F^{126}$ mutant is used as an example to detail the expression and purification procedures which are pertinent to all other mutants studied.

3.1.2 Small scale expression of the $Q^{122}FM(Y)F^{126}$ mutant

The *E.coli* culture was grown on the Luria-Bertani (LB) agar plates containing 100 μg/ml ampicillin and 34 μg/ml chloramphenicol. From the selected plates, two colonies were picked up and grown in two 15-ml tubes.

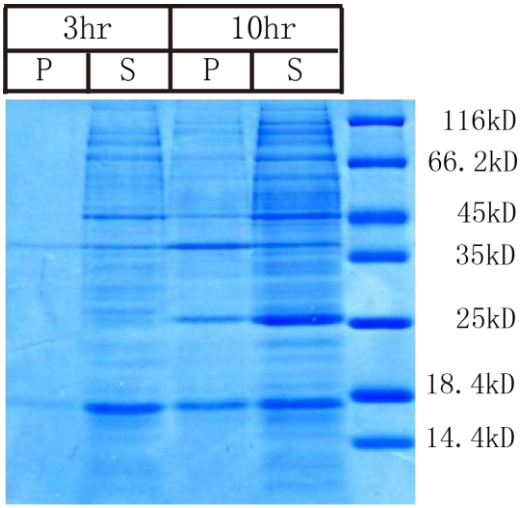

Figure 3.1.1: Small scale expression of $Q^{122}FM(Y)F^{126}$. Pellt (P) and supernatant (S) with different incubation time (3 hours and 10 hours) are show in the 15% SDS-PAGE gel.

The expression of the protein was tested at different incubation time periods. The aliquots of 0.2 to 1.0 mM of IPTG were added when the optical density at 600 nm (OD_{600}) reached 0.6~0.7 units and 10 ml culture**s** were harvested. Cells were sedimented down by centrifugation at 14000 rpm for 5 minutes. The cell pellet was resuspended and sonicated (1s on and 1s off). After that, supernatant and pellet were separated by centrifugation and the pellet was resolved in the same buffer. A sample from both supernatant and pellet were heated at 95°C for 5min and loaded to 15% SDS-PAGE (Figure 3.1.1). From the result, it is proposed that 0.2 mM IPTG and 10 hours incubation of the cells provide the optimal conditions for higher yields of the soluble protein.

3.1.3 Large scale expression of the $Q^{122}FM(Y)F^{126}$ mutant

The His-tagged $Q^{122}FM(Y)F^{126}$ mutant is expressed in *Escherichia coli Rosetta*(DE3) host cells. Uniformly ^{13}C,^{15}N -labeled protein is produced in 500ml of M9 salts minimum media containing 100 µg/ml ampicillin and 34 µg/ml chloramphenicol and is supplemented with extra 0.0456 g/L $CaCl_2$ at 37°C with $^{15}NH_4Cl$ (1.0 g/L) and ^{13}C 6-glucose (2.0 g/L) as the sole nitrogen and carbon sources. The protein expression was induced at OD_{600} equals 0.6~0.7 with 0.2mM IPTG. After 10 hours incubation cells were harvested by centrifugation at 8000 rpm for 20 mins.

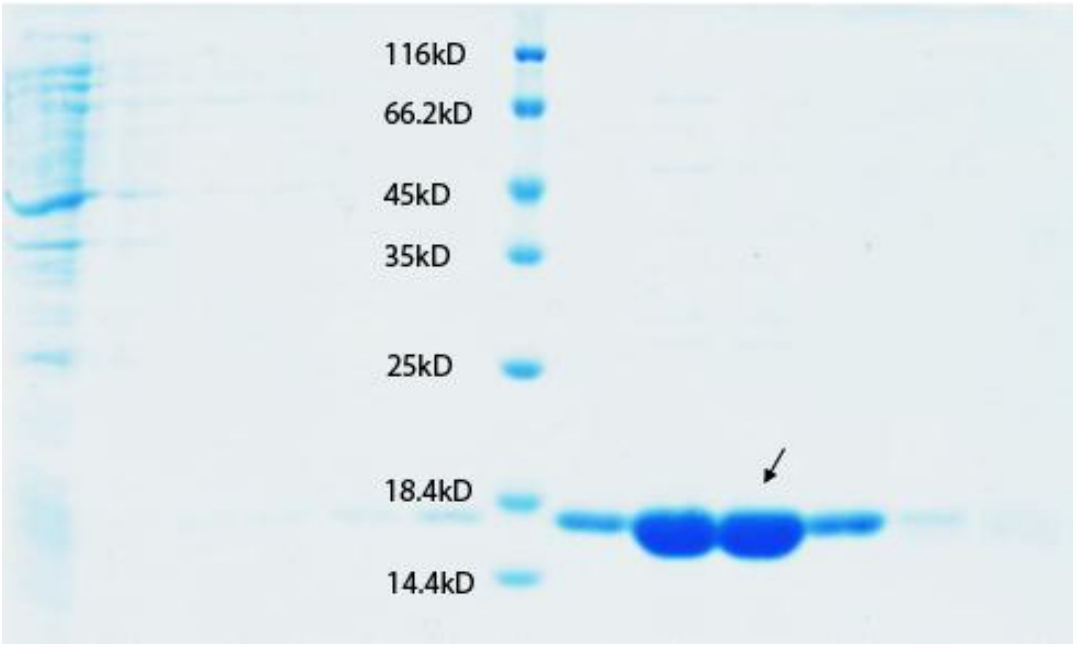

Figure 3.1.2: SDS-PAGE (15%) analysis of purified $Q^{122}FM(Y)F^{126}$ mutant. Arrow indicates the pure $Q^{122}FM(Y)F^{126}$ mutant protein.

3.1.4 Purification ofthe $Q^{122}FM(Y)F^{126}$ mutant

A cell pellet harvested from M9 media was resuspended in 20ml phosphate buffer. The harvested culture was lysed by sonication (3s on, 3s off) at 4°C in the Binding Buffer (pH 6.8). Cell lysate was then centrifuged at 18000 rpm for 30 min at 4°C.

The lysate was applied to a HisTrap HP column (GE Healthcare) and eluted with a 25–250 mM imidazole gradient (Figure 3.1.3). The protein is separated well from the cell supernatant in the first purification process. Buffer exchange was performed to remove the high amount of imidazole that is present in the protein sample. For this purpose either Superdex 75 prep grade column (GE Healthcare) or a series of HiTrap desalting column

were used. Depending on the protein load after the purification with HiTrap desalting column the samples were pure enough and enabling us to limit the final purification step to only the HiTrap desalting column resulting inconsiderable time saving. After this step, the phosphate buffer is exchanged to MES buffer (pH 6.0). The purified recombinant $Q^{122}FM(Y)F^{126}$ protein has a C-terminal His tag (LEHHHHHH). The concentration of ^{15}N-labeled and ^{13}C, ^{15}N-labeled $Q^{122}FM(Y)F^{126}$ was about 1 mM, and all the samples for NMR contained 20 mM MES buffer (pH 6.0), 100 mM KCl, 2mM DTT, in 96% H_2O/4% D_2O.

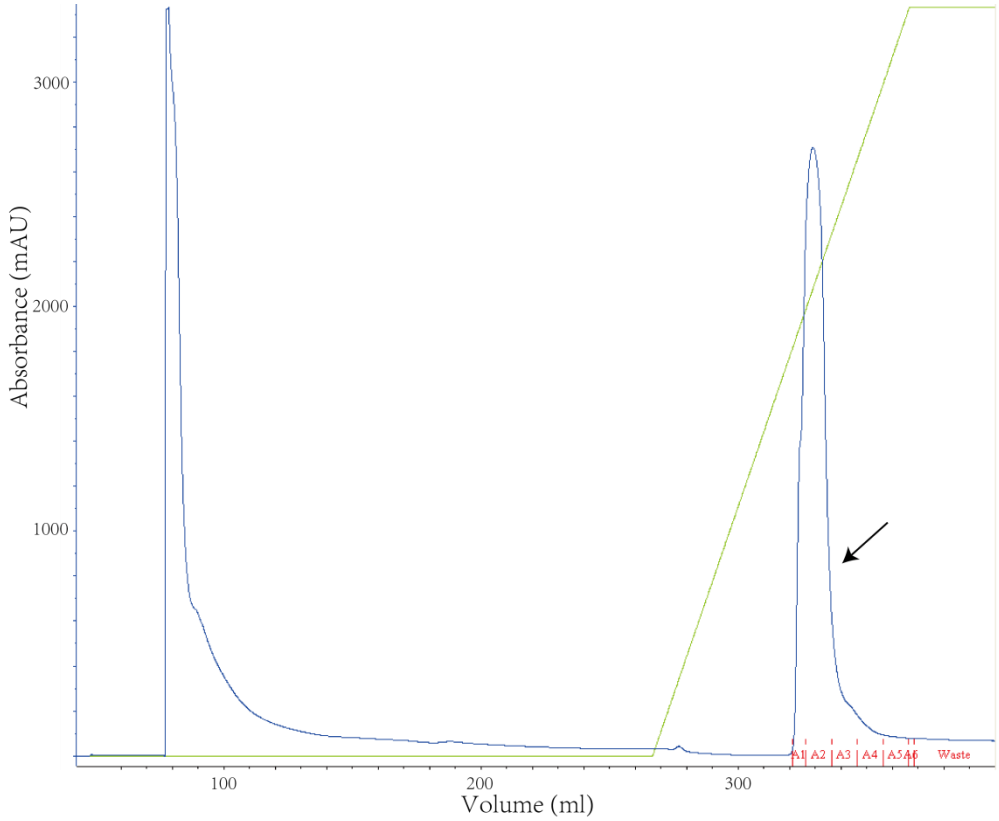

Figure 3.1.3: UV absorption curve of $Q^{122}FM(Y)F^{126}$ during HisTrap HP column. The protein was eluted with a 25–250 mM imidazole gradient (the yellow line) and resulted in a sharp peak which is collected as the sample. Depending on the protein load after the purification with HiTrap desalting column the samples were more than 97% pure as evinced by SDS-PAGE.

3.2 Structural characterization of the $Q^{122}FM(Y)F^{126}$ mutant

3.2.1 Backbone assignment of $Q^{122}FM(Y)F^{126}$

For the backbone assignment, 2D [^{1}H, ^{15}N]-TROSY (Figure 3.2.2) and 3D HNCO, HNCA (Figure 3.2.3), and HNCACB (Figure 3.2.4) spectra were acquired. Reverse labeling of phenylalanine (Figure 3.2.6) and a dual amino acid-selective ^{13}C–^{15}N labeling technique (Figure 3.2.8) are also used to finish the backbone assignment. Totally, >98% of the total number backbone amides of $Q^{122}FM(Y)F^{126}$ were assigned (for more details see below). M1 and A2 cannot be identified presumably due to the fast exchange of the amide protons with water.

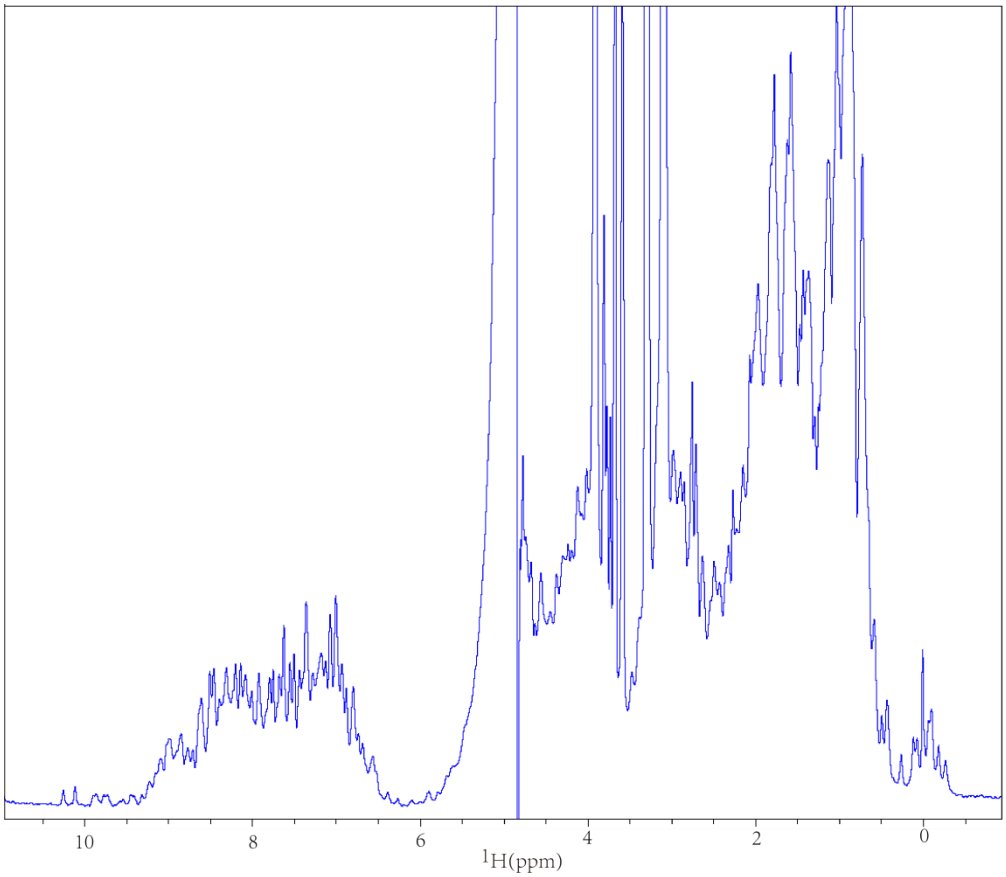

Figure 3.2.1: 1D ^{1}H NMR spectrum of $Q^{122}FM(Y)F^{126}$ mutant at 298K showing good dispersion of $^{1}H^{N}$ resonances in H^{N} region and $^{1}H\alpha$ protons. Strong peaks at 4.8 ppm represents water signal.

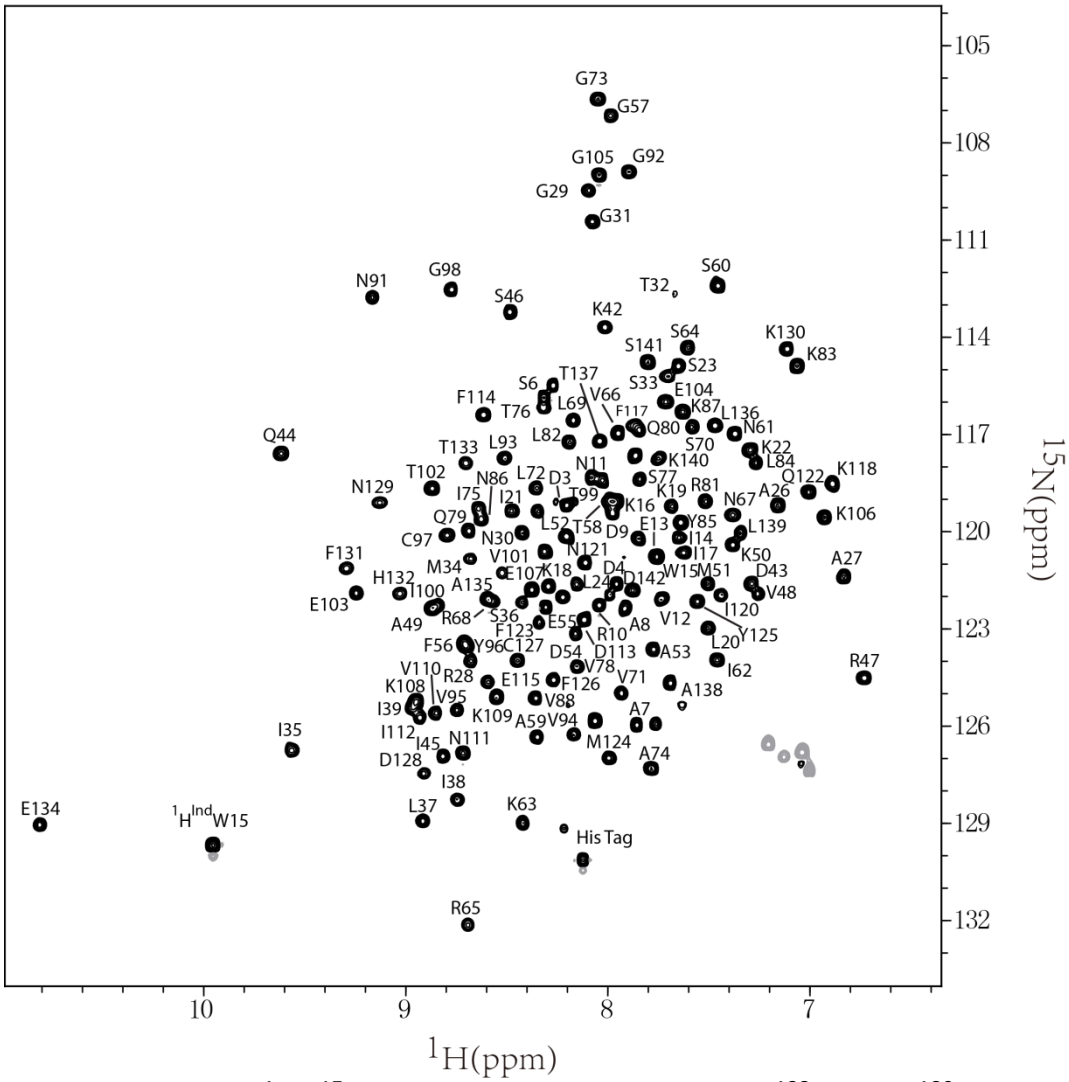

Figure 3.2.2: 2D [^{1}H, ^{15}N]-TROSY spectrum of the Q^{122}FM(Y)F^{126} mutant. The cross peaks are labeled by one-letter amino acid code and the residue number.

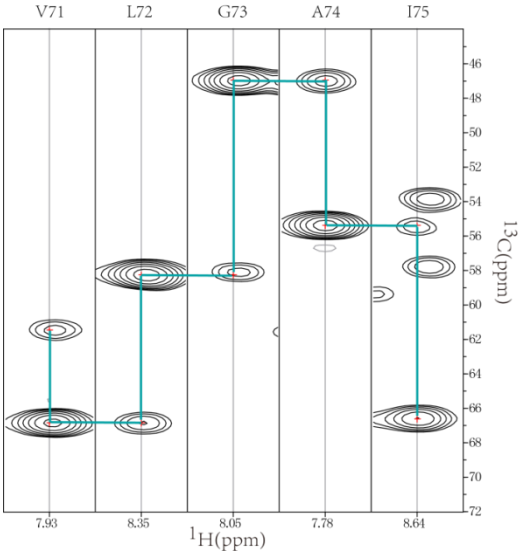

Figure 3.2.3: Strip plots from the TROSY-HNCA spectrum of the $Q^{122}FM(Y)F^{126}$ mutant. Shown are $^{1}H/^{15}N/^{13}C\alpha$ and $^{1}H/^{15}N/^{13}C\alpha$-1 cross-peaks bound into the $^{1}H/^{15}N/^{13}C\alpha/^{13}C\alpha$-1 spin systems (vertical cyan lines) and sequential $^{13}C\alpha/^{13}C\alpha$-1 connectivities (horizontal cyan lines) using the program CARA (www.nmr.ch).

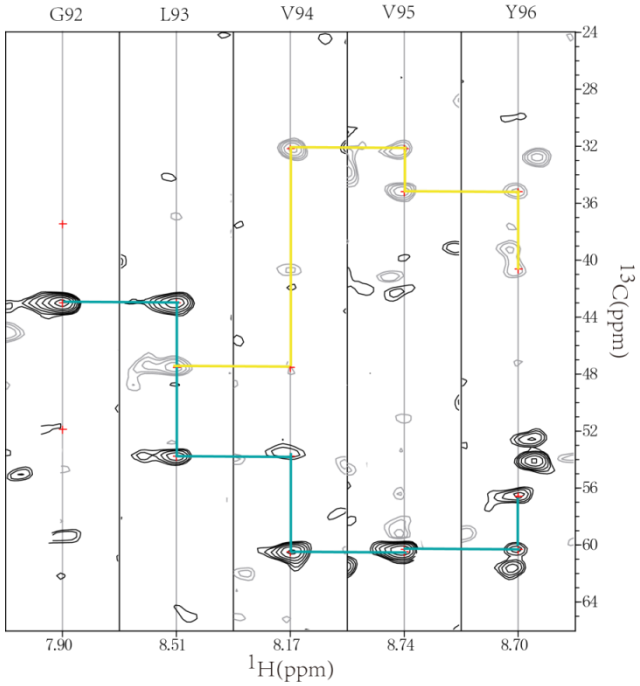

Figure 3.2.4: Strip plots from the TROSY-HNCACB spectrum of $Q^{122}FM(Y)F^{126}$ mutant. Shown are $^{1}H/^{15}N/^{13}C\alpha/^{13}C\beta$ and $^{1}H/^{15}N/^{13}C\alpha$-1/$^{13}C\beta$-1 cross-peaks bound into the $^{1}H/^{15}N/^{13}C\alpha/^{13}C\alpha$-1/$^{13}C\beta/^{13}C\beta$-1 spin systems (vertical cyan and yellow lines for Cα and Cβ) and sequential $^{13}C\alpha/^{13}C\alpha$-1 connectivities (horizontal cyan and yellow lines) using the program CARA (www.nmr.ch).

3.2.1.1 Reverse labeling of $Q^{122}FM(Y)F^{126}$

Based on 3D TROSY-HNCA and TROSY-HNCACB spectra, we have assigned about 80% of the backbone spin systems. However, as there are several prolines and phenylalanines near the mutation region in the protein sequence (Figure 3.2.5), we extended the triple resonance experiments with spectra utilizing the reverse $^{15}N/^{14}N$ isotope labeling strategy (*100*) to help resolve ambiguous phenylalanine assignments.

$P^{89}P^{90}$NGLVVYCGTIVTEEGKEKKVNIDF^{114}E$P^{116}F^{117}$KP^{119}INQF^{123}MYF^{126}

CDNKF^{131}HT^{134}

Figure 3.2.5: Sequence of a fragment of $Q^{122}FM(Y)F^{126}$ (from P89 to T134). Prolines and phenylalanines are highlighted in cyan are red, respectively.

Following this method, an extra 100 mg/L unlabeled phenylalanine amount was added to the medium just before induction to get a uniformly ^{15}N-labeled sample in which only the phenylalanine is bearing the ^{14}N isotopes. The 2D [^{1}H, ^{15}N]-TROSY spectrum (Figure 3.2.6) was recorded. In this spectrum, the phenylalanine showed cross-peaks with markedly reduced volumes than the other kind of residues. A comparison with uniformly labeled 2D [^{1}H, ^{15}N]-TROSY spectrum (Figure 3.2.2) provided residue-type specific assignment of phenylalanines. However, as some phenylalanine show only weak cross-peaks in the fully-labeled sample most

likely due to conformational exchange line broadening and due to spectral overlap one residue F117 eluded assignment at this stage.

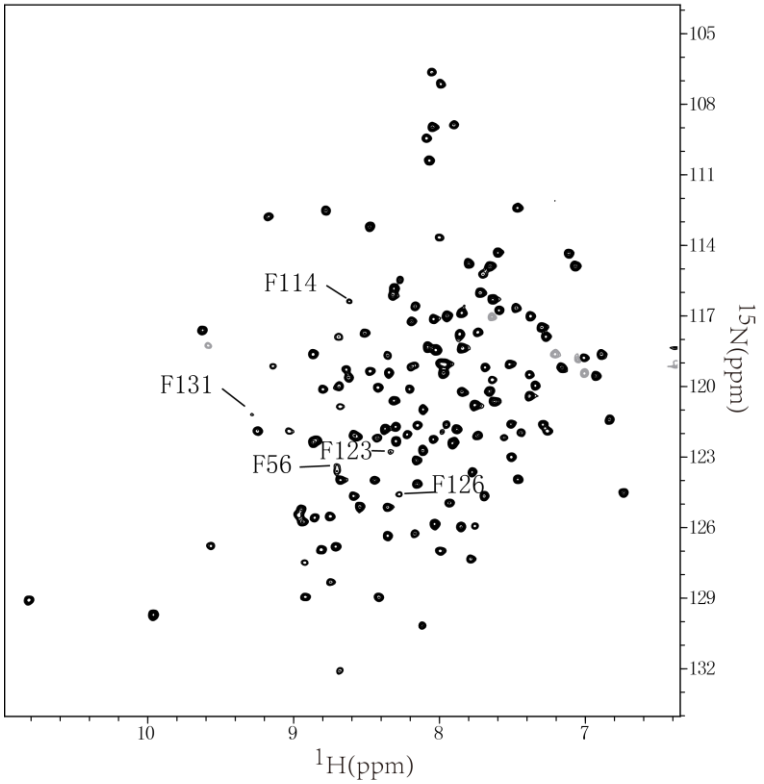

Figure 3.2.6: 2D [^{1}H, ^{15}N]-TROSY spectrum of Q^{122}FM(Y)F^{126} with reverse ^{15}N/^{14}N isotope labeling of phenylalanines. The cross peaks are labeled by phenylalanine one-letter code and the residue number.

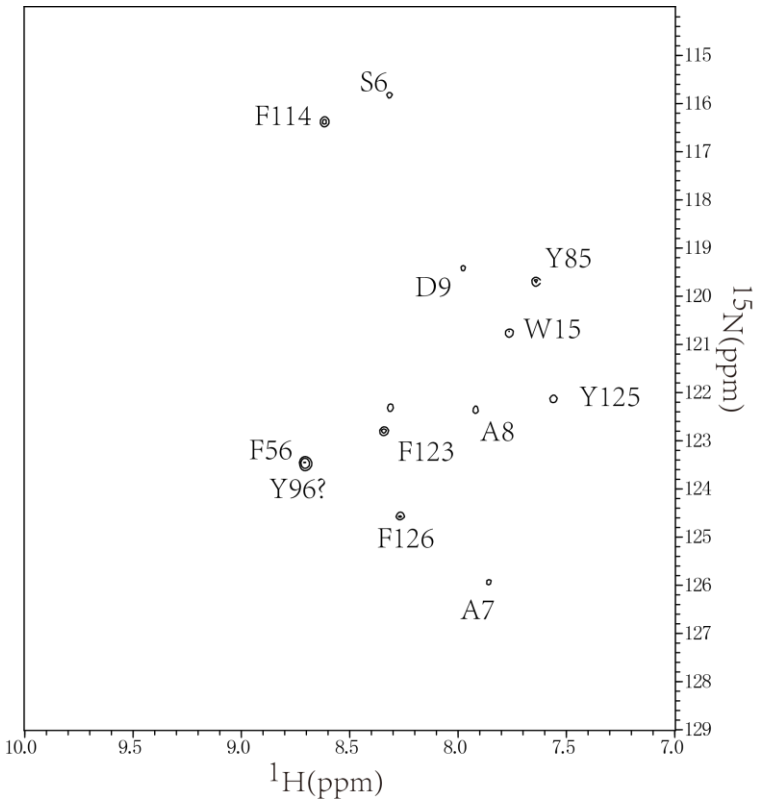

Figure 3.2.7: 2D [^{1}H, ^{15}N]-TROSY spectrum of Q^{122}FM(Y)F^{126} with only phenylalanines ^{15}N-labeled. By choosing sufficiently low contour level of the spectrum it shows scrambling of less than 10% of the ^{15}N-isotopes from phenylalanine to other aromatic and non-aromatic residues. The cross peaks are labeled by one letter amino-acid code and the residue number. The question mark at Y96 implies a small contribution of Y96 to the cross-peak assigned to F56.

3.2.1.2 Selective labeling of Q^{122}FM(Y)F^{126}

Selective labeling method was used to help complete the backbone assignment. Similarly with the reverse labeling method, extra amount of 100 mg/L ^{15}N-labeled phenylalanine was added to the medium just before induction of protein expression to obtain a sample in which only the phenylalanines containing NMR detectable ^{15}N-isotopes are expected. The resulting the2D [^{1}H, ^{15}N]-TROSY spectrum (Figure 3.2.7) showed that about

10% of ^{15}N-isotopes were scrambled to other amino acids predominantly aromatics, alanine and serine, *e.g.* S6, A7, A8, D9, W15, Y85 and Y125. Also since the cross-peaks stemming from F56 and Y96 overlap both residues contribute to the same cross-peak detected in the spectrum. Thus, though majority of phenylalanines were indeed highlighted, it appears still difficult to assign F117 with the high degree of probability.

3.2.1.3 Dual amino acid-selective ^{13}C–^{15}N labeling of Q^{122}FM(Y)F^{126}

The difficulties with F117 identification can be traced to the location of F117 in the structurally flexible loop potentially resulting in resonance lines broadening due to conformational exchange in the intermediate (in the NMR time scale) kinetic regime. To solve this problem with assignment of F117, a dual amino acid-selective ^{13}C–^{15}N labeling technique (*102*) was applied. In the method, all the phenylalanines are ^{15}N-labeled, and all the other residues are ^{13}C-labeled. That means that the glucose in M9 medium was ^{13}C-labeled, and an extra amount of 100 mg/L ^{15}N-labeled phenylalanine was added to the medium just before induction followed by recording of 3D HNCA spectrum (Figure 3.2.8). We can compare this with the uniformly ^{13}C, ^{15}N-labeled sample's 3D HNCA spectrum (Figure 3.2.8). In the uniformly ^{13}C, ^{15}N-labeled sample's 3D HNCA spectrum, Cα of F117 is stronger than Cα-1 of F117 (Figure 3.2.8A). By contrast, in dual amino acid-selective

^{13}C-^{15}N-labeled sample's 3D HNCA spectrum, Cα-1 of F117 is stronger than Cα of F117 (Figure 3.2.8B). For other residues which are not phenylalanine like V71 (Figure 3.2.8C, D), in both condition Cα is stronger than Cα-1. Thus, although indeed severely broadened by conformational exchange resonances stemming from F117 have been successfully assigned.

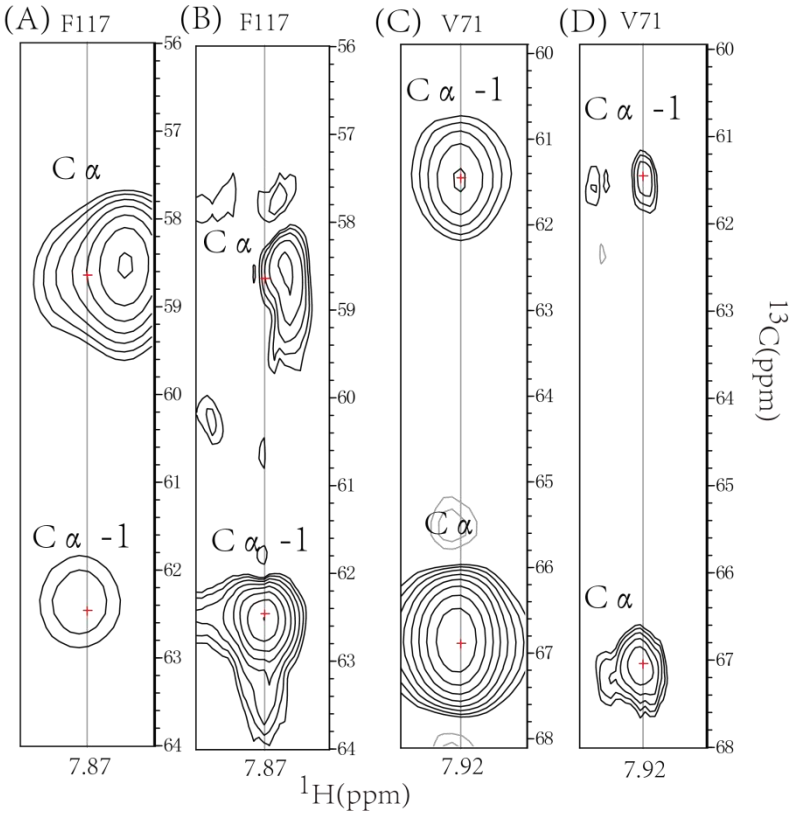

Figure 3.2.8: Slides from different 3D HNCA Spectrum of $Q^{122}FM(Y)F^{126}$ mutant. (A) Strip of F117 from normal ^{13}C, ^{15}N-labeled sample's 3D HNCA spectrum. (B) Strip of F117 from dual amino acid-selective ^{13}C-^{15}N-labeled sample's 3D HNCA spectrum. (C) Strip of V71 from uniformly ^{13}C, ^{15}N-labeled sample's 3D HNCA spectrum. (D) Strip of V71 from dual amino acid-selective ^{13}C-^{15}N-labeled sample's 3D HNCA spectrum.

3.2.2 Side-chain and NOE assignment of $Q^{122}FM(Y)F^{126}$

Side-chain ^{1}H and ^{13}C were assigned using iterative analysis of the 3D ^{15}N-NOESY-HSQC and ^{13}C-NOESY-HMQC spectra coupled with structure calculations using CYANA program (*108*). The ^{15}N-resolved NOESY spectra were collected in the phase-sensitive manner, with mixing times of 200 ms. The ^{13}C-resolved NOESY spectra contain both aromatic and aliphatic carbons and hydrogens. The assignment process was facilitated by comparison with chemical shifts deposited in the Biological Magnetic Resonance Data Bank (www.bmrb.wisc.edu) for individual domains(*103-105*). Totally, the assignment completeness is more than 98% except M1 and A2. The short-range and medium range NOE connectivities were used to establish the sequence-specific^{1}H NMR assignment and to identify elements of the regular secondary structure. Typically, from the Figure 3.2.11, it is revealed that $Q^{122}FM(Y)F^{126}$ has four α-helices located in residues S6-A27, I45-S60, R65-Y85 and T133-D142, which is consistent with the Dihedral angle data generated from TALOS (*112*).

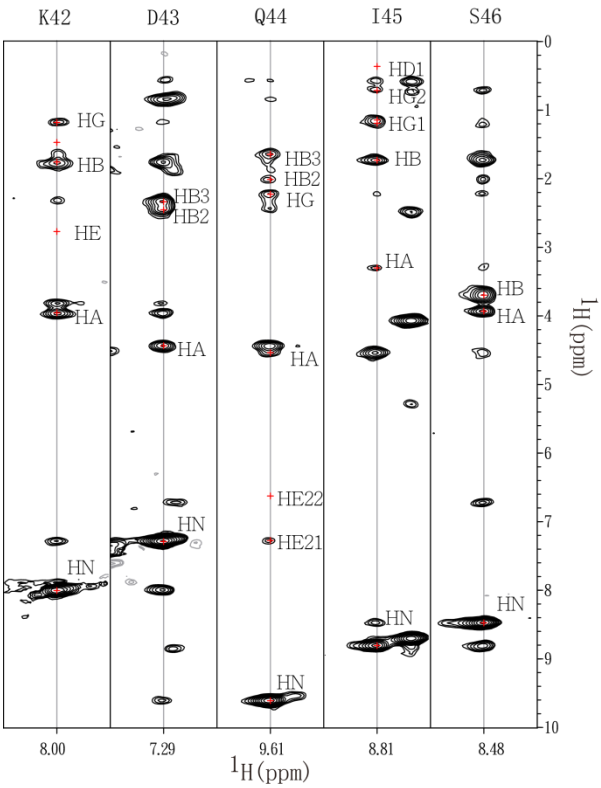

Figure 3.2.9: Slides from the 3D ^{15}N-resolved NOESY spectrum of the Q^{122}FM(Y)F^{126} mutant. The assignment of individual protons is shown in the spectrum.

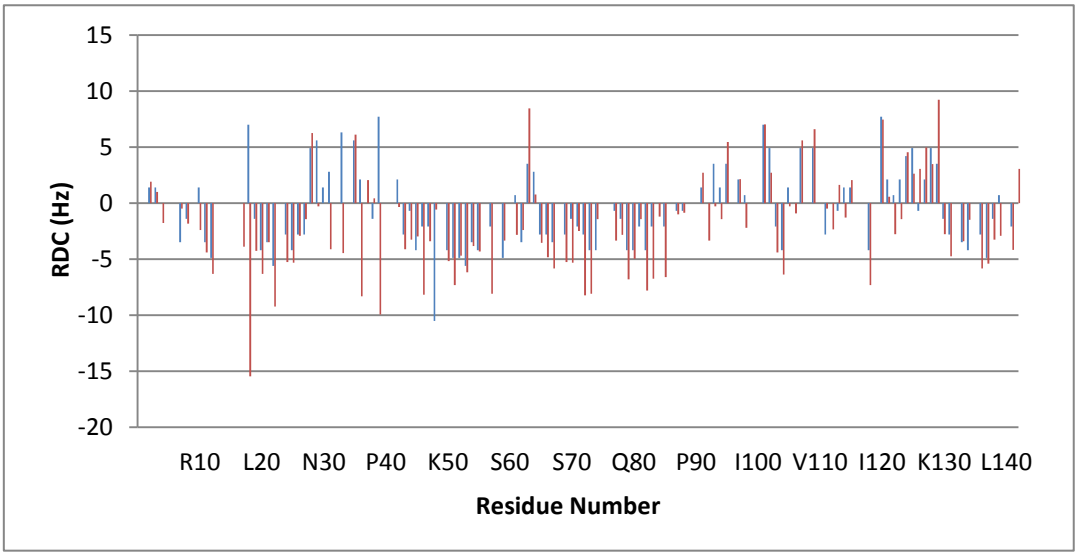

Figure 3.2.10: Observed [^{1}H^{N}, ^{15}N]-RDC values *versus* residue number using phages *Pf1* as an anisotropic alignment medium.

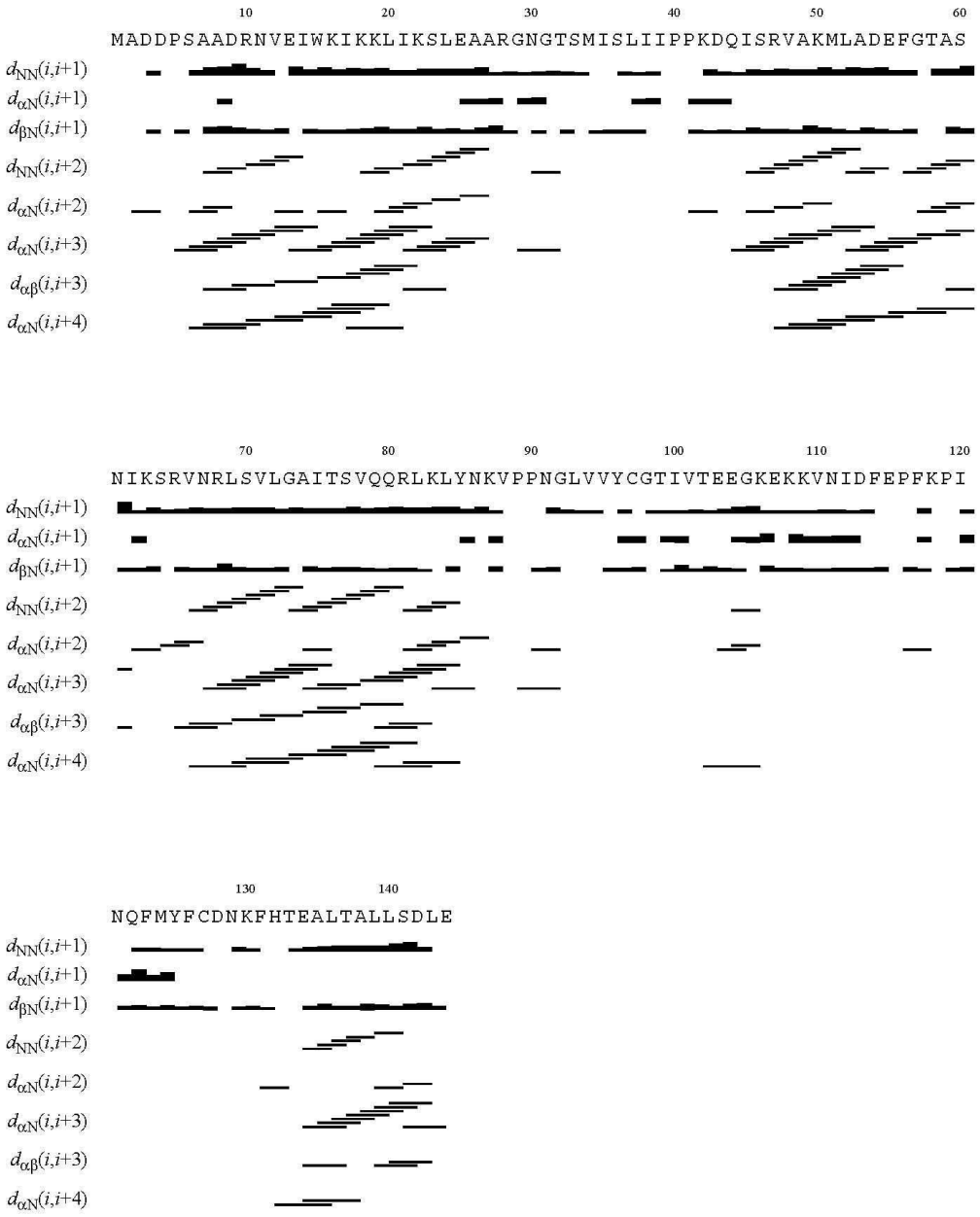

Figure 3.2.11: Sequential connectivities *versus* the residue number. Strong and weak NOE intensities for the sequential d_{NN}, $d_{\alpha N}$, $d_{\beta N}$ and $d_{\alpha\beta}$ connectivities are indicated by thick and thin horizontal bars, respectively, indicating four α-helices located in S6-A27, I45-S60, R65-Y85 and T133-D142 of $Q^{122}FM(Y)F^{126}$.

3.2.3 Residue dipolar coupling analysis

Residual dipolar couplings (RDC) are expressed in Hz and contain information about the orientation of the internuclear vector relative to the molecular susceptibility tensor. *Pf1* bacteriophages are used as a convenient alignment media providing sufficiently strong anisotropic alignment of protein to be detected as relative shifts of the $^{1}H^{N}$multiplets. The sample preparation described below is for *Pf1* phages in 10 mM potassium phosphate buffer, pH 6.0, 2 mM $MgCl_2$, and 0.05 % NaN_3. The aliquots of *Pf1* (SIGMA) were directly added into the eRF1 mutant $Q^{122}FM(Y)F^{126}$ (0.65 mM) to determine the optimum phages concentration to induce partial alignment of the protein. Concentrations tried were 20, 15 and 10 mg/ml of *Pf1*. Approximately 10 mg/ml bacteriophages *Pf1* were found to be sufficient for protein alignment without excessive line broadening due to the spurious RDCs between $^{1}H^{N}$ and other remote protons. The sample appeared to be clear and free of precipitates, as opposed to the higher concentrations tried. 2D [^{1}H-^{15}N] TROSY and anti-TROSY experiments were measured for the sample at both isotropic and anisotropic conditions. Observed [$^{1}H^{N}$, ^{15}N]-RDCs are shown in Figure 3.2.10. The 3D structure of the N-domain obtained via NOEs and chemical shifts data was verified against experimental RDCs as described below.

3.2.4 Backbone relaxation studies

NMR relaxation experiments of proteins provide uniquely detailed and quantitative information about the conformational dynamics on the pico- and nanosecond time scale. The ^{15}N relaxation experiments for Q^{122}FM(Y)F^{126} were performed at 25°Con a 700 MHz Bruker Avance II spectrometer. Longitudinal relaxation time T_1 were measured with eight relaxation delays, 0.075, 0.15, 0.3, 0.375, 0.525, 0.675, 0.9375 and 1.2 s. Transverse relaxation time T_2 were measured with eight relaxation delays, 12.5, 25, 50, 62.5, 87.5, 112.5, 156.25, and 200 ms. The spectra measuring ^{1}H-^{15}N NOE were acquired with a 2 s relaxation delay, followed by a 3 s period of proton saturation. The reference spectra in the absence of proton saturation were recorded with a relaxation delay of 5 s. The exponential curve fitting and data analysis were carried out using Origin (Origin Lab). Figure 3.2.13 shows the obtained ^{15}N R1 and R2 relaxation rates and ^{1}H-^{15}N NOEs. As shown in Figure 3.2., in the N-terminal part located in the residues D3-I14, the protein exhibits obvious increase in R1 and a decrease in the R2 values indicating that this part is more flexible than other part. Detailed comparison of the intra-molecular dynamics in the N-domain mutants is provided in the following sections.

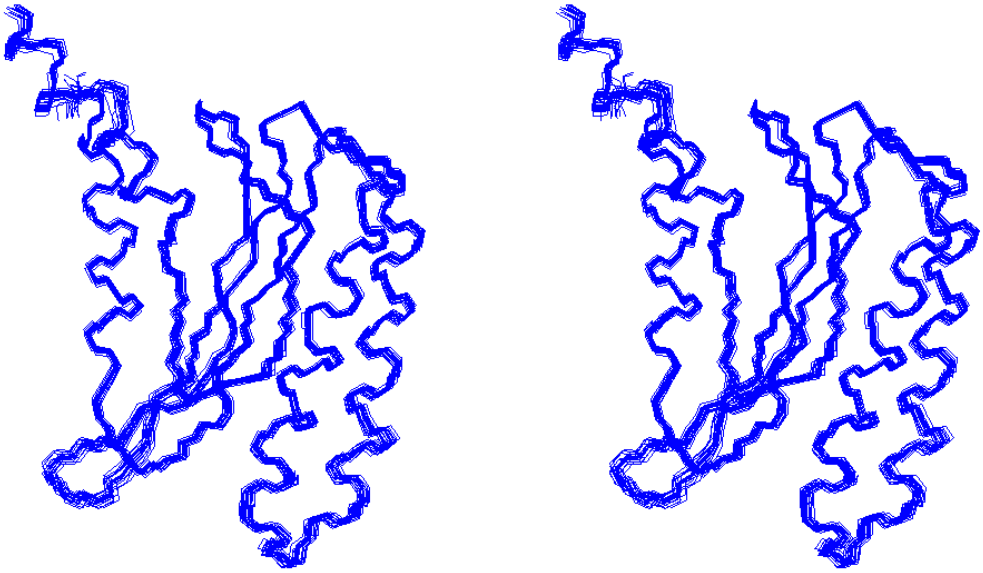

Figure 3.2.12: Three-dimensional solution structure of the $Q^{122}FM(Y)F^{126}$ mutant. 20 lowest energy conformers were shown in the lines representation.

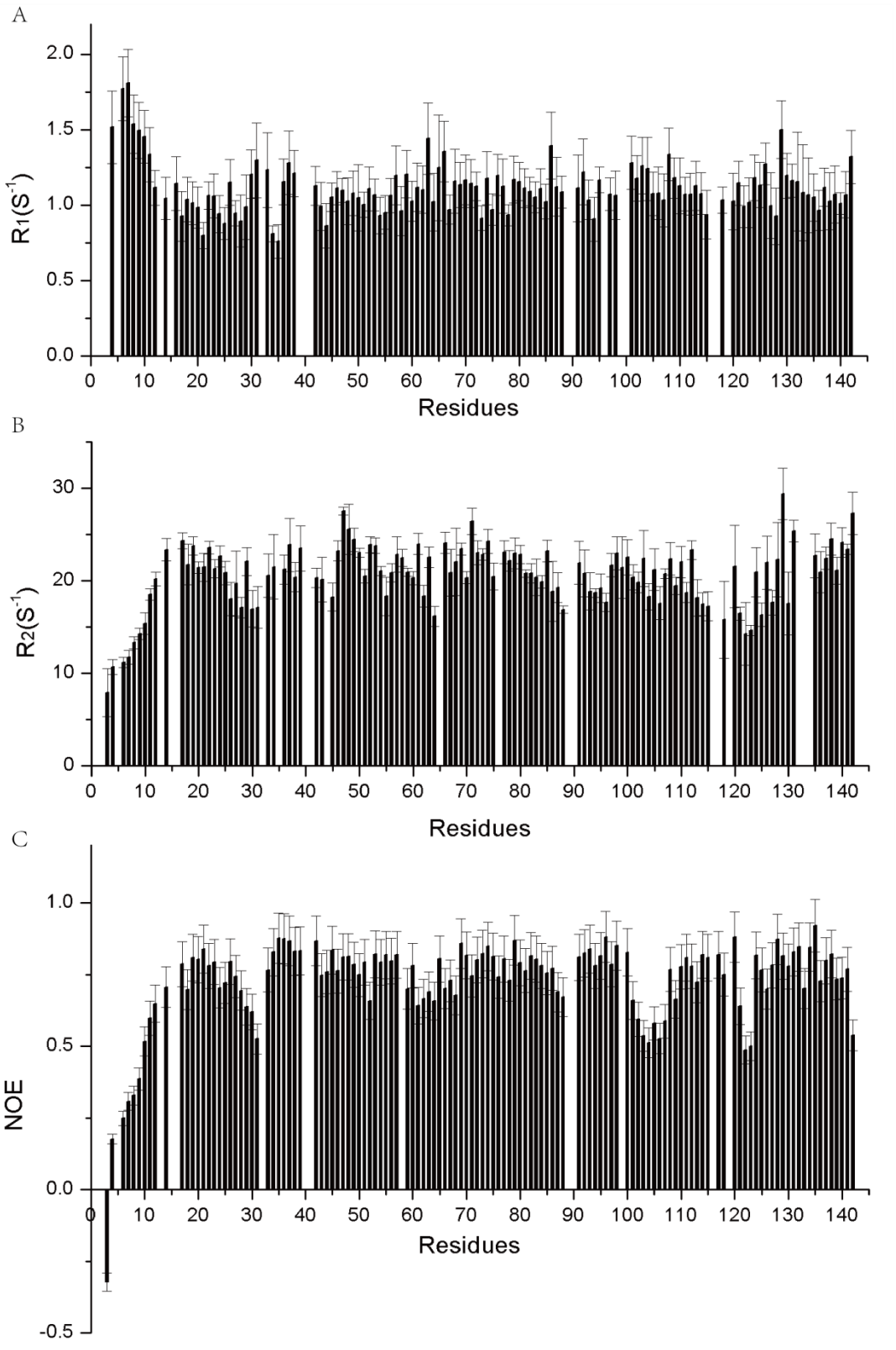

Figure 3.2.13: Backbone ^{15}N-relaxation rates of the Q^{122}FM(Y)F^{126} mutant. (A) Experimental longitudinal (R1) ^{15}N relaxation rates, (B) experimental longitudinal (R2) ^{15}N transverse rates, (C) ^{1}H-^{15}N heteronuclear NOEs *versus* residue numbers.

3.2.5 Structure determination of $Q^{122}FM(Y)F^{126}$

NOE distance restraints for the calculated structures of wt N-domain and $Q^{122}FM(Y)F^{126}$ mutant were obtained from ^{15}N-NOESY-HSQC and ^{13}C-NOESY-HMQC spectra, respectively. NOE distance restraints for the calculated structures of Y125Fmutant and E55Qmutant were obtained from ^{15}N-NOESY-HSQC. Backbone dihedral angle restraints (φ and ψ) were derived from the backbone $^{13}C'$, $^{13}C_{\alpha}$, $^{13}C_{\beta}$, $^{1}H_{\alpha}$, $^{1}H_{\beta}$, $^{1}H^{N}$ chemical shift values using TALOS (*112*). Residual dipolar couplings containing information regarding the orientation of the internuclear vector relative to the molecular susceptibility tensor were used for structure verification purposes. Hydrogen bond restraints were obtained by identifying the slow exchange amide protons mainly in the regular secondary structures. Structure calculations were performed using CYANA 3.0(*108, 109*) and visualized using MOLMOL (*110*) and PyMOL (Delano Scientific). Quality of the final structures was assessed using PROCHECK-NMR (*111*).

Totally, >98% of the complete backbone and >95% of the side-chain ^{1}H resonance of $Q^{122}FM(Y)F^{126}$ were assigned, including those of aromatic rings. A total of 1316 distance restraints experimentally derived from NOEs, 77 distance restraints derived from hydrogen bonds and 269 dihedral angle restraints derived from TALOS were used in the structure calculations.

Table 3.2: Structure statistics for the selected 20 structures of $Q^{122}FM(Y)F^{126}$ mutant[a]

NMR restraints	
Total unambiguous distance restraints	1316
Intra residual	321
Sequential (| i – j | = 1)	423
Short-range (| i – j | <=1)	744
Medium (2 ≤ | i – j | ≤ 4)	262
Long range (| i – j | ≥ 5)	310
RDC restraints	117
Hydrogen bond restraints	77
RMSD from the average atomic coordinates（residues 6-140, Å）	
Backbone atoms	0.39 ± 0.07
All heavy atoms	1.00 ± 0.06
Ramachandran analysis (%)	
Residues in most favored regions	74.6
Residues in additional allowed regions	24.6
Residues in generously allowed regions	0.8
Residues in disallowed regions	0.0

a, None of the structure exhibits distance violations greater than 0.2 Å or dihedral angle violations greater than 5°

Table 3.2 lists the structural statistics about the quality and variation within the 20 conformers representing 3D NMR structure. For the region from residue S6 to L140, the RMSD values to the mean structure were 0.39Å for backbone atoms and 1.00 Å for all heavy atoms. The experimental RDC correlate well with the couplings generated from a representative conformer (the conformer with the smallest RMSD to the mean structure) (Figure 3.2.15). Based on the Ramachandran plot for φ and ψ angles of $Q^{122}FM(Y)F^{126}$, 74.6% of residues are found in the most favored regions,

24.6% in the additionally allowed region, 0.8% in the generously allowed regions and no angles in the disallowed regions. This plot is prepared using CYANA (*113*).

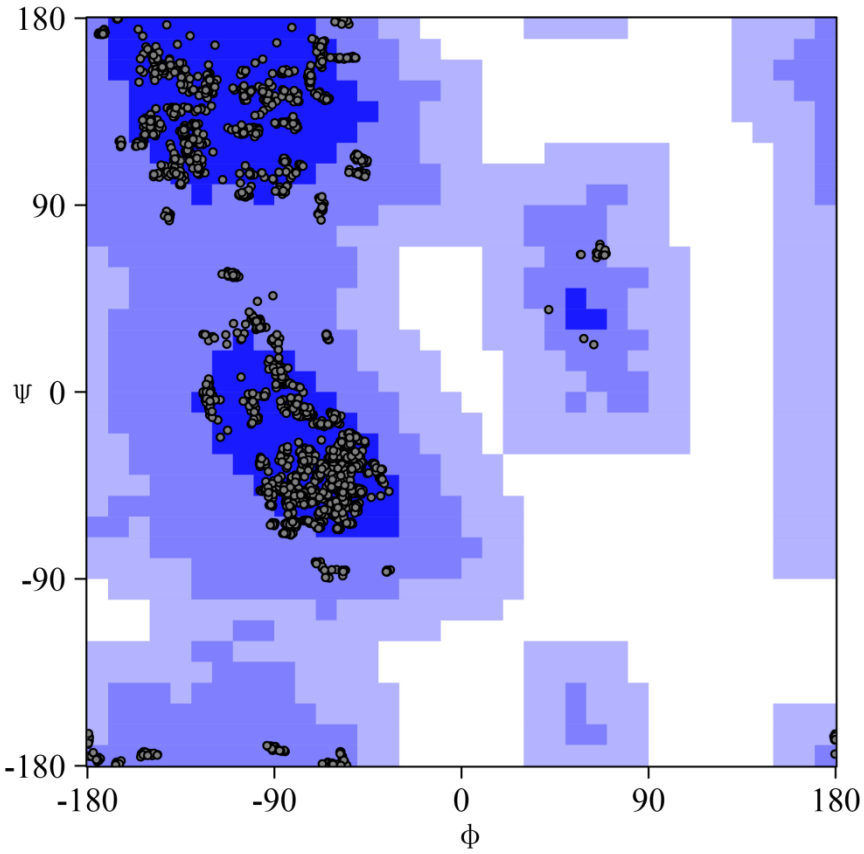

Figure 3.2.14: Ramachandran plot of residues φ and ψ angles of $Q^{122}FM(Y)F^{126}$. The most favored regions are in blue, the additionally allowed regions are in light blue, the generously allowed regions are in lightest blue and the disallowed regions are white. This plot is prepared using CYANA (*108*).

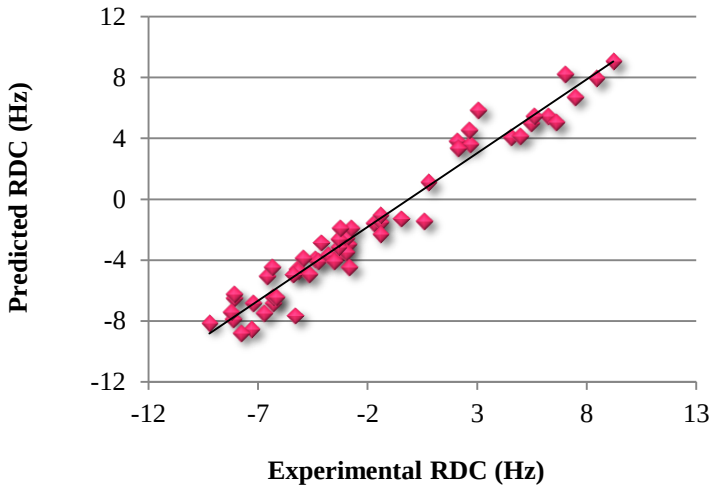

Figure 3.2.15: The correlation between experimental and theoretical ^{15}N-^{1}H dipolar couplings predicted using the representative conformer of $Q^{122}FM(Y)F^{126}$. Alignment Tensor: axial component = -6.6; R = 0.97 with rhombicity = 0.44.

3.2.6 Description of NMR structure of $Q^{122}FM(Y)F^{126}$

The NMR-derived tertiary structure of $Q^{122}FM(Y)F^{126}$ contains 3 β sheets and 4 α-helices linked with four loops. The four α-helices are sequentially named α1 (S6-A27), α2 (I45-S60), α3 (R65-Y85), and α4 (T133-D142), respectively, from N-terminus (Figure 3.2.16), and the three anti-parallel β-sheet are composed of β1 (I35-I39), β2 (L93-T102), β3 (G105-F114) (Figure 3.2.16). In crystal structure, another β-sheet β4 (Q122-C127) is formed. Four α-helices form a left-handed bundle. A long loop of 22 residues connects sheets β3 and β4, and a shorter loop of 19 residues connects helix α3 and sheet β3. The strand β4 has some hydrophobic residues, like I120, N121, F123, M124, Y125, F126 and C127. These hydrophobic interactions provide the hydrophobic core of the structure of $Q^{122}FM(Y)F^{126}$, which is

altered in the mutant comparing with wt N-domain. Some highly conserved negatively charged residues are found on the surface of the protein. They probably play a significant role in stabilizing the conformation of the protein.

The highly conserved motifs YxCxxxF (M124-F131) plays an important role in the stop-codon recognition. The mutations T122Q, S123F, L124M and L126F are located in this region. Comparing the structure of $Q^{122}FM(Y)F^{126}$ with the crystal structure of eRF1 (*7*), one significant difference is that the side chain of F126 flipped to the opposite side of β4 where F126 is situated. Thus, the side-chain of F126 cannot interact with residues located in proximal α4. By contrast, through the 3D ^{13}C-NOESY-HMQC spectrum, clear NOEs contacts between F126 and α2 can be seen. Thus, the presence of F126 perturbs the wt conformation of the YxCxxxF motif, and the β4 in crystal structure cannot be directly aligned with the NMR structure of $Q^{122}FM(Y)F^{126}$ mutant. Also, the conformation of the GTS loop is rearranged compared with the crystal structures. These changes alter the solution structure of $Q^{122}FM(Y)F^{126}$ mutant relative to the wild-type crystal structure.

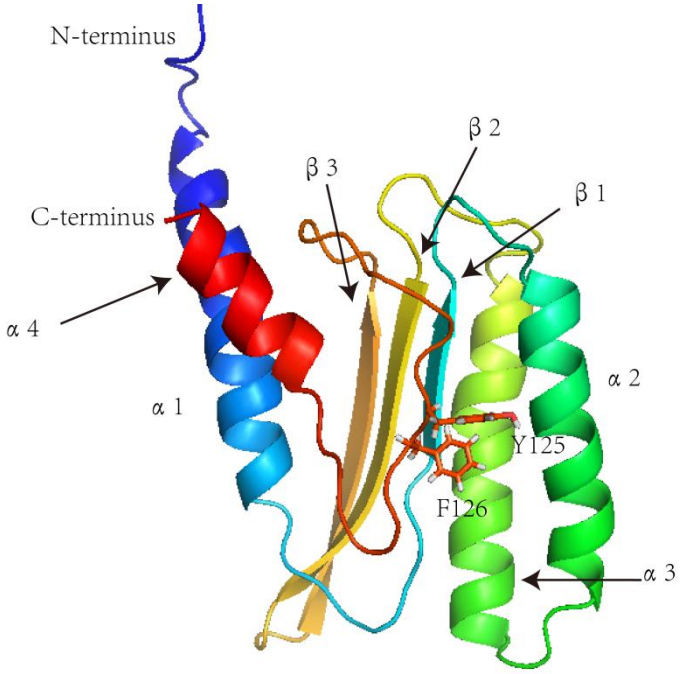

Figure 3.2.16: NMR structure of $Q^{122}FM(Y)F^{126}$. The $Q^{122}FM(Y)F^{126}$ mutant was shown in the ribbon representation; the four α-helices (α1, α2, α3, and α4) and the three β-sheets are labeled; the side-chain of Y125 and F126 were shown in the sticks representation.

3.3 Structural characterization of wild-type N-domain

3.3.1 Resonance assignment of wild-type N-domain

All NMR spectra were acquired using 600 or 700 MHz Bruker Avance II spectrometers at 25°C. Chemical shifts were referenced to DSS directly for ^{1}H and indirectly for ^{13}C and ^{15}N spins. The raw data was processed using TopSpin 2.1 (www.bruker-biospin.com) and analyzed using CARA (www.nmr.ch). Linear prediction was used to improve spectral resolution in the indirect dimensions where constant-time acquisition was used.

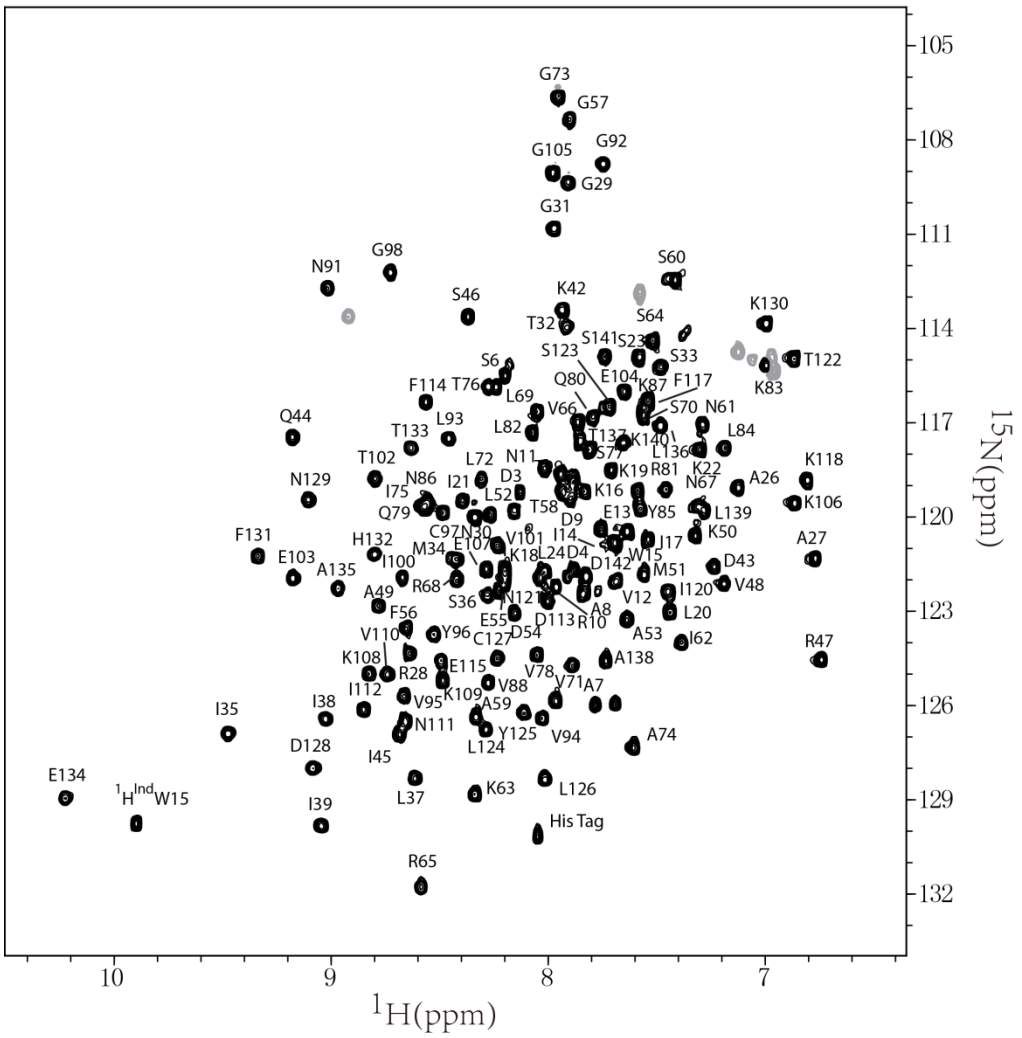

Figure 3.3.1: 2D [^{1}H, ^{15}N]-TROSY spectrum of the wild-type N-domain of eRF1. The cross-peaks are labeled by the one-letter amino acid code and the residue number.

The crucial step to analyze protein by NMR spectroscopy is the process of sequential assignment. Assignments of ^{1}H, ^{15}N and ^{13}C signals of wt N-domain were performed by using 2D [^{1}H, ^{15}N]-TROSY (*99*), [^{1}H, ^{13}C]-HSQC, 3D TROSY-HNCA. Side-chain ^{1}H and ^{13}C were assigned using iterative analysis of the 3D ^{15}N-NOESY-HSQC and ^{13}C-NOESY-HMQC spectra coupled with structure calculations. The ^{15}N-resolved NOESY spectra were collected in the phase-sensitive manner, with mixing times of 200 ms. The ^{13}C-resolved NOESY spectra contain both aromatic and aliphatic carbons and protons. The assignment process was facilitated by comparison with chemical shifts deposited in the Biological Magnetic Resonance Data Bank (www.bmrb.wisc.edu) for individual domains (*103-105*).

3.3.2 Backbone relaxation studies of wt N-domain

Similarly with $Q^{122}FM(Y)F^{126}$, for wt N-domain, longitudinal relaxation time T_1 were measured with 8 relaxation delays,0.075,0.15, 0.3, 0.375, 0.525, 0.675, 0.9375, 1.2 s. Transverse relaxation time T_2 were measured with eight relaxation delays, 12.5, 25, 50, 62.5, 87.5, 112.5, 156.25, and 200 ms. The spectra measuring ^{1}H-^{15}N NOE were acquired with a 2 s relaxation delay, followed by a 3 s period of proton saturation. In the absence of proton saturation, the spectra were recorded with a relaxation delay of 5 s. The

exponential curve fitting and data analysis were carried out using Origin (Origin Lab). Figure 3.3.2 shows the obtained ^{15}N R1 and R2 relaxation rates and ^{1}H-^{15}N NOEs. As shown in Figure 3.3.2, in the N-termainal part approximately D3-I14, there is obvious increase in R1 and a decrease in the R2 values. It is supposed that this part is more flexible than other part.

3.3.3 Structure Determination of wt N-domain

NOE distance restraints for the calculated structures of wt N-domain were obtained from ^{15}N-NOESY-HSQC and ^{13}C-NOESY-HMQC spectra, respectively. Backbone dihedral angle restraints (φ and ψ) were derived from the backbone ^{13}C', $^{13}C_{\alpha}$, $^{13}C_{\beta}$, $^{1}H_{\alpha}$, $^{1}H_{\beta}$, $^{1}H^{N}$ chemical shift values using TALOS (*107*). Hydrogen bond restraints were obtained from crystal structure, and they were used to help structure determination at the beginning stage. Structure calculations were performed using CYANA 3.0 (*108, 109*) and visualized using MOLMOL (*110*) and PyMOL (Delano Scientific).

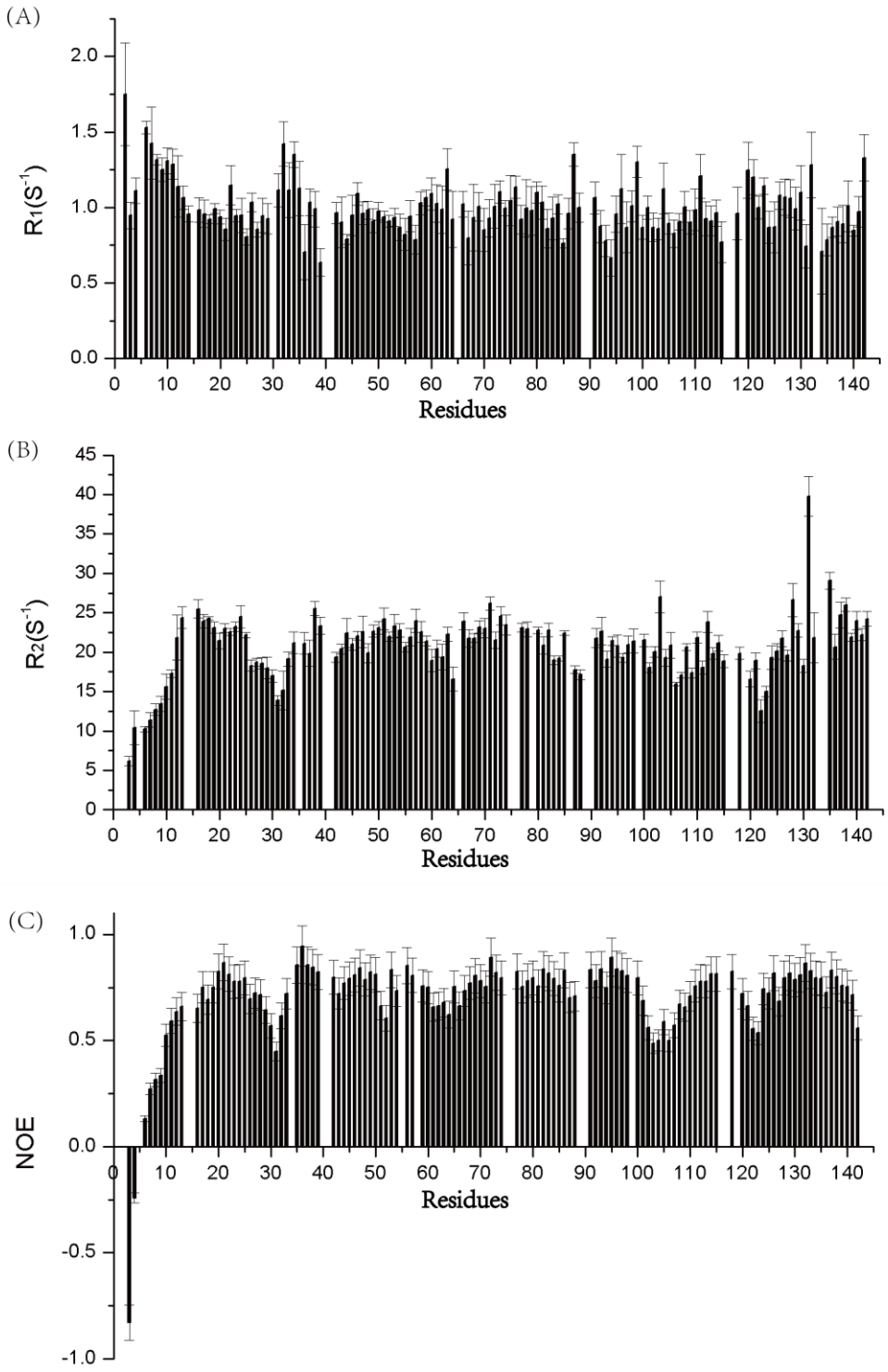

Figure 3.3.2: Backbone relaxation parameters of wt N-domain. (A) Experimental longitudinal (R_1) ^{15}N relaxation rate (B) Experimental longitudinal (R_2) ^{15}N transverse rate (C) ^{1}H-^{15}N heteronuclear NOEs for wt N-domain.

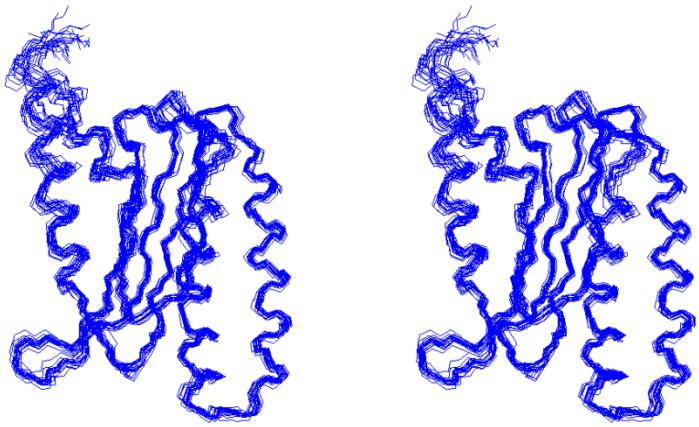

Figure 3.3.3: Three-dimensional solution structure of wt N-domain. 20 lowest energy conformers are shown in the lines representation.

Table 3.3: Structure statistics for the selected 20 structures of wt N-domain[a].

NMR restraints	
Total unambiguous distance restraints	2139
Intra residual	616
Sequential (| i – j | = 1)	622
Short-range (| i – j | <=1)	1238
Medium (2 ≤ | i – j | ≤ 4)	418
Long range (| i – j | ≥ 5)	483
Hydrogen bond restraints	77
RMSD from the average atomic coordinates（residues 6-140, Å）	
Backbone atoms	0.78 ± 0.18
All heavy atoms	1.14 ± 0.16
Ramachandran analysis (%)	
Residues in most favored regions	66.9
Residues in additional allowed regions	27.2
Residues in generously allowed regions	5.8
Residues in disallowed regions	0.1

a None of the structure exhibits distance violations greater than 0.2 Å or dihedral angle violations greater than 5°.

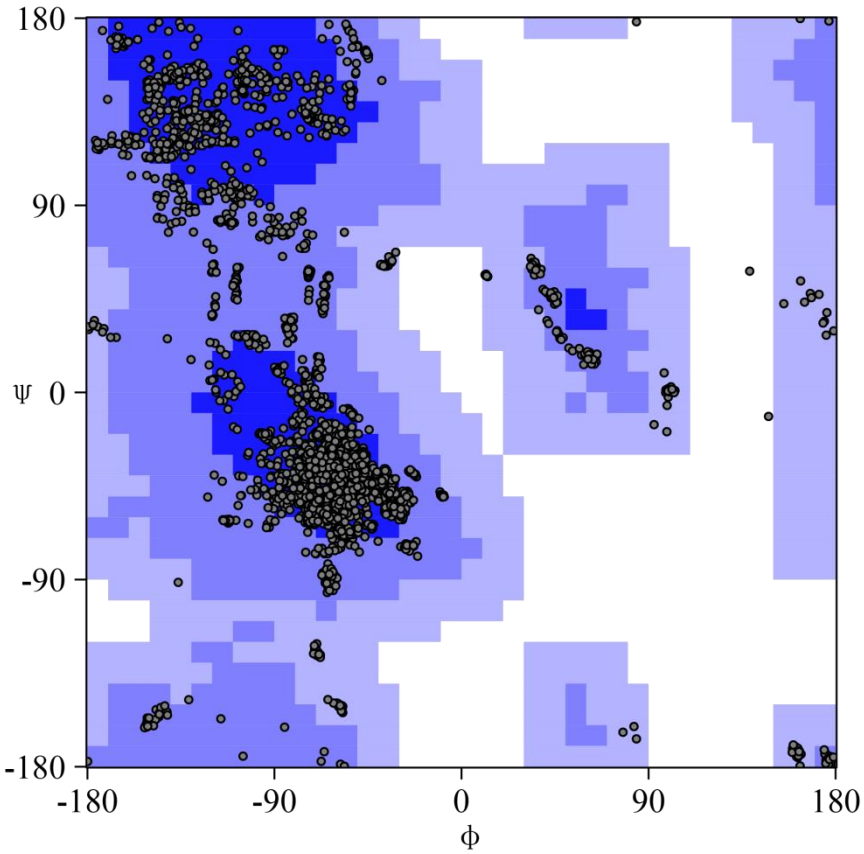

Figure 3.3.4: Ramachandran plot of residues φ and ψ angles of wt N-domain. 66.9% in most favored regions, 27.2% in additionally allowed region, 5.8% in generously allowed regions and 0.1% in disallowed regions. This plot is made from CYANA (*108*).

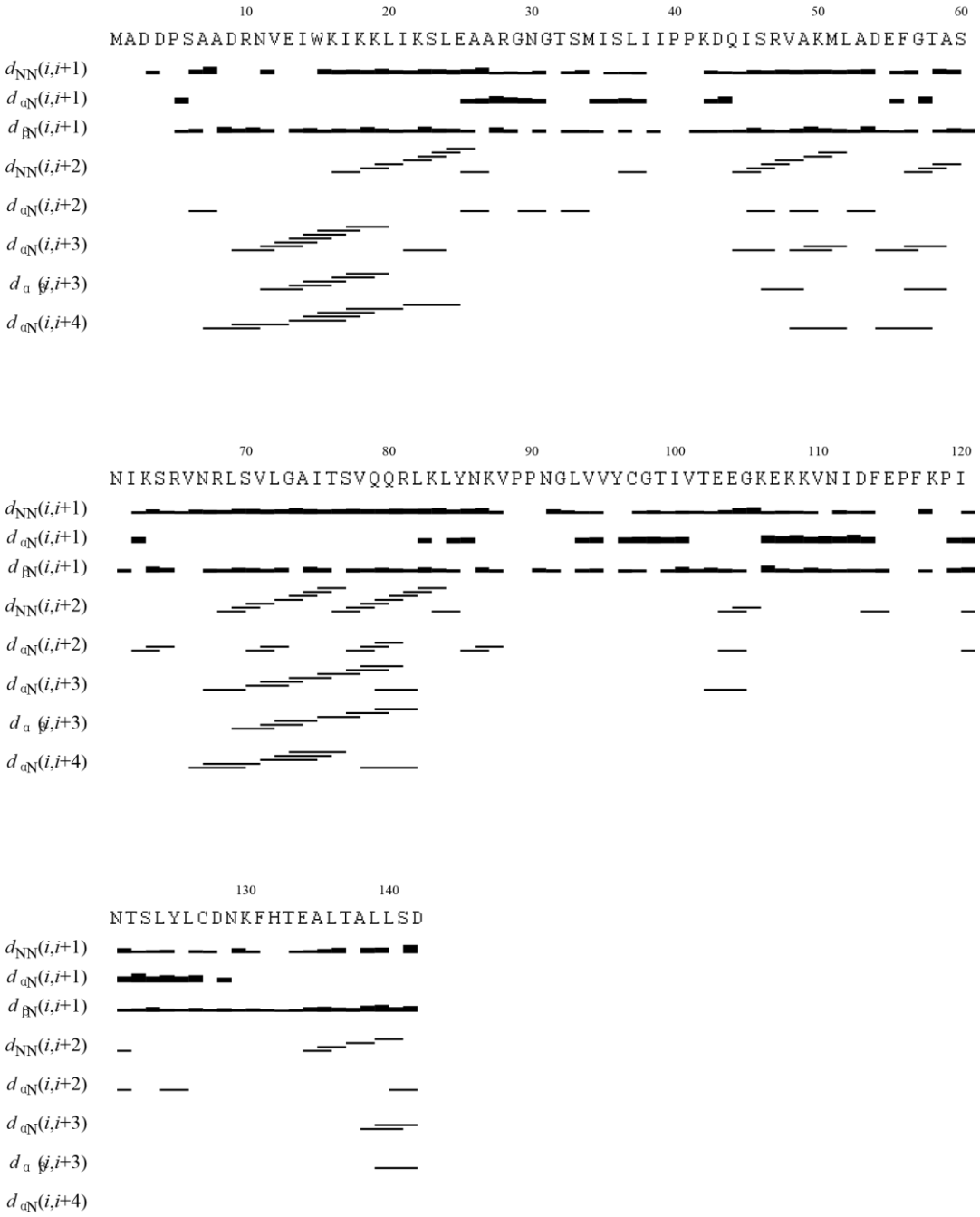

Figure 3.3.5: Sequential connectivities are plotted against the residue number. Strong and weak NOE intensities for the sequential d_{NN}, $d_{\alpha N}$, $d_{\beta N}$ and $d_{\alpha\beta}$ connectivities are indicated by thick and thin horizontal bars, respectively. N-domain contains four α-helices located in the residues S6-A27, I45-S60, R65-Y85 and T133-D142.

3.3.4 The GTS loop in N-domain adopts distinctly different conformations

To understand the structural effect of the quadruple mutations (*i.e.* T122Q, S123F, L124M, and L126F) that lead to unipotency for UGA in the mutant eRF1, we determined the solution structures of wt N-domain and $Q^{122}FM(Y)F^{126}$, and compared them with the corresponding crystal structure of N-domain in full-length eRF1 (*7*). The solution structures were verified against measured residual dipolar couplings, and the structure determination statistics are reported in Table 3.2. As expected, the NMR solution structure of wt N-domain matches closely with the crystal structure of N-domain in full-length eRF1 (Figure 3.3.7A). The only significant deviations observed between them are positioning of the N-terminal part of helix α3 and conformation of the GTS loop.

The global structure of $Q^{122}FM(Y)F^{126}$ is well superimposable with wt N-domain (Figure 3.3.8A). Their structural differences are confined to the β-strand β4 that contains the point mutations, as well as the GTS loop. Likewise, helix α3 of $Q^{122}FM(Y)F^{126}$ is also repositioned relative to wt N-domain (Figure 3.3.8A). Although the four point mutations are spatially remote from the GTS loop, structural alteration occurs to the GTS loop in $Q^{122}FM(Y)F^{126}$ is evident from the difference in amide chemical shift for the GTS loop and several other residues including C97 and T99 (Figure 3.3.8B).

Furthermore, different GTS loop conformations are also confirmed by clear differences in the NOEs patterns between wt N-domain and $Q^{122}FM(Y)F^{126}$ (Figure 3.3.7B). The alternative conformation of the GTS loop in $Q^{122}FM(Y)F^{126}$ is maintained via an intricate propagation of structural perturbations from the site of mutations situated at the beginning of strand β4 of the β-sheet that constitutes the core of N-domain (Figure 3.3.8A). In wt N-domain, this strand forms a well-defined network of hydrogen bonds with the adjacent strand starting from L124 to D128, as seen from the alternating directions of the side-chains of consecutive residues. In $Q^{122}FM(Y)F^{126}$, the regular hydrogen-bonding network is disrupted starting from M124. Mutation L126F is critical for breaking the regularity, since the phenylalanine aromatic ring is found flipped to the opposite direction of the side-chain of L126, thus as a consequence, altering direction of the side-chain of C127. As the side-chain of C127 is moved away from the hydrophobic core formed between the β-sheet, helix α2, and helix α3, the N-terminal part of helix α3 is able to move closer to the GTS loop. The phenylalanine substitution at position 126 in three of the ciliates that are unipotent for UGA suggests that similar structural features may have causal effect on the UGA-unipotency in those organisms (Figure 3.3.6). Nevertheless, the overall structural alteration in $Q^{122}FM(Y)F^{126}$ is likely to be an additive effect from all of the point mutations (*97*).

Remarkably, the GTS loop adopts distinct conformations in all three situations, namely the crystal and solution structures of wt N-domain as well as the solution structure of $Q^{122}FM(Y)F^{126}$ (Figure 3.3.8C). This means that the GTS loop has the flexibility to adopt different conformations even within wt N-domain. In fact, the GTS loop in the solution structures has very defined conformations, as backbone RMSD of the loop region (N30-M34) in wt N-domain and $Q^{122}FM(Y)F^{126}$ are 0.32 ± 0.28 Å and 0.05 ± 0.02 Å, respectively. This suggests that the observed GTS loop conformations are distinctly different equilibrium conformations. Close inspection of the GTS loop reveals that side-chains of the individual residues have different solvent exposure between the three structures, hinting at the possibility that alternative GTS loop conformations provide distinct functional groups for interaction. Functional implication of the GTS loop in stop-codon recognition had been reported (*61*). Furthermore, two different mutants of eRF1, *i.e.* T32A and S33A, were found to exhibit opposite effects on their *in vitro* release activity, namely 32/30/75% (for UAA/UAG/UGA) and 100/90/63%, respectively. Coincidentally, the side-chain of T32 in the structure of $Q^{122}FM(Y)F^{126}$ is hidden from the solvent, suggesting that T32 is not required for interacting with UGA (right panel in Figure 3.3.8C).

Interestingly, we found that in $Q^{122}FM(Y)F^{126}$, but not in wt N-domain, the resonance stemming from the hydroxyl proton of S70 can be observed

(Figure 3.3.7C), protected by potential hydrogen bonding to the carbonyl oxygen of S33 (Figure 3.3.8C). Residue S70 is critical for UGA-decoding, as point mutation S70A restricts eRF1 to recognize UAA and UAG only (*93*). Hence, the structure of $Q^{122}FM(Y)F^{126}$ has shown how S70 helps to stabilize the GTS loop in conformation that may be associated with UGA recognition.

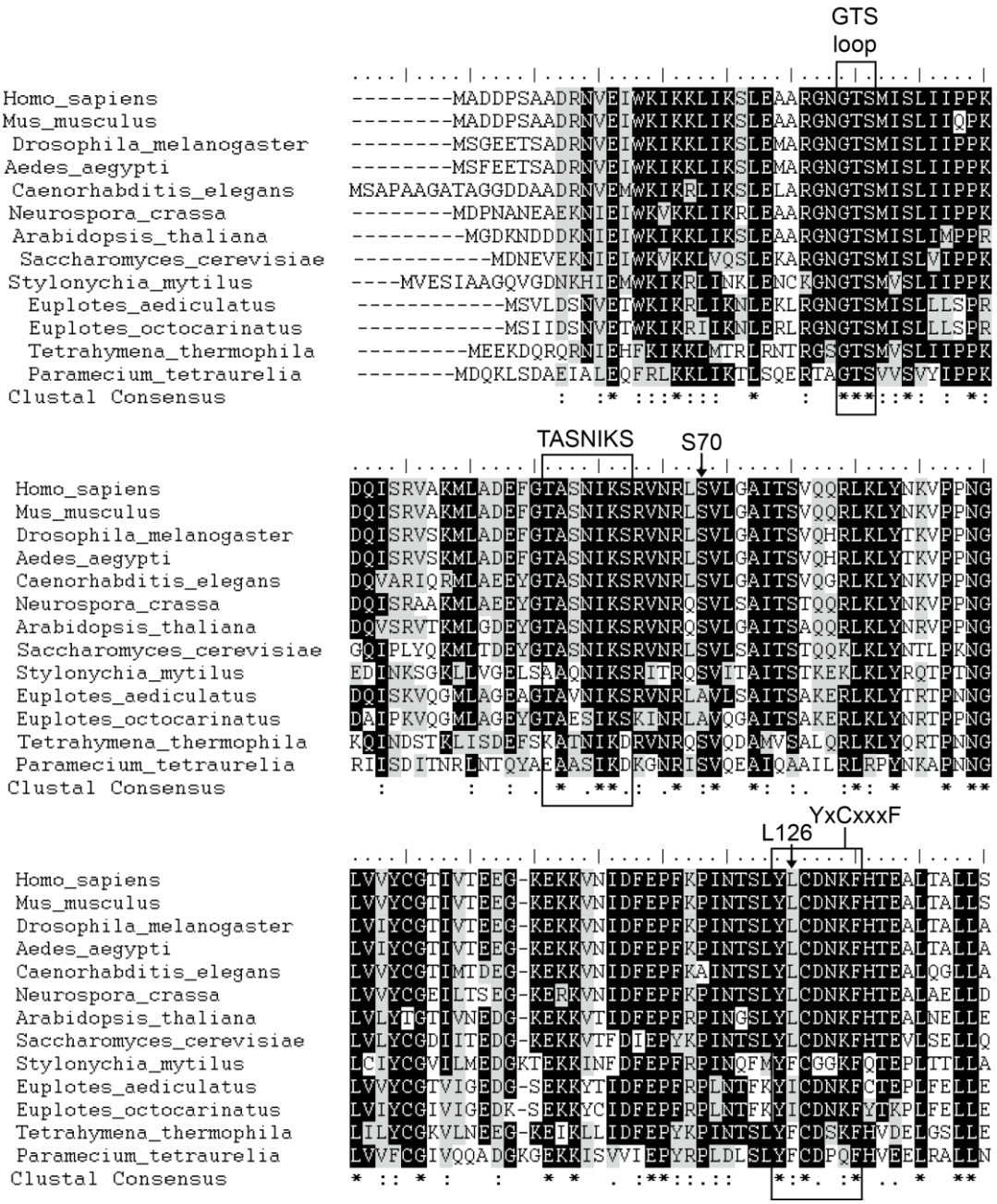

Figure 3.3.6: Sequence conservation of the GTS loop. Multiple sequence alignment of the amino acid sequences of eRF1 N-domain from different eukaryotic organisms using ClustalW2 online server (http://www.ebi.ac.uk/Tools/msa/clustalw2/). Numbering of the residues is according to the human's. The GTS loop is strictly conserved. Substitution S70A occurs in *E. aediculatus* and *E. octocarinatus*, which are variant-code organisms with UAR as stop-codons. Conversely, substitution L126F occurs in *S. mytilus*, *T. thermophila*, and *P. tetraurelia*, all of whichareunipotentfor UGA.

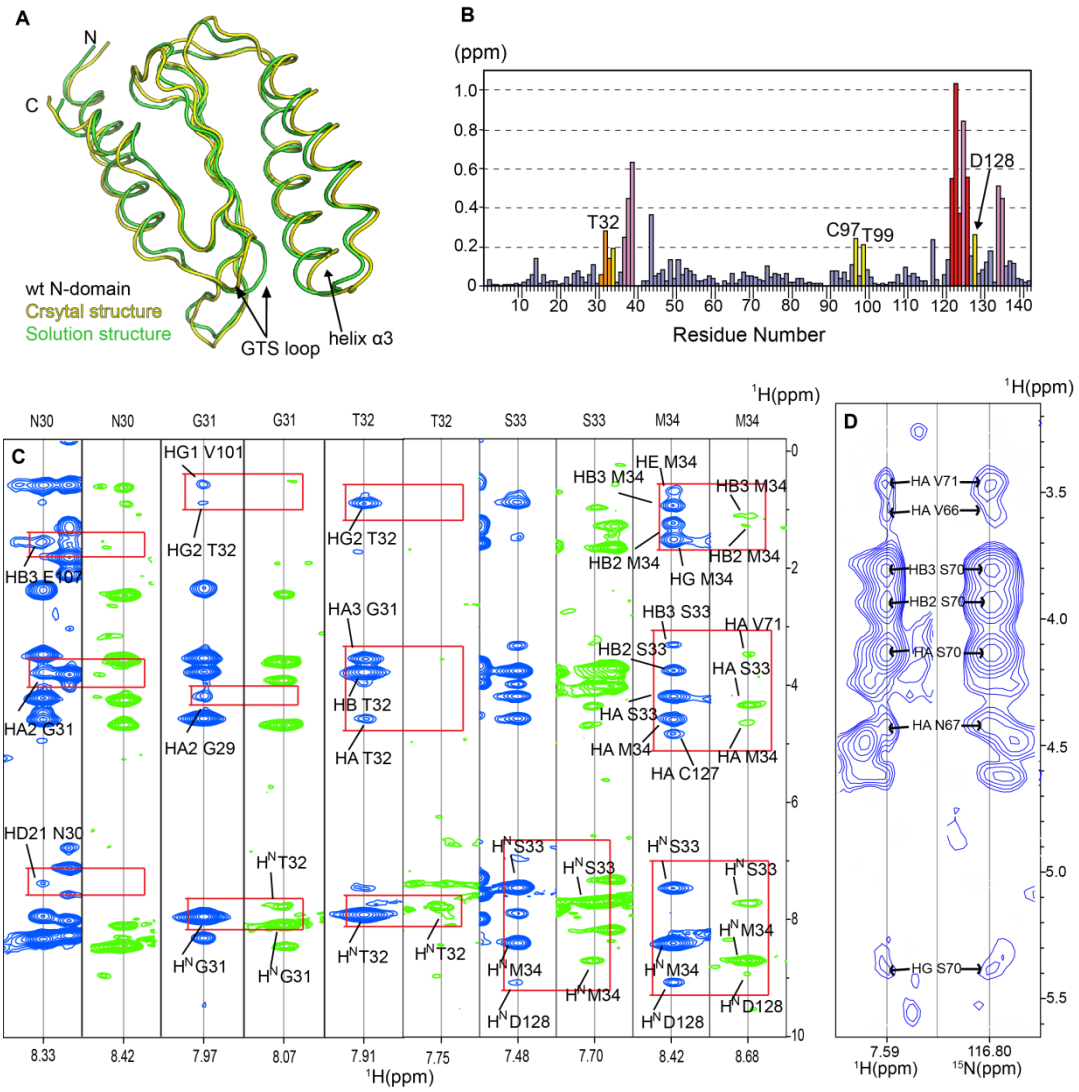

Figure 3.3.7: The GTS loop in $Q^{122}FM(Y)F^{126}$ has a conformation distinct from wt N-domain. (A) Superposition of the crystal structure (yellow) and solution structure (green) of wt N-domain, showing distinct conformations of the GTS loop and spatial deviation of helix α3. (B) Plot of the differences in amide chemical shift between wt N-domain and $Q^{122}FM(Y)F^{126}$ as calculated by $\Delta\delta_{NH} = [(\Delta\delta_H)^2 + (0.14*\Delta\delta_N)^2]^{1/2}$. Specific residues are highlighted as follows: point mutations (red), residues close to the point mutations in space (pink), the GTS loop (orange), and residues close to the GTS loop in space (yellow) (Figure 3.3.7B). (C) Differences in the NOE patterns as observed from the amides of N30 to M34 between wt N-domain (blue) and $Q^{122}FM(Y)F^{126}$ (green) show that their GTS loops have distinct conformations. (D) The NOE cross-peak of HG S70 as observed from the amide of S70 indicates participation of the hydroxyl group in hydrogen bonding. This NOE cross-peak was not observed in wt N-domain.

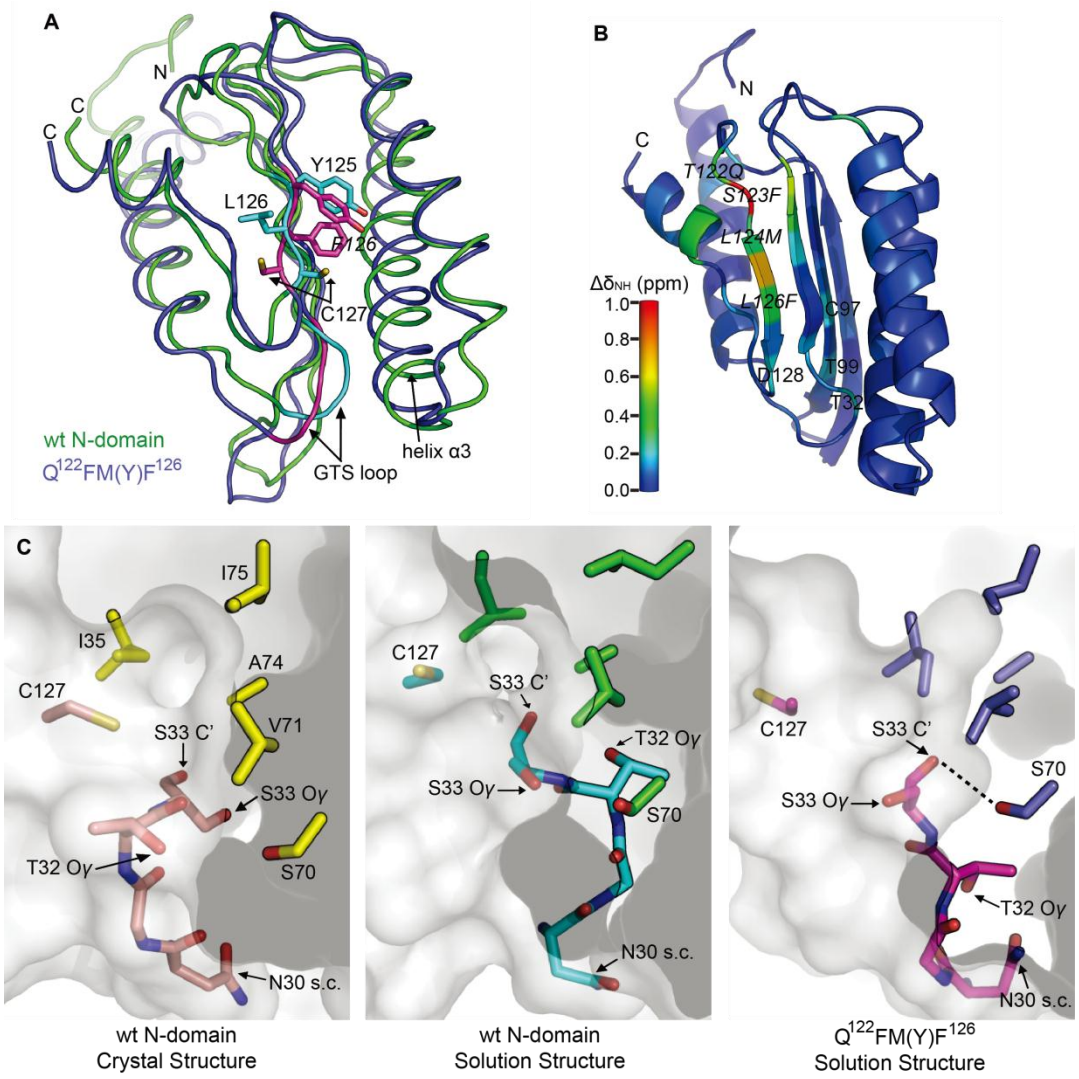

Figure 3.3.8: Structural comparison between wt N-domain and $Q^{122}FM(Y)F^{126}$. (A) Superposition of the solution structures of wt N-domain (green) and $Q^{122}FM(Y)F^{126}$ (blue). Regions that are structurally distinct between the two were highlighted in cyan (wt N-domain) and magenta ($Q^{122}FM(Y)F^{126}$). (B) Differences in amide chemical shift between wt N-domain and $Q^{122}FM(Y)F^{126}$ were calculated by $\Delta\delta_{NH} = [(\Delta\delta_H)^2 + (0.14*\Delta\delta_N)^2]^{1/2}$, and were mapped onto the structure of wt N-domain according to the color scale. The four mutated residues were denoted in italics. (C) Conformations of the GTS loop (residues N30 to S33) found in the crystal structure of wt N-domain (left panel), the solution structure of wt N-domain (middle panel), and the solution structure of $Q^{122}FM(Y)F^{126}$ (right panel). Positions of the residues that form the hydrophobic core above the GTS loop were shown by their side-chains only. Hydrogen bonding between the hydroxyl group of S70 and the carbonyl oxygen of S33 in $Q^{122}FM(Y)F^{126}$ mutant was denoted by a dashed line. The distance between the hydrogen donor and the acceptor is 2.67 ± 0.09 Å.

3.3.5 The GTS loop is a flexible ‘hotspot’

Heteronuclear relaxation parameters of wt N-domain and $Q^{122}FM(Y)F^{126}$ have shown that the GTS loop is relatively more dynamic than the bulk of N-domain on ps-ns timescale (Figure 3.3.9). It was reported that the ligand-binding sites are often found at or close to the flexible regions of the proteins (*114, 115*). Although it is not possible to localize the stop-codon binding site based on the fast timescale dynamics of N-domain, it is interesting to note that the GTS loop being one of the flexible ‘hotspots’ coincides with the structural discrepancy between wt N-domain and $Q^{122}FM(Y)F^{126}$ as well as the implicated functional role of the GTS loop in stop-codon recognition. A study had shown that flexible ‘hotspots’ on the ps-ns timescale in that particular protein are associated with the larger amplitude motions on the µs-ms timescale (*116*). It would be an attractive hypothesis to infer that the observed flexibility of the GTS loop on ps-ns timescale represents a prerequisite for it to switch between conformations upon encountering the stop-codon. Apparently, the dynamic properties of wt N-domain and $Q^{122}FM(Y)F^{126}$ do not differ significantly from each other (Figure 3.3.9). Hence, this led us to conclude that although the switching between omnipotency and unipotency of eRF1 can be sufficiently explained by the alteration of the GTS loop conformation, it is not reflected by the backbone relaxation data.

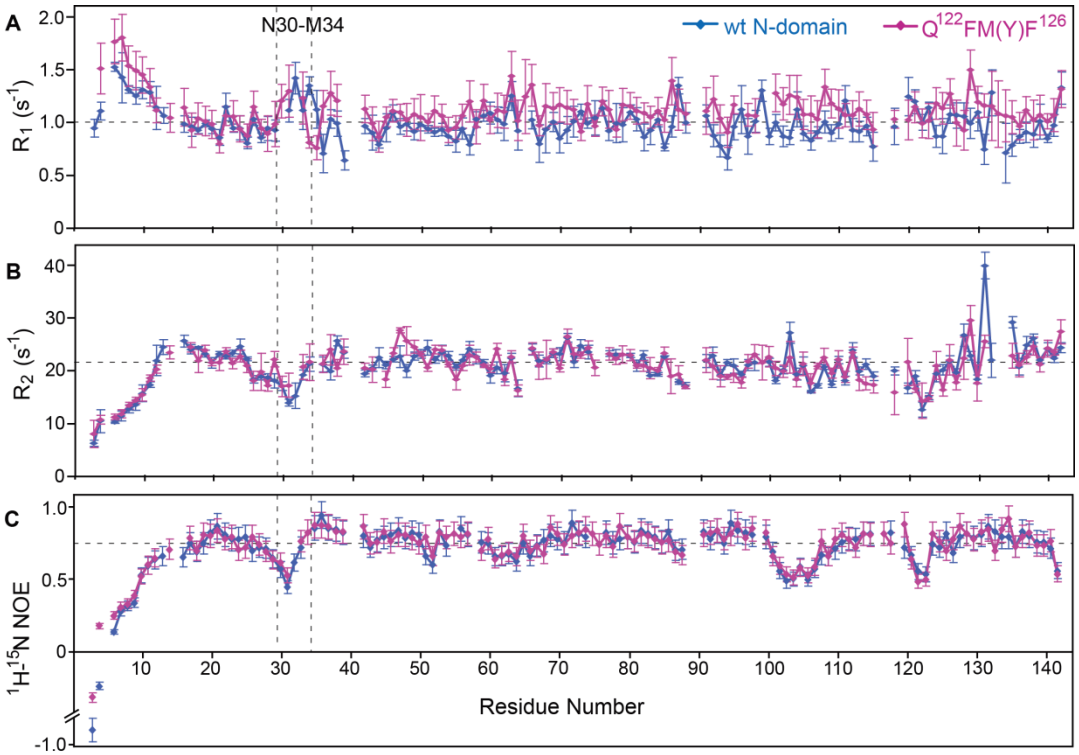

Figure 3.3.9: The dynamic properties of wt N-domain and $Q^{122}FM(Y)F^{126}$. Plots of the longitudinal relaxation rate R_1 (A), the transverse relaxation rate R_2 (B) and the heteronuclear ^{15}N, ^{1}H-steady-state NOE values (C) of the amide ^{15}N-nuclei of wt N-domain and $Q^{122}FM(Y)F^{126}$ measured at 25°C. The GTS loop region (N30-M34) is highlighted. The standard error is indicated by the error bars, and the average values of the respective relaxation parameters (residues 16-142) are indicated by horizontal dashed lines.

3.4 Structural characterization of Y125F mutant

3.4.1 Sequential assignment of Y125F

Assignments of amino acids of Y125F were performed by backbone ^{15}N and ^{13}C signals using 2D [^{1}H, ^{15}N]-TROSY (*99*) and 3D ^{15}N-NOESY-HSQC. The assignment process was facilitated by comparison with assignments from $Q^{122}FM(Y)F^{126}$ mutant.

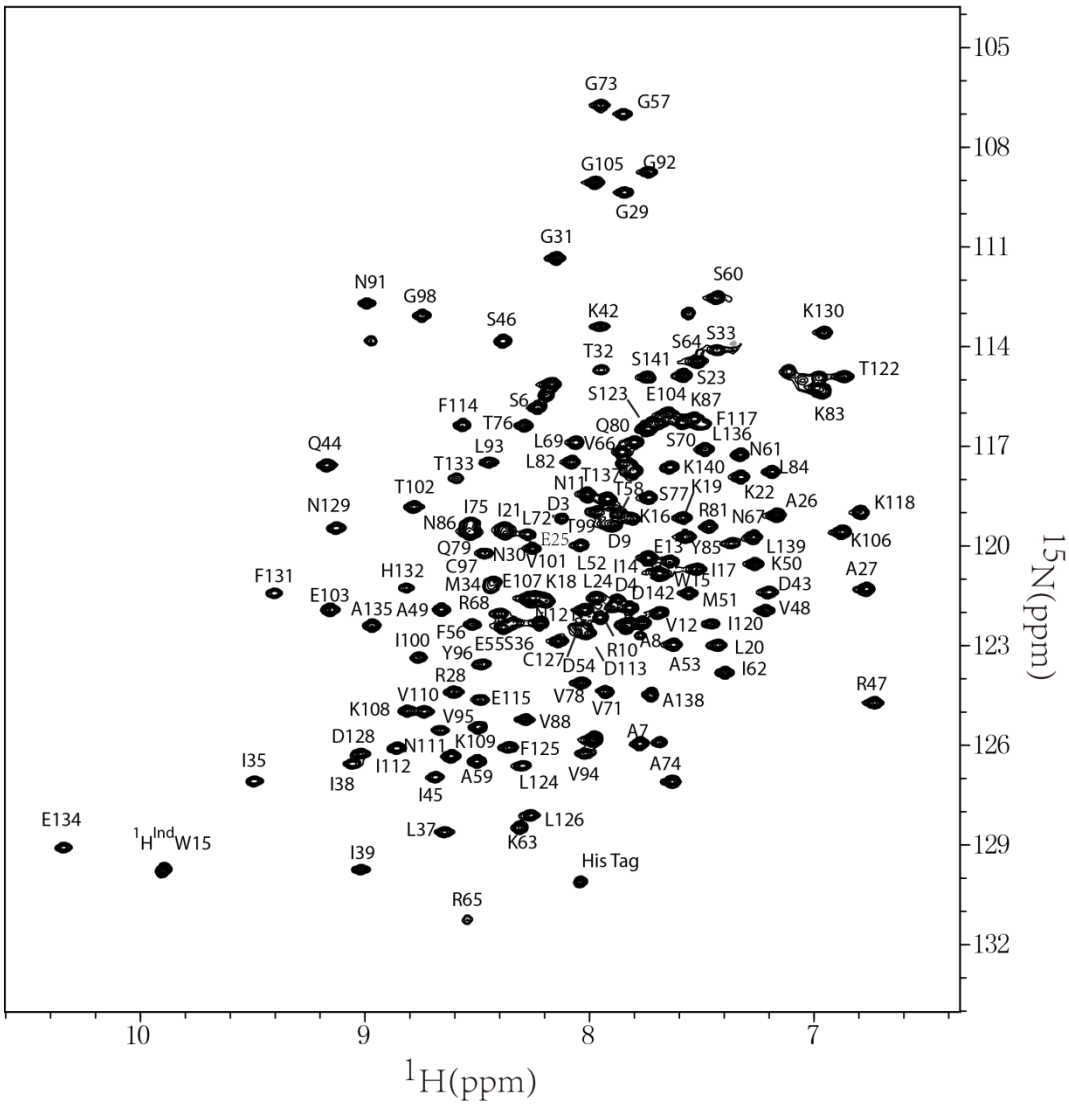

Figure 3.4.1: 2D [^{1}H, ^{15}N]-TROSY Spectrum of Y125F mutant. The cross-peaks show good dispersion and are labeled by the one-letter amino acid code and the residue number.

3.4.2 Structure determination of the Y125F mutant

NOE distance restraints for the calculated structures of Y125F mutant and E55Q mutant were obtained from ^{15}N-NOESY-HSQC. Totally, >98% of the complete backbone and >95% of the side-chain ^{1}H resonance of $Q^{122}FM(Y)F^{126}$ were assigned, including that of some aromatic rings. A total of 1333 distance restraints experimentally derived from NOEs, 77 distance restraints derived from hydrogen bonds. Also the distance restraints from crystal structure are used to help generate high quality structure.

Table 3.4: Structure statistics for the selected 20 structures of Y125F mutant[a]

NMR restraints	
Total unambiguous distance restraints	1333
Intra residual	413
Sequential (| i – j | = 1)	466
Short-range (| i – j | <=1)	879
Medium (2 ≤ | i – j | ≤ 4)	246
Long range (| i – j | ≥ 5)	208
Distance restraints[b]	1101
Hydrogen bond restraints	77
RMSD from the average atomic coordinates（residues 6-140, Å）	
Backbone atoms	0.82 ± 0.15
All heavy atoms	1.41 ± 0.13
Ramachandran analysis (%)	
Residues in most favored regions	82.1
Residues in additional allowed regions	16.3
Residues in generously allowed regions	1.5
Residues in disallowed regions	0.0

a None of the structure exhibits distance violations greater than 0.2 Å or dihedral angle violations greater than 5°.
b the distance restraints are from the crystal structure of eRF1 (*7*).

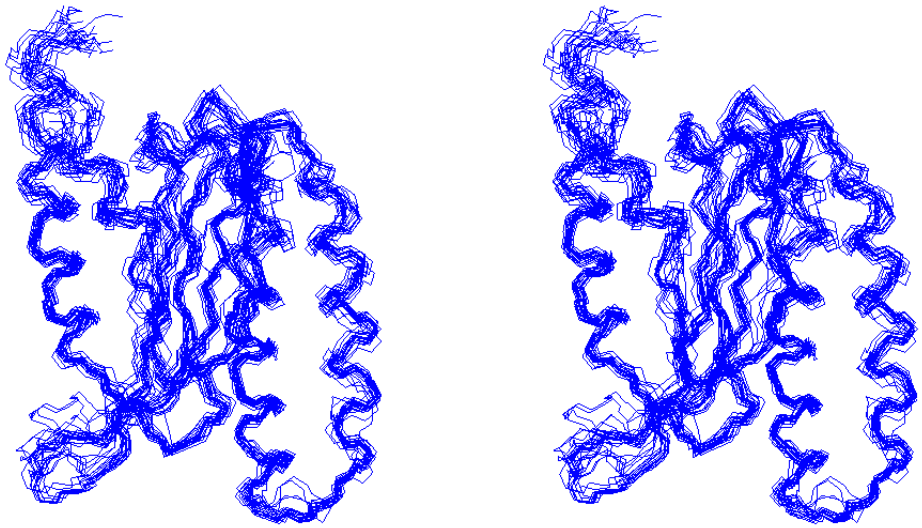

Figure 3.4.2: Three-dimensional solution structure of Y125F. 20 lowest energy conformers are shown in the lines representation.

3.4.3 Comparison of GTS loop conformations

YxCxxxF motif plays an important role in discrimination of stop codon (*69*). *Stylonychia* has the same UGA-only type of stop-codon recognition (*94*). By introducing the St-eRF1 pentapeptide QFMYF (positions 122–126), the UAA and UAG responses are eliminated in Hs-eRF1 (*97*).

Though comparing of structure of Y125F and the crystal structure of wild type N-domain, it is revealed that the conformations of GTS loops are quite similar (Figure 3.4.3). The side-chain of F125 and the side-chain of M51 are flipped out, and the distance between ^{1}Hβ of position 125 (Y125 in the wild type N-domain and F125 in the Y125F mutant) and ^{1}Hε of M51 increased

from 4.54 ± 0.12 Å to 8.05 ±0.16 Å. *In vitro* release factor activity of Y125F against UAA and UGA is similar with wild type, but the release factor activity against UAG is only one third of the wild type (Table 3.1). This is consistent with the obtained structural information of the mutant. In another study, it is revealed that in the pentapeptide QFMYF, Q^{122}, F^{123}, M^{124}, and F^{126} strongly affect the discrimination ability (*97*), and Y^{125} is a universal conserved residue (Figure 3.3.6) in different species. Possibly, the Y^{125} plays a less important role than the other four residues in the pentapeptide. The conformations of GTS loop in wild type and Y125F are similar, resulting in the similar release factor activity against UAA and UGA. However, the direction of side-chain of residue in position 125 is changed, which possibly reduce the ability to recognize UAG.

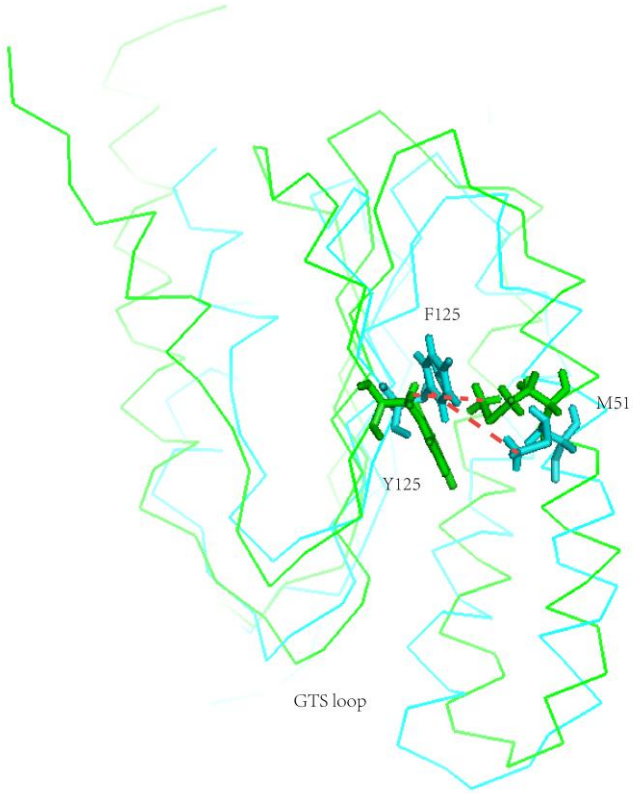

Figure 3.4.3: Superposition of the crystal structure of wt N-domain (green) and Y125F (cyan). The side-chains of residues in position 125 and 51 are shown in the sticks representation.

Chapter IV Discussion

4.1 Selectivity of stop-codon recognition is modulated by multiple GTS loop conformations

The strictly conserved GTS loop of N-domain is emerging as being implicated in decoding or even in direct contact with the stop-codon (*71, 117, 118*). The most significant insight from the finding of distinct GTS loop conformations in wild type N-domain and $Q^{122}FM(Y)F^{126}$ is that the bias in stop-codon selectivity is most probably determined not only by the structural determinants but rather a combination of structure and underlying conformational dynamics in the GTS loop, and not by the loss or replacement of certain amino acids by mutations in the remote region of the eRF1. Indeed, T32A mutant of eRF1 has been shown to exhibit tendency towards UGA-unipotency (*61*). By having the same amino acid sequence as wild type at the positions from 122 to 126, why is T32A mutant showing the same attribute as $Q^{122}FM(Y)F^{126}$? The same question can be asked about the various mutants isolated from previous studies. In many cases, the point mutations scattered across a large part of N-domain resulted in the same bias of stop-codon selectivity. This paradox can only be explained in two ways: (i) the loss of interaction with only one out of three nucleotides of a stop-codon could still support the peptide release for that particular stop-codon, or (ii) the different point mutations are responsible to modulate the structure of the part of N-domain that actually interacts with the

stop-codon. On top of these two scenarios, the interactions of N-domain with the ribosome might further augment the complexity of analysis.

In fact, there is sufficient experimental evidence to support and elaborate on the second scenario above. In the context of our proposed mechanism, point mutation that alters selectivity of stop-codon recognition is likely to modulate the structure of the GTS loop, or even its capacity to switch between different conformations. Indeed, many of these point mutations hit on the residues that constitute the hydrophobic core right above the GTS loop, *e.g.* I35, V71, V78, and C127 (*61, 72, 73*). Remarkably, the width of this hydrophobic core is directly related to the differential positioning of helix α3 as observed in the structures of wt N-domain and $Q^{122}FM(Y)F^{126}$ (Figure 3.3.9A & Figure 3.3.8A). The width, measured as the distance between the amides of M34 and V71, is reduced from 7.68 Å and 7.38 ± 0.18 Å in the crystal and solution structures of wt N-domain, respectively, to 6.56 ± 0.13 Å in $Q^{122}FM(Y)F^{126}$. In light of these observations, it is attractive to hypothesize that repositioning of helix α3 in N-domain occurs during stop-codon recognition as the GTS loop is sampling different configurations. Besides helix α3, helix α2 could also play a role in modulating the selectivity of stop-codon recognition. First of all, M51 and E55 on helix α2 are able to alter stop-codon recognition patterns (*72, 74*). Secondly, the TASNIKS motif was found to confer distinct requirement of eRF3 upon eRF1 on decoding

UAA/UAG and UGA (*73*). As T58 in the TASNIKS motif was observed to interact with the 15-mer RNA (experimental data on RNA binding is generated in K.Pervushin's lab and to be published elsewhere) and the NIKS motif had also been implicated in ribosome binding (*68*), interactions between helix α2 and the ribosome is highly possible. Furthermore, P41 and P89, which may be critical for the formation of the β-turns that connect the core β-sheet to helices α2 and α3, were also found to affect stop-codon recognition (*72, 119*).

4.2 RF activity of C127 mutants of eRF1 with omni-, bi- and uni-potent specificity

Although the distinct GTS loop conformation in $Q^{122}FM(Y)F^{126}$ compared to wt N-domain implicates a functional role of the GTS loop in stop-codon recognition, one may argue that loss of UAA- and UAG-decoding capability in the mutant might be caused by the substituted residues directly. To prove the non-direct implication of the 122-128 region of eRF1 in stop-codon decoding, the RF activity of the variant-code (*Euplotes*and *Stylonychia*) eRF1s with C127 mutations has been determined in an *in vitro* Caskey assay (*120*). C127 is an invariant residue in family of eRF1s and is located neighbor to F126 in the $Q^{122}FM(Y)F^{126}$ mutant that possesses the same stop-codon specificity as *Stylonychia* eRF1 (Figure 3.3.9A).

As was shown earlier C127A and C127S mutants of human eRF1 exhibited tendency towards UGA unipotency (*69*), while C127S mutant of *Euplotes* eRF1 restored efficient recognition of UGA stop-codon without changing of UAA and UAG stop-codon decoding in the readthrough RF assay (*73*). We have shown that C127A and C127S mutants of *Euplotes* eRF1 also restored recognition of UGA stop-codon but RF activity towards UAG was reduced for both mutants (Figure 4.). However, insertion of the same C127A and C127S mutations into *Stylonychia* eRF1 with UGA-only specificity caused total abolishment of RF activity towards UGA (Figure 4.1). The different effects of the same C127 mutation on the recognition of UGA by human, *Euplotes* and *Stylonychia*e RF1s are a very hard argument in favor of suggestion that C127 does not participate directly in UGA recognition.

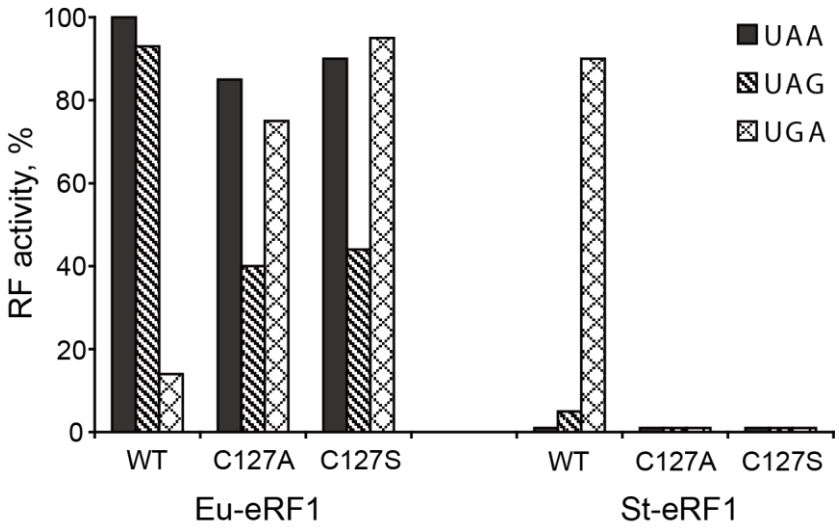

Figure 4.1: RF activity of C127 mutants of eRF1 with omni-, bi- and uni-potent specificity. *In vitro* RF activity of chimeric eRF1 constructs containing the whole N-terminal domains (positions 1-144) of *Euplotes* eRF1 (wt Eu-eRF1) or *Stylonychia* eRF1 (wt St-eRF1) and Eu-eRF1 and St-eRF1 mutants with C127 substitutions in the N-terminal domains. All eRF1 constructs contain MC-domain of human eRF1 (positions 145-437). (Data supplied by L. Frolova as private communication to K. Pervushin).

4.3 A model of N-domain bound in the pre-termination complex

Prior to solving the high-resolution structures of eRF1-bound pre-termination complex (pre-TC), understanding of the mechanism of translation termination in eukaryotes will have to rely on combining all the biochemical, structural, and genetics data from different studies. Our structural study of N-domain enable us to explain how eRF1 decodes different stop-codon by adopting distinct GTS loop conformations, thus implying direct access of the GTS loop to the stop-codon. In addition, the study on N-domain-RNA interactions has shown that N-domain potentially interacts with Helix 44 of 18S rRNA (the model is generated in

K.Pervushin's lab and to be published elsewhere). Based on these results, we propose a structural model that encompasses currently known interactions between N-domain of eRF1 and the A site of eukaryotic ribosome (Figure 4.2).

The model shows that it is possible for the GTS loop to contact the stop-codon while helix α1 is positioned next to the decoding region of Helix 44. Although helix α1 is not in the exact position to interact with Helix 44, a slight forward movement of the stop-codon towards the P site will compensate for this discrepancy. Interestingly, it was reported that 2-nt toeprint shift occurs when the eRF1·eRF3·GTP complex binds to the pre-TC (*76*). On the other side of N-domain, the side-chains of A53, N61, R65, R68, and Q79 are facing 18S rRNA. Residues R65 and R68 affect the binding of eRF1 to the ribosome (*68*), while each of the point mutants, A53K, N61K and Q79K/R, was shown to substantially reduce the level of stop-codon readthrough in comparison to wild type, indicating enhanced ribosome binding due to the lysine or arginine substitution (*121*). In our model, the GTS loop is close enough to the stop-codon to allow photoactivatable cross-linking with the second and third stop-codon positions (*71*). In the eRF1/pre-TC cross-linking experiments, the KSR loop (positions 63-65) and V66 were suggested to be in contact with the first stop-codon position (*70, 71*). Although within margins of cross-linking

experiments, in our model these residues are not located in the direct proximity of the uridine of the stop-codon, thereby requiring further experiments to resolve this issue.

In this orientation of N-domain, a hinge motion between N-domain and M-domain would allow the GGQ motif to reach the 3'-CAA tail of P-site tRNA, while C-domain would be required to move away from helix α1. The latter is well demonstrated by the competitive binding experiments (*122*) (experiments are performed in K.Pervushin's lab and to be published elsewhere). Hence, a major domain rearrangement between N-domain and C-domain is likely to occur during which N-domain accommodates itself into the A site.

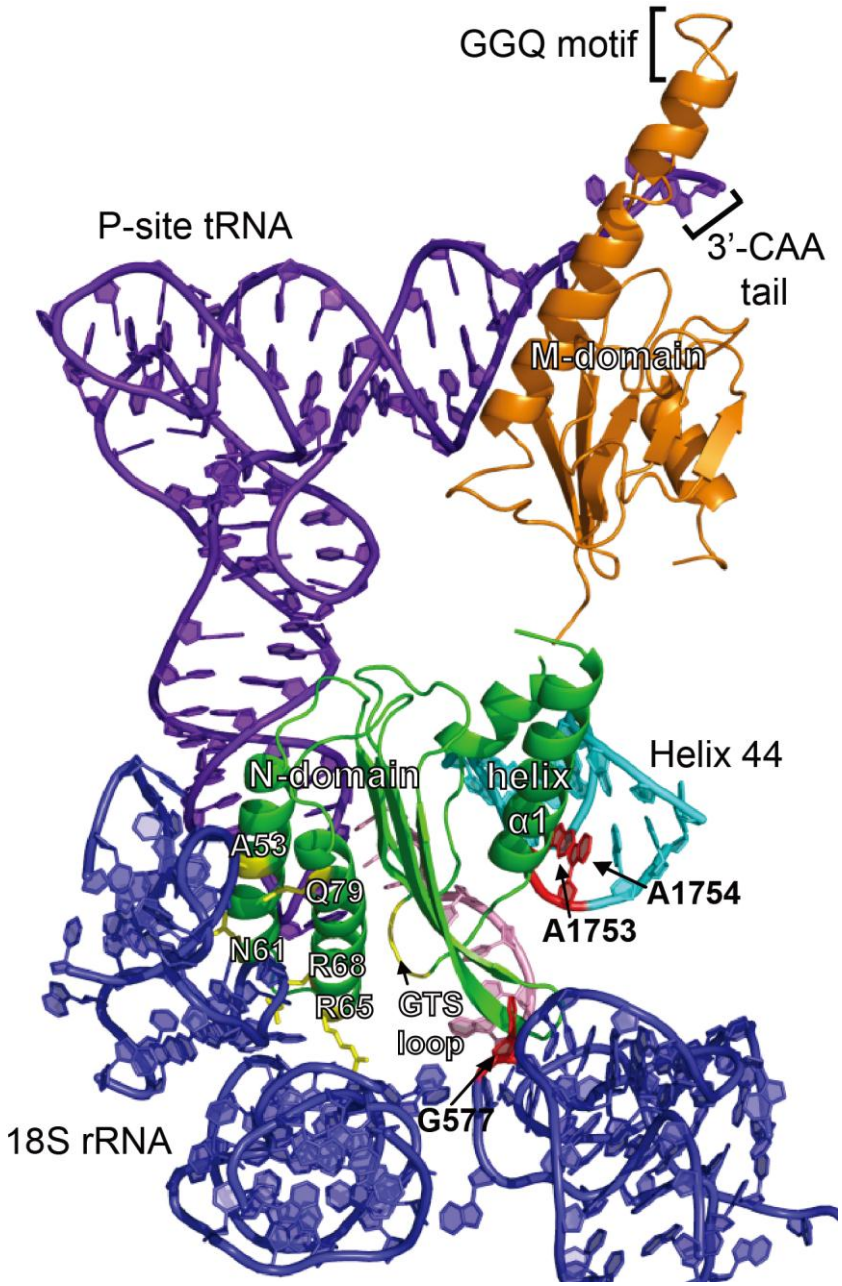

Figure 4.2: A model of eRF1 bound to the A site of eukaryotic ribosome. NM-domain of eRF1 (green and orange) was docked onto the A site of 18S rRNA (blue) with P-site bound tRNA (purple) and mRNA (pink) (PDB ID: 3IZ7), based on the insights derived from the interactions between helix α1 of N-domain and the decoding region of Helix 44 (cyan), as well as the putative role of the GTS loop in stop-codon recognition. The corresponding nucleotides critical for tRNA selection in prokaryotic ribosome and selected residues of eRF1 are highlighted in red and yellow, respectively.

4.4 Conclusions

In summary, by solving the solution structure of $Q^{122}FM(Y)F^{126}$ mutant, the Y125F mutant of eRF1 N-domain and the wild type N-domain, we built a correlation between the structure and the results of stop-codon recognition assays pointing to the strictly conserved GTS loop to be directly involved in the contact with mRNA. We propose that structural variability in the GTS loop may rely on the switching between omnipotency and unipotency of eRF1, implying the direct access of the GTS loop to the stop-codon. However, the details of the mechanism by which the class-I release factor recognize the stop-codons are not very clear, in future structures of different mutants need to be explored to clarify the details of the stop-codon recognition mechanism.

References

1. Wimberly, B. T., Brodersen, D. E., Clemons, W. M., Jr., Morgan-Warren, R. J., Carter, A. P., Vonrhein, C., Hartsch, T., and Ramakrishnan, V. (2000) Structure of the 30S ribosomal subunit, *Nature 407*, 327-339.
2. Brenner, S., Barnett, L., Katz, E. R., and Crick, F. H. (1967) UGA: a third nonsense triplet in the genetic code, *Nature 213*, 449-450.
3. Brenner, S., Stretton, A. O., and Kaplan, S. (1965) Genetic code: the 'nonsense' triplets for chain termination and their suppression, *Nature 206*, 994-998.
4. Scolnick, E., Tompkins, R., Caskey, T., and Nirenberg, M. (1968) Release factors differing in specificity for terminator codons, *Proc Natl Acad Sci U S A 61*, 768-774.
5. Capecchi, M. R., and Klein, H. A. (1969) Characterization of three proteins involved in polypeptide chain termination, *Cold Spring Harb Symp Quant Biol 34*, 469-477.
6. Scolnick, E. M., and Caskey, C. T. (1969) Peptide chain termination. V. The role of release factors in mRNA terminator codon recognition, *Proc Natl Acad Sci U S A 64*, 1235-1241.
7. Song, H., Mugnier, P., Das, A. K., Webb, H. M., Evans, D. R., Tuite, M. F., Hemmings, B. A., and Barford, D. (2000) The crystal structure of human eukaryotic release factor eRF1--mechanism of stop codon recognition and peptidyl-tRNA hydrolysis, *Cell 100*, 311-321.
8. Goldstein, J. L., Beaudet, A. L., and Caskey, C. T. (1970) Peptide chain termination with mammalian release factor, *Proc Natl Acad Sci U S A 67*, 99-106.
9. Konecki, D. S., Aune, K. C., Tate, W., and Caskey, C. T. (1977) Characterization of reticulocyte release factor, *J Biol Chem 252*, 4514-4520.
10. Frolova, L., Le Goff, X., Rasmussen, H. H., Cheperegin, S., Drugeon, G., Kress, M., Arman, I., Haenni, A. L., Celis, J. E., Philippe, M., and et al. (1994) A highly conserved eukaryotic protein family possessing properties of polypeptide chain release factor, *Nature 372*, 701-703.
11. Grentzmann, G., Brechemier-Baey, D., Heurgue, V., Mora, L., and Buckingham, R. H. (1994) Localization and characterization of the gene encoding release factor RF3 in Escherichia coli, *Proc Natl Acad Sci U S A 91*, 5848-5852.
12. Zhouravleva, G., Frolova, L., Le Goff, X., Le Guellec, R., Inge-Vechtomov, S., Kisselev, L., and Philippe, M. (1995) Termination of translation in eukaryotes is governed by two interacting polypeptide chain release factors, eRF1 and eRF3, *Embo J 14*, 4065-4072.
13. Laurberg, M., Asahara, H., Korostelev, A., Zhu, J., Trakhanov, S., and Noller, H. F. (2008) Structural basis for translation termination on the 70S ribosome, *Nature 454*, 852-857.
14. Ban, N., Nissen, P., Hansen, J., Moore, P. B., and Steitz, T. A. (2000) The complete atomic structure of the large ribosomal subunit at 2.4 A resolution, *Science 289*, 905-920.
15. Schluenzen, F., Tocilj, A., Zarivach, R., Harms, J., Gluehmann, M., Janell, D., Bashan, A., Bartels, H., Agmon, I., Franceschi, F., and Yonath, A. (2000) Structure of functionally activated small ribosomal subunit at 3.3 angstroms resolution, *Cell 102*, 615-623.
16. Czworkowski, J., Wang, J., Steitz, T. A., and Moore, P. B. (1994) The crystal structure of elongation factor G complexed with GDP, at 2.7 A resolution, *Embo J 13*, 3661-3668.

17. Nissen, P., Kjeldgaard, M., Thirup, S., Polekhina, G., Reshetnikova, L., Clark, B. F., and Nyborg, J. (1995) Crystal structure of the ternary complex of Phe-tRNAPhe, EF-Tu, and a GTP analog, *Science 270*, 1464-1472.
18. Ito, K., Ebihara, K., Uno, M., and Nakamura, Y. (1996) Conserved motifs in prokaryotic and eukaryotic polypeptide release factors: tRNA-protein mimicry hypothesis, *Proc Natl Acad Sci U S A 93*, 5443-5448.
19. Selmer, M., Al-Karadaghi, S., Hirokawa, G., Kaji, A., and Liljas, A. (1999) Crystal structure of Thermotoga maritima ribosome recycling factor: a tRNA mimic, *Science 286*, 2349-2352.
20. Ito, K., Uno, M., and Nakamura, Y. (2000) A tripeptide 'anticodon' deciphers stop codons in messenger RNA, *Nature 403*, 680-684.
21. Weixlbaumer, A., Jin, H., Neubauer, C., Voorhees, R. M., Petry, S., Kelley, A. C., and Ramakrishnan, V. (2008) Insights into translational termination from the structure of RF2 bound to the ribosome, *Science 322*, 953-956.
22. Jin, H., Kelley, A. C., Loakes, D., and Ramakrishnan, V. (2010) Structure of the 70S ribosome bound to release factor 2 and a substrate analog provides insights into catalysis of peptide release, *Proc Natl Acad Sci U S A 107*, 8593-8598.
23. Korostelev, A., Zhu, J., Asahara, H., and Noller, H. F. (2010) Recognition of the amber UAG stop codon by release factor RF1, *Embo J 29*, 2577-2585.
24. Freistroffer, D. V., Kwiatkowski, M., Buckingham, R. H., and Ehrenberg, M. (2000) The accuracy of codon recognition by polypeptide release factors, *Proc Natl Acad Sci U S A 97*, 2046-2051.
25. Jorgensen, F., Adamski, F. M., Tate, W. P., and Kurland, C. G. (1993) Release factor-dependent false stops are infrequent in Escherichia coli, *J Mol Biol 230*, 41-50.
26. Jenner, L. B., Demeshkina, N., Yusupova, G., and Yusupov, M. (2010) Structural aspects of messenger RNA reading frame maintenance by the ribosome, *Nat Struct Mol Biol 17*, 555-560.
27. Korostelev, A., Asahara, H., Lancaster, L., Laurberg, M., Hirschi, A., Zhu, J., Trakhanov, S., Scott, W. G., and Noller, H. F. (2008) Crystal structure of a translation termination complex formed with release factor RF2, *Proc Natl Acad Sci U S A 105*, 19684-19689.
28. Vestergaard, B., Van, L. B., Andersen, G. R., Nyborg, J., Buckingham, R. H., and Kjeldgaard, M. (2001) Bacterial polypeptide release factor RF2 is structurally distinct from eukaryotic eRF1, *Mol Cell 8*, 1375-1382.
29. Young, D. J., Edgar, C. D., Poole, E. S., and Tate, W. P. (2010) The codon specificity of eubacterial release factors is determined by the sequence and size of the recognition loop, *Rna 16*, 1623-1633.
30. Field, A., Hetrick, B., Mathew, M., and Joseph, S. (2010) Histidine 197 in release factor 1 is essential for a site binding and peptide release, *Biochemistry 49*, 9385-9390.
31. Basu, G., Sivanesan, D., Kawabata, T., and Go, N. (2004) Electrostatic potential of nucleotide-free protein is sufficient for discrimination between adenine and guanine-specific binding sites, *J Mol Biol 342*, 1053-1066.
32. Poole, E. S., Brown, C. M., and Tate, W. P. (1995) The identity of the base following the stop codon determines the efficiency of in vivo translational termination in Escherichia

coli, *Embo J 14*, 151-158.

33. Schmeing, T. M., Huang, K. S., Strobel, S. A., and Steitz, T. A. (2005) An induced-fit mechanism to promote peptide bond formation and exclude hydrolysis of peptidyl-tRNA, *Nature 438*, 520-524.
34. Frolova, L. Y., Tsivkovskii, R. Y., Sivolobova, G. F., Oparina, N. Y., Serpinsky, O. I., Blinov, V. M., Tatkov, S. I., and Kisselev, L. L. (1999) Mutations in the highly conserved GGQ motif of class 1 polypeptide release factors abolish ability of human eRF1 to trigger peptidyl-tRNA hydrolysis, *Rna 5*, 1014-1020.
35. Shaw, J. J., and Green, R. (2007) Two distinct components of release factor function uncovered by nucleophile partitioning analysis, *Mol Cell 28*, 458-467.
36. Trobro, S., and Aqvist, J. (2007) A model for how ribosomal release factors induce peptidyl-tRNA cleavage in termination of protein synthesis, *Mol Cell 27*, 758-766.
37. Seit-Nebi, A., Frolova, L., Justesen, J., and Kisselev, L. (2001) Class-1 translation termination factors: invariant GGQ minidomain is essential for release activity and ribosome binding but not for stop codon recognition, *Nucleic Acids Res 29*, 3982-3987.
38. Mora, L., Heurgue-Hamard, V., Champ, S., Ehrenberg, M., Kisselev, L. L., and Buckingham, R. H. (2003) The essential role of the invariant GGQ motif in the function and stability in vivo of bacterial release factors RF1 and RF2, *Mol Microbiol 47*, 267-275.
39. Dincbas-Renqvist, V., Engstrom, A., Mora, L., Heurgue-Hamard, V., Buckingham, R., and Ehrenberg, M. (2000) A post-translational modification in the GGQ motif of RF2 from Escherichia coli stimulates termination of translation, *Embo J 19*, 6900-6907.
40. Zavialov, A. V., Mora, L., Buckingham, R. H., and Ehrenberg, M. (2002) Release of peptide promoted by the GGQ motif of class 1 release factors regulates the GTPase activity of RF3, *Mol Cell 10*, 789-798.
41. Trobro, S., and Aqvist, J. (2009) Mechanism of the translation termination reaction on the ribosome, *Biochemistry 48*, 11296-11303.
42. Youngman, E. M., Brunelle, J. L., Kochaniak, A. B., and Green, R. (2004) The active site of the ribosome is composed of two layers of conserved nucleotides with distinct roles in peptide bond formation and peptide release, *Cell 117*, 589-599.
43. Brunelle, J. L., Shaw, J. J., Youngman, E. M., and Green, R. (2008) Peptide release on the ribosome depends critically on the 2' OH of the peptidyl-tRNA substrate, *Rna 14*, 1526-1531.
44. Zaher, H. S., Shaw, J. J., Strobel, S. A., and Green, R. (2011) The 2'-OH group of the peptidyl-tRNA stabilizes an active conformation of the ribosomal PTC, *Embo J 30*, 2445-2453.
45. Shin, D. H., Brandsen, J., Jancarik, J., Yokota, H., Kim, R., and Kim, S. H. (2004) Structural analyses of peptide release factor 1 from Thermotoga maritima reveal domain flexibility required for its interaction with the ribosome, *J Mol Biol 341*, 227-239.
46. Vestergaard, B., Sanyal, S., Roessle, M., Mora, L., Buckingham, R. H., Kastrup, J. S., Gajhede, M., Svergun, D. I., and Ehrenberg, M. (2005) The SAXS solution structure of RF1 differs from its crystal structure and is similar to its ribosome bound cryo-EM structure, *Mol Cell 20*, 929-938.

47. Zoldak, G., Redecke, L., Svergun, D. I., Konarev, P. V., Voertler, C. S., Dobbek, H., Sedlak, E., and Sprinzl, M. (2007) Release factors 2 from Escherichia coli and Thermus thermophilus: structural, spectroscopic and microcalorimetric studies, *Nucleic Acids Res 35*, 1343-1353.
48. He, S. L., and Green, R. (2010) Visualization of codon-dependent conformational rearrangements during translation termination, *Nat Struct Mol Biol 17*, 465-470.
49. Hetrick, B., Lee, K., and Joseph, S. (2009) Kinetics of stop codon recognition by release factor 1, *Biochemistry 48*, 11178-11184.
50. Kisselev, L., Ehrenberg, M., and Frolova, L. (2003) Termination of translation: interplay of mRNA, rRNAs and release factors?, *Embo J 22*, 175-182.
51. Freistroffer, D. V., Pavlov, M. Y., MacDougall, J., Buckingham, R. H., and Ehrenberg, M. (1997) Release factor RF3 in E.coli accelerates the dissociation of release factors RF1 and RF2 from the ribosome in a GTP-dependent manner, *Embo J 16*, 4126-4133.
52. Grentzmann, G., Kelly, P. J., Laalami, S., Shuda, M., Firpo, M. A., Cenatiempo, Y., and Kaji, A. (1998) Release factor RF-3 GTPase activity acts in disassembly of the ribosome termination complex, *Rna 4*, 973-983.
53. Mikuni, O., Ito, K., Moffat, J., Matsumura, K., McCaughan, K., Nobukuni, T., Tate, W., and Nakamura, Y. (1994) Identification of the prfC gene, which encodes peptide-chain-release factor 3 of Escherichia coli, *Proc Natl Acad Sci U S A 91*, 5798-5802.
54. Zavialov, A. V., Buckingham, R. H., and Ehrenberg, M. (2001) A posttermination ribosomal complex is the guanine nucleotide exchange factor for peptide release factor RF3, *Cell 107*, 115-124.
55. Klaholz, B. P., Myasnikov, A. G., and Van Heel, M. (2004) Visualization of release factor 3 on the ribosome during termination of protein synthesis, *Nature 427*, 862-865.
56. Gao, H., Zhou, Z., Rawat, U., Huang, C., Bouakaz, L., Wang, C., Cheng, Z., Liu, Y., Zavialov, A., Gursky, R., Sanyal, S., Ehrenberg, M., Frank, J., and Song, H. (2007) RF3 induces ribosomal conformational changes responsible for dissociation of class I release factors, *Cell 129*, 929-941.
57. Valle, M., Sengupta, J., Swami, N. K., Grassucci, R. A., Burkhardt, N., Nierhaus, K. H., Agrawal, R. K., and Frank, J. (2002) Cryo-EM reveals an active role for aminoacyl-tRNA in the accommodation process, *Embo J 21*, 3557-3567.
58. Spahn, C. M., Blaha, G., Agrawal, R. K., Penczek, P., Grassucci, R. A., Trieber, C. A., Connell, S. R., Taylor, D. E., Nierhaus, K. H., and Frank, J. (2001) Localization of the ribosomal protection protein Tet(O) on the ribosome and the mechanism of tetracycline resistance, *Mol Cell 7*, 1037-1045.
59. Frolova, L. Y., Merkulova, T. I., and Kisselev, L. L. (2000) Translation termination in eukaryotes: polypeptide release factor eRF1 is composed of functionally and structurally distinct domains, *Rna 6*, 381-390.
60. Ito, K., Ebihara, K., and Nakamura, Y. (1998) The stretch of C-terminal acidic amino acids of translational release factor eRF1 is a primary binding site for eRF3 of fission yeast, *Rna 4*, 958-972.
61. Cheng, Z., Saito, K., Pisarev, A. V., Wada, M., Pisareva, V. P., Pestova, T. V., Gajda, M., Round, A., Kong, C., Lim, M., Nakamura, Y., Svergun, D. I., Ito, K., and Song, H. (2009)

Structural insights into eRF3 and stop codon recognition by eRF1, *Genes Dev 23*, 1106-1118.

62. Merkulova, T. I., Frolova, L. Y., Lazar, M., Camonis, J., and Kisselev, L. L. (1999) C-terminal domains of human translation termination factors eRF1 and eRF3 mediate their in vivo interaction, *FEBS Lett 443*, 41-47.
63. Eurwilaichitr, L., Graves, F. M., Stansfield, I., and Tuite, M. F. (1999) The C-terminus of eRF1 defines a functionally important domain for translation termination in Saccharomyces cerevisiae, *Mol Microbiol 32*, 485-496.
64. Ebihara, K., and Nakamura, Y. (1999) C-terminal interaction of translational release factors eRF1 and eRF3 of fission yeast: G-domain uncoupled binding and the role of conserved amino acids, *Rna 5*, 739-750.
65. Ben-Shem, A., Garreau de Loubresse, N., Melnikov, S., Jenner, L., Yusupova, G., and Yusupov, M. (2011) The structure of the eukaryotic ribosome at 3.0 A resolution, *Science 334*, 1524-1529.
66. Ben-Shem, A., Jenner, L., Yusupova, G., and Yusupov, M. (2010) Crystal structure of the eukaryotic ribosome, *Science 330*, 1203-1209.
67. Ito, K., Frolova, L., Seit-Nebi, A., Karamyshev, A., Kisselev, L., and Nakamura, Y. (2002) Omnipotent decoding potential resides in eukaryotic translation termination factor eRF1 of variant-code organisms and is modulated by the interactions of amino acid sequences within domain 1, *Proc Natl Acad Sci U S A 99*, 8494-8499.
68. Frolova, L., Seit-Nebi, A., and Kisselev, L. (2002) Highly conserved NIKS tetrapeptide is functionally essential in eukaryotic translation termination factor eRF1, *Rna 8*, 129-136.
69. Seit-Nebi, A., Frolova, L., and Kisselev, L. (2002) Conversion of omnipotent translation termination factor eRF1 into ciliate-like UGA-only unipotent eRF1, *EMBO Rep 3*, 881-886.
70. Chavatte, L., Seit-Nebi, A., Dubovaya, V., and Favre, A. (2002) The invariant uridine of stop codons contacts the conserved NIKSR loop of human eRF1 in the ribosome, *Embo J 21*, 5302-5311.
71. Bulygin, K. N., Khairulina, Y. S., Kolosov, P. M., Ven'yaminova, A. G., Graifer, D. M., Vorobjev, Y. N., Frolova, L. Y., Kisselev, L. L., and Karpova, G. G. (2010) Three distinct peptides from the N domain of translation termination factor eRF1 surround stop codon in the ribosome, *Rna 16*, 1902-1914.
72. Bertram, G., Bell, H. A., Ritchie, D. W., Fullerton, G., and Stansfield, I. (2000) Terminating eukaryote translation: domain 1 of release factor eRF1 functions in stop codon recognition, *Rna 6*, 1236-1247.
73. Fan-Minogue, H., and Bedwell, D. M. (2008) Eukaryotic ribosomal RNA determinants of aminoglycoside resistance and their role in translational fidelity, *Rna 14*, 148-157.
74. Kolosov, P., Frolova, L., Seit-Nebi, A., Dubovaya, V., Kononenko, A., Oparina, N., Justesen, J., Efimov, A., and Kisselev, L. (2005) Invariant amino acids essential for decoding function of polypeptide release factor eRF1, *Nucleic Acids Res 33*, 6418-6425.
75. Kong, C., Ito, K., Walsh, M. A., Wada, M., Liu, Y., Kumar, S., Barford, D., Nakamura, Y., and Song, H. (2004) Crystal structure and functional analysis of the eukaryotic class II release factor eRF3 from S. pombe, *Mol Cell 14*, 233-245.

76. Alkalaeva, E. Z., Pisarev, A. V., Frolova, L. Y., Kisselev, L. L., and Pestova, T. V. (2006) In vitro reconstitution of eukaryotic translation reveals cooperativity between release factors eRF1 and eRF3, *Cell 125*, 1125-1136.
77. Frolova, L., Le Goff, X., Zhouravleva, G., Davydova, E., Philippe, M., and Kisselev, L. (1996) Eukaryotic polypeptide chain release factor eRF3 is an eRF1- and ribosome-dependent guanosine triphosphatase, *Rna 2*, 334-341.
78. Kononenko, A. V., Mitkevich, V. A., Dubovaya, V. I., Kolosov, P. M., Makarov, A. A., and Kisselev, L. L. (2008) Role of the individual domains of translation termination factor eRF1 in GTP binding to eRF3, *Proteins 70*, 388-393.
79. Baierlein, C., and Krebber, H. (2010) Translation termination: new factors and insights, *RNA Biol 7*, 548-550.
80. Orlova, M., Yueh, A., Leung, J., and Goff, S. P. (2003) Reverse transcriptase of Moloney murine leukemia virus binds to eukaryotic release factor 1 to modulate suppression of translational termination, *Cell 115*, 319-331.
81. Gross, T., Siepmann, A., Sturm, D., Windgassen, M., Scarcelli, J. J., Seedorf, M., Cole, C. N., and Krebber, H. (2007) The DEAD-box RNA helicase Dbp5 functions in translation termination, *Science 315*, 646-649.
82. Bolger, T. A., Folkmann, A. W., Tran, E. J., and Wente, S. R. (2008) The mRNA export factor Gle1 and inositol hexakisphosphate regulate distinct stages of translation, *Cell 134*, 624-633.
83. Weirich, C. S., Erzberger, J. P., Flick, J. S., Berger, J. M., Thorner, J., and Weis, K. (2006) Activation of the DExD/H-box protein Dbp5 by the nuclear-pore protein Gle1 and its coactivator InsP6 is required for mRNA export, *Nat Cell Biol 8*, 668-676.
84. Khoshnevis, S., Gross, T., Rotte, C., Baierlein, C., Ficner, R., and Krebber, H. (2010) The iron-sulphur protein RNase L inhibitor functions in translation termination, *EMBO Rep 11*, 214-219.
85. Konecki, D. S., Aune, K. C., Tate, W., and Caskey, C. T. (1977) Characterization of reticulocyte release factor, *J Biol Chem 252*, 4514-4520.
86. Klaholz, B. P., Pape, T., Zavialov, A. V., Myasnikov, A. G., Orlova, E. V., Vestergaard, B., Ehrenberg, M., and van Heel, M. (2003) Structure of the Escherichia coli ribosomal termination complex with release factor 2, *Nature 421*, 90-94.
87. Ma, B., and Nussinov, R. (2004) Release factors eRF1 and RF2: a universal mechanism controls the large conformational changes, *J Biol Chem 279*, 53875-53885.
88. Hauryliuk, V., Zavialov, A., Kisselev, L., and Ehrenberg, M. (2006) Class-1 release factor eRF1 promotes GTP binding by class-2 release factor eRF3, *Biochimie 88*, 747-757.
89. Pisareva, V. P., Pisarev, A. V., Hellen, C. U., Rodnina, M. V., and Pestova, T. V. (2006) Kinetic analysis of interaction of eukaryotic release factor 3 with guanine nucleotides, *J Biol Chem 281*, 40224-40235.
90. Salas-Marco, J., and Bedwell, D. M. (2004) GTP hydrolysis by eRF3 facilitates stop codon decoding during eukaryotic translation termination, *Mol Cell Biol 24*, 7769-7778.
91. Mitkevich, V. A., Kononenko, A. V., Petrushanko, I. Y., Yanvarev, D. V., Makarov, A. A., and Kisselev, L. L. (2006) Termination of translation in eukaryotes is mediated by the

quaternary eRF1*eRF3*GTP*Mg2+ complex. The biological roles of eRF3 and prokaryotic RF3 are profoundly distinct, *Nucleic Acids Res 34*, 3947-3954.

92. Liang, H., Wong, J. Y., Bao, Q., Cavalcanti, A. R., and Landweber, L. F. (2005) Decoding the decoding region: analysis of eukaryotic release factor (eRF1) stop codon-binding residues, *J Mol Evol 60*, 337-344.
93. Eliseev, B., Kryuchkova, P., Alkalaeva, E., and Frolova, L. (2011) A single amino acid change of translation termination factor eRF1 switches between bipotent and omnipotent stop-codon specificity, *Nucleic Acids Res 39*, 599-608.
94. Lozupone, C. A., Knight, R. D., and Landweber, L. F. (2001) The molecular basis of nuclear genetic code change in ciliates, *Curr Biol 11*, 65-74.
95. Chavatte, L., Kervestin, S., Favre, A., and Jean-Jean, O. (2003) Stop codon selection in eukaryotic translation termination: comparison of the discriminating potential between human and ciliate eRF1s, *Embo J 22*, 1644-1653.
96. Kervestin, S., Frolova, L., Kisselev, L., and Jean-Jean, O. (2001) Stop codon recognition in ciliates: Euplotes release factor does not respond to reassigned UGA codon, *EMBO Rep 2*, 680-684.
97. Lekomtsev, S., Kolosov, P., Bidou, L., Frolova, L., Rousset, J. P., and Kisselev, L. (2007) Different modes of stop codon restriction by the Stylonychia and Paramecium eRF1 translation termination factors, *Proc Natl Acad Sci U S A 104*, 10824-10829.
98. Dubovaia, V. I., Kolosov, P. M., Alkalaeva, E. Z., Frolova, L., and Kiselev, L. L. (2006) [Influence of individual domains of the translation termination factor eRF1 on induction of the GTPase activity of the translation termination factor eRF3], *Mol Biol (Mosk) 40*, 310-316.
99. Pervushin, K., Riek, R., Wider, G., and Wuthrich, K. (1997) Attenuated T2 relaxation by mutual cancellation of dipole-dipole coupling and chemical shift anisotropy indicates an avenue to NMR structures of very large biological macromolecules in solution, *Proc Natl Acad Sci U S A 94*, 12366-12371.
100. Kelly, M. J., Krieger, C., Ball, L. J., Yu, Y., Richter, G., Schmieder, P., Bacher, A., and Oschkinat, H. (1999) Application of amino acid type-specific 1H- and 14N-labeling in a 2H-, 15N-labeled background to a 47 kDa homodimer: potential for NMR structure determination of large proteins, *J Biomol NMR 14*, 79-83.
101. Kainosho, M., and Tsuji, T. (1982) Assignment of the three methionyl carbonyl carbon resonances in Streptomyces subtilisin inhibitor by a carbon-13 and nitrogen-15 double-labeling technique. A new strategy for structural studies of proteins in solution, *Biochemistry 21*, 6273-6279.
102. Yabuki, T., Kigawa, T., Dohmae, N., Takio, K., Terada, T., Ito, Y., Laue, E. D., Cooper, J. A., Kainosho, M., and Yokoyama, S. (1998) Dual amino acid-selective and site-directed stable-isotope labeling of the human c-Ha-Ras protein by cell-free synthesis, *J Biomol NMR 11*, 295-306.
103. Oda, Y., Muramatsu, T., Yumoto, F., Ito, M., and Tanokura, M. (2004) Backbone (1)H, (13)C and (15)N resonance assignment of the N-terminal domain of human eRF1, *J Biomol NMR 30*, 109-110.

104. Ivanova, E. V., Kolosov, P. M., Birdsall, B., Kisselev, L. L., and Polshakov, V. I. (2006) NMR assignments of the middle domain of human polypeptide release factor eRF1, *J Biomol NMR 36 Suppl 1*, 8.

105. Mantsyzov, A. B., Ivanova, E. V., Birdsall, B., Kolosov, P. M., Kisselev, L. L., and Polshakov, V. I. (2007) NMR assignments of the C-terminal domain of human polypeptide release factor eRF1, *Biomol NMR Assign 1*, 183-185.

106. Zweckstetter, M. (2008) NMR: prediction of molecular alignment from structure using the PALES software, *Nat Protoc 3*, 679-690.

107. Cornilescu, G., Delaglio, F., and Bax, A. (1999) Protein backbone angle restraints from searching a database for chemical shift and sequence homology, *J Biomol NMR 13*, 289-302.

108. Guntert, P., Mumenthaler, C., and Wuthrich, K. (1997) Torsion angle dynamics for NMR structure calculation with the new program DYANA, *J Mol Biol 273*, 283-298.

109. Herrmann, T., Guntert, P., and Wuthrich, K. (2002) Protein NMR structure determination with automated NOE assignment using the new software CANDID and the torsion angle dynamics algorithm DYANA, *J Mol Biol 319*, 209-227.

110. Koradi, R., Billeter, M., and Wuthrich, K. (1996) MOLMOL: a program for display and analysis of macromolecular structures, *J Mol Graph 14*, 51-55, 29-32.

111. Laskowski, R. A., Rullmannn, J. A., MacArthur, M. W., Kaptein, R., and Thornton, J. M. (1996) AQUA and PROCHECK-NMR: programs for checking the quality of protein structures solved by NMR, *J Biomol NMR 8*, 477-486.

112. Cornilescu, G., Delaglio, F., and Bax, A. (1999) Protein backbone angle restraints from searching a database for chemical shift and sequence homology, *Journal of Biomolecular Nmr 13*, 289-302.

113. Guntert, P., Mumenthaler, C., and Wuthrich, K. (1997) Torsion angle dynamics for NMR structure calculation with the new program DYANA, *Journal of Molecular Biology 273*, 283-298.

114. Jarymowycz, V. A., and Stone, M. J. (2006) Fast time scale dynamics of protein backbones: NMR relaxation methods, applications, and functional consequences, *Chem Rev 106*, 1624-1671.

115. Ishima, R., and Torchia, D. A. (2000) Protein dynamics from NMR, *Nat Struct Biol 7*, 740-743.

116. Henzler-Wildman, K. A., Lei, M., Thai, V., Kerns, S. J., Karplus, M., and Kern, D. (2007) A hierarchy of timescales in protein dynamics is linked to enzyme catalysis, *Nature 450*, 913-916.

117. Wang, Y., Chai, B., Wang, W., and Liang, A. (2010) Functional characterization of polypeptide release factor 1b in the ciliate Euplotes, *Biosci Rep 30*, 425-431.

118. Bulygin, K. N., Khairulina, Y. S., Kolosov, P. M., Ven'yaminova, A. G., Graifer, D. M., Vorobjev, Y. N., Frolova, L. Y., and Karpova, G. G. (2011) Adenine and guanine recognition of stop codon is mediated by different N domain conformations of translation termination factor eRF1, *Nucleic Acids Res 39*, 7134-7146.

119. Velichutina, I. V., Hong, J. Y., Mesecar, A. D., Chernoff, Y. O., and Liebman, S. W. (2001)

Genetic interaction between yeast Saccharomyces cerevisiae release factors and the decoding region of 18 S rRNA, *J Mol Biol 305*, 715-727.

120. Caskey, C. T., Beaudet, A. L., and Tate, W. P. (1974) Mammalian release factor; in vitro assay and purification, *Methods Enzymol 30*, 293-303.

121. Hatin, I., Fabret, C., Rousset, J. P., and Namy, O. (2009) Molecular dissection of translation termination mechanism identifies two new critical regions in eRF1, *Nucleic Acids Res 37*, 1789-1798.

122. Wong, L. E., Li, Y., Pillay, S., Frolova, L., and Pervushin, K. (2012) Selectivity of stop codon recognition in translation termination is modulated by multiple conformations of GTS loop in eRF1, *Nucleic Acids Res*.